

Understanding Recent Snow Cover Changes in the Pan-Arctic

Xiaogang Shi

A dissertation submitted in partial fulfillment of the requirements for the degree of

Doctor of Philosophy

University of Washington

2012

Reading Committee:

Dennis P. Lettenmaier, Chair

Stephen J. Déry

Erkan Istanbuluoglu

Program Authorized to Offer Degree:

Department of Civil and Environmental Engineering

University of Washington

Abstract

Understanding Recent Snow Cover Changes in the Pan-Arctic

Xiaogang Shi

Chair of the Supervisory Committee:

Professor Dennis P. Lettenmaier

Department of Civil and Environmental Engineering

Over the pan-Arctic land area, surface air temperature (SAT) has risen by almost twice the global average in recent decades, and many other changes have been observed across the region, indicating a system-wide response to a changing climate. These changes motivate this study, the goal of which is to identify the roles of hydroclimate indicators in snow cover extent (SCE) changes, and to evaluate the impact of snow cover recession on frozen soil heat content (SHC) over the pan-Arctic land region. I do so by exploring the variability and trends in surface energy fluxes, SCE and SHC, as well as their corresponding correlations. This work comprises four related studies. First, high latitude surface radiative fluxes produced by a suite of satellite, global reanalysis, and land surface model-derived data were compared with in situ observations. The results show that relative to other data sources, the Variable

Infiltration Capacity (VIC) land surface model provides good estimates of surface radiative fluxes. Second, the relative roles of surface energy fluxes in the observed spring and summer SCE recession were identified. My analyses indicate that surface net radiation (SNR) provides the primary energy source and sensible heat (SH) plays a secondary role in observed changes of SCE. Compared with SNR and SH, latent heat has only a minor influence on snow cover changes. Third, by comparing with the corresponding satellite product, the ability of VIC to reconstruct spatial and temporal changes of SCE was assessed. The relationships between snow cover and hydroclimate changes over each snow cover sensitivity zone (SCSZ) for North America and Eurasia were also identified. We find that VIC is able to reconstruct spatial and temporal changes of observed SCE, and the snow cover recession is mainly driven by statistically significant decreases in snow surface albedo and increased SAT, as well as statistically significant increased atmospheric water vapor pressure. Finally, I explored the effects of snow cover recession and increases in SAT on SHC. I found that increasing SAT during late spring and early summer has the greatest influence on SHC changes, and reduced SCE plays a secondary role, which is only significant in SCSZ.

Table of Contents

List of Figures	iv
List of Tables	ix
Acknowledgements	xii
Dedication	xiii
1. Introduction	1
2. Surface Radiative Fluxes over the Pan-Arctic Land Region: Variability and Trends	6
2.1. Introduction	6
2.2. Data Sets	8
2.2.1 In Situ Data	9
2.2.2 Satellite Data	9
2.2.3 Reanalysis Data	11
2.2.4 Temperature Index Scheme	12
2.3. Results	13
2.3.1 Evaluation of Data Sets Using in Situ Observations	13
2.3.1.1 Mean Diurnal Cycle	14
2.3.1.2 Mean Seasonal Cycle	16
2.3.2 Regional-Scale Comparisons	22
2.3.2.1 Temporal Variability	22
2.3.2.2 Spatial Variability	25
2.3.2.2.1 DSW	25
2.3.2.2.2 DLW	26
2.3.2.2.3 Albedo	28
2.3.2.3. Latitudinal Variability	30
2.3.3 Trend Analysis	32
2.4. Summary and Conclusions	39
3. The Role of Surface Energy Fluxes in Pan-Arctic Snow Cover Changes	41

3.1. Introduction	41
3.2. Data Sets	43
3.2.1 Snow Cover Extent Data	44
3.2.2 Surface Energy Fluxes Data.....	46
3.3. Results.....	48
3.3.1 Temporal Analyses of SCE and Surface Energy Fluxes.....	48
3.3.2 Correlations between Observed SCE and Modeled Surface Energy Fluxes.....	52
3.3.3 Role of Surface Energy Fluxes in Snow Cover Changes.....	54
3.4. Summary and Discussion.....	58
4. Relationships between Recent Pan-Arctic Snow Cover and Hydroclimate Trends	61
4.1. Introduction	61
4.2. Data Sets	64
4.2.1 Observed and Modeled Snow Cover Extent Data	64
4.2.2 Hydroclimatic Forcing Data.....	66
4.3. Results and Discussion.....	70
4.3.1 Spatial and Temporal Variability of SCE.....	71
4.3.2 Temporal Analyses of Surface Energy Fluxes	78
4.3.3 Correlations between Observed SCE and Modeled Surface Energy Fluxes.....	83
4.3.4 Role of Surface Energy Fluxes in Snow Cover Changes.....	83
4.3.5 Causes of Pan-Arctic Snow Cover Changes.....	86
4.4. Conclusions.....	94
5. The Effects of Pan-Arctic Snow Cover and Air Temperature Changes on Frozen Soil Heat Content	96
5.1. Introduction	96
5.2. Data Sets	99
5.2.1 Observed SCE and SAT Data	99
5.2.2 Modeled SH.....	101
5.3. Results.....	102
5.3.1 Definition of Study Zones.....	102
5.3.2 Experimental Design Based on SCE and SAT Trends.....	105

5.3.3 SHC Trends.....	111
5.3.4 Effects of SCE and SAT Changes on SHC.....	116
5.4. Conclusions	122
6. Conclusions.....	124
References.....	127
Curriculum Vitae	148

List of Figures

Figure Number	Page
2.1 Geographical distribution of GEBA observation sites for DSW (32 sites), DLW (3 sites), and albedo (2 sites) over the pan-Arctic land region. The color bar at right indicates the number of archived years of data.....	10
2.2 The mean diurnal cycle anomaly of DSW from TIND, ERA-40, ERA-Interim and ISCCP relative to the observations for the six index stations over the pan-Arctic for winter (DJF), spring (MAM), summer (JJA), and autumn (SON)	15
2.3 Mean seasonal cycles and biases of a) DSW, b) DLW, and c) albedo from TIND, ERA-40, ERA-Interim, and ISCCP with GEBA observations averaged for all the available stations	19
2.4 Monthly time series (left-hand) and mean seasonal cycle (right-hand) of a) DSW; b) DLW; c) albedo from TIND (dashed), ERA-40 (dotted), ERA-Interim (blue solid), and ISCCP (black solid) for the pan-Arctic land region. All the units where applicable are W/m^2	23
2.5 Spatial distribution of seasonal mean DSW from ERA-40, and the difference between ERA-40 and TIND, ERA-Interim, and ISCCP for the pan-Arctic land area	27
2.6 Spatial distribution of seasonal mean DLW from ERA-40, and the difference between ERA-40 and TIND, ERA-Interim, and ISCCP for the pan-Arctic land area	29
2.7 Spatial distribution of seasonal mean albedo from ERA-40, and the difference between ERA-40 and TIND, ERA-Interim, and ISCCP for the pan-Arctic land area	31

2.8 Annual mean a) DSW, b) DLW, and c) albedo versus latitude from TIND, ERA40, ERA-Interim, and ISCCP for the pan-Arctic	33
2.9 GEBA annual DSW trend plots for all periods with trends significant at 95% using the Mann-Kendall non-parametric test at a) Lulea, Sweden, b) Oestersund, Sweden, and c) Aleksandrovscoe, Russia. Each line represents a period for which the trend slope is given by the color of the line and the period length is given by the length of the line (starting and ending at the start and end of the period, respectively)	36
3.1 Study domain with 100 km resolution EASE grid mesh	43
3.2 Spring and summer snow cover area fraction over the pan-Arctic land areas in North America and Eurasia from VIC and satellite observations	49
3.3 Scatterplots of surface energy fluxes: (a) SNR, (b) SH, and (c) LH versus satellite SCF over North America and Eurasia during spring and summer. The sign of star means that the correlation has a significance level $p < 0.025$	51
3.4 Relative role of spring and summer surface energy fluxes averaged only over snow-covered (a) North America and (b) Eurasia.....	55
3.5 Latitudinal profiles of the changes in spring and summer surface energy fluxes over North America and Eurasia snow covered areas. The blue line shows the weight (fraction of snow cover in each latitudinal band)	57
4.1 Spatial distribution of monthly mean SCE from the VIC model (VIC) and NOAA satellite observations (OBS) over North America and Eurasia from April through June for the period 1972-2006. The percentages on the map show the snow cover area fractions from VIC and NOAA for each month over the 35-year period of analysis.....	72

4.2 Monthly time series of snow cover fraction (SCF) and their trends (the unit of trend slope is in $year^{-1}$) derived from the VIC model (VIC, dashed lines) and NOAA observations (OBS, solid lines) for the period 1972-2006 for North America and Eurasia over the pan-Arctic land area.....	74
4.3 Latitudinal variations of the SCE trends and their area fractions derived from the VIC model (VIC) and NOAA satellite observations (OBS) over (a) North American and (b) Eurasian Snow Covered Zones (SCZs), including the Snow Covered Sensitivity Zones (SCSZs) and Snow Covered Non-sensitivity Zones (SCNZs) as indicated by the arrows, from April through June for the period 1972-2006. The percentage under each bar chart is the trend significance for each 5° (N) of latitude (expressed as a confidence level).....	77
4.4 Snow cover area weights (the fraction of snow-covered area falling within each 5° (N) latitude band) for North American and Eurasian SCSZs from April through June for the period 1972-2006	81
4.5 Correlations between three surface energy fluxes: SNR, SH, and LH versus NOAA satellite SCE observations for each latitude band in the North American and Eurasian SCSZs for April, May and June. The significance level of $p < 0.025$ (dashed line) was calculated by the Student t-test	82
4.6 Latitudinal variations in the changes of surface energy fluxes in the North American and Eurasian SCSZs from April through June for the period 1972-2006 by 5° latitude band. The number in each bar denotes the relative role of the total energy attributable to snow cover changes	85
4.7 Relative role of three surface energy fluxes' changes during the April to June part of the year areally-averaged over each SCSZ for (a) North America and (b) Eurasia for the period 1972-2006. The number in each bar denotes the contribution of the total energy attributable to snow cover changes	87

4.8 Correlations between NOAA SCE observations and fifteen hydroclimatic characteristics in the North American and Eurasian SCSZs from April to June for the period 1972-2006. The correlation is statistically significant at a level of $p < 0.025$ when its absolute value is greater than 0.34. X denotes that the correlation is not significant. The abbreviations for the hydroclimate variables are defined as follows: surface net radiation (SNR), sensible heat (SH), latent heat (LH), net shortwave radiation (SW), snow surface albedo (ALB), downward shortwave radiation (DSW), diurnal temperature range (DTR), atmospheric water vapor pressure (VP), downward longwave radiation (DLW), cloud cover (CC), precipitation (P), surface air temperature (SAT), daily maximum temperature (T_{max}), daily minimum temperature (T_{min}), and wind speed (WS).....	92
5.1 (a) Spatial distribution of monthly mean snow cover extent (SCE) from NOAA satellite observations (OBS) over North America and Eurasia in the pan-Arctic land region (non-snow covered zone (NSCZ) and snow covered zone (SCZ)) for April (top panel), May (middle panel), and June (bottom panel) for the period 1972-2006. The SCE trends in 5° latitude bands and their area fractions over (b) North American and (c) Eurasian SCZ, including the snow covered sensitivity zone (SCSZ) and snow covered non-sensitivity zones (SCNZ) as indicated by the arrows. The percentage under each bar chart is the trend significance for each 5° (N) of latitude.....	104
5.2 Experimental design for accessing the effects of pan-Arctic snow cover and air temperature changes on soil heat content (SHC) in NSCZ, SCSZ, and SCNZ over North America and Eurasia from April through June for the period 1972-2006.....	109
5.3 Area comparisons of NSCZ, SCSZ, and SCNZ in North America and Eurasia from April through June for the period 1972-2006	110
5.4 Trend analyses for SHC for SHC averaged over a thermal profile from the surface to the depth of each soil thermal node derived from VIC in NSCZ, SCSZ, and SCNZ	

over (a) North America and (b) Eurasia from April through June for the period 1972-2006. The significance level (expressed as a CL) was calculated using a two-sided Mann-Kendall trend test. Trend slope (TS) units are $mJm^{-2}year^{-1}$ 114

5.5 Correlations between observed SCE and simulated SHC in NSCZ, SCSZ, and SCNZ over North America and Eurasia from April through June for the period 1972-2006. The correlation is statistically significant at a level of $p < 0.025$ when its absolute value is greater than 0.34117

5.6 Correlations between observed SAT and simulated SHC in NSCZ, SCSZ and SCNZ over North America and Eurasia from April through June for the period 1972-2006. The correlation is statistically significant at a level of $p < 0.025$ when its absolute value is greater than 0.34118

List of Tables

Table Number	Page
2.1 Basic information of surface radiative flux data sets.....	8
2.2 MAE and MBE of DSW mean diurnal cycle anomaly from ERA-40, ERA-Interim, ISCCP, and TIND against the observed data averaged for the six index stations over the pan-Arctic for winter (DJF), spring (MAM), summer (JJA), and autumn (SON). (All units where applicable are W/m ²).....	17
2.3 Correlations for deseasonalized monthly anomalies of DSW, DLW and albedo between ERA-40, ERA-Interim, ISCCP, TIND, and the GEBA observations	17
2.4 Trend analysis details for GEBA annual and seasonal DSW at 12 stations over the pan-Arctic land region. The significance level (<i>p</i> -value) achieved by two-sided Mann-Kendall test.....	35
2.5 DSW trend tests at Lulea (1413), Oestersund (2104) and corresponding grid cells from TIND, ISCCP, ERA-40, ERA-Interim, and ERA-40-Interim. The significance level (<i>p</i> -value) achieved by two-sided Mann-Kendall test	38
3.1 Monotonic trends in spring and summer SCE over North America and Eurasia from the VIC model and satellite observations (OBS) in the pan-Arctic land region. The significance level (<i>p</i> -value) was calculated by two-sided Mann-Kendall test. (the unit of trend slope is in year ⁻¹)	50
3.2 Trend analyses for spring and summer surface energy fluxes over snow-covered North America and Eurasia generated from VIC. The significance level (<i>p</i> -value) was calculated by two-sided Mann-Kendall trend test.	53

3.3 Trend analyses for the terms related with SNR during spring and summer over snow-covered North America and Eurasia generated from VIC. The significance level (<i>p</i> -value) was calculated by two-sided Mann-Kendall trend test. (the unit of total change during the 35-year period for fluxes is W/m^2 ; the unit for T_{min} and T_{max} is $^{\circ}C$; no unit for Albedo and RH)	59
4.1 Correlation coefficients due to the linear trend and the variability for the monthly time series of SCE derived from VIC and NOAA observations in the North American and Eurasian SCSZs for the period 1972-2006. The significance level (<i>p</i> -value) was calculated using a two-tailed Student t-test with 33 degrees of freedom	75
4.2 Trend analyses for three surface energy fluxes (surface net radiation (SNR), sensible heat (SH), and latent heat (LH)) from April to June for 1972-2006 in the North American and Eurasian SCSZs generated from VIC. The significance level (<i>p</i> -value) was calculated using a two-sided Mann-Kendall trend test. Trend slope units are $Wm^{-2}year^{-1}$	79
4.3 Total changes for twelve pan-Arctic hydroclimatic characteristics from April to June during the period 1972-2006 in the North American and Eurasian SCSZs. The significance level (<i>p</i> -value) was calculated using a two-sided Mann-Kendall trend test. The unit of total change for radiation fluxes (net shortwave radiation (SW), downward shortwave radiation (DSW), and downward longwave radiation (DLW)) is Wm^{-2} . Units for diurnal temperature range (DTR), surface air temperature (SAT), daily maximum temperature (T_{max}), and daily minimum temperature (T_{min}) are $^{\circ}C$; for atmospheric water vapor pressure (VP) <i>hPa</i> ; for precipitation (P) <i>mm</i> ; and for wind speed (WS) ms^{-1} . Snow surface albedo (ALB) and cloud cover (CC) are dimensionless	90
5.1 Trend analyses for observed snow cover extent (SCE) in the snow covered sensitivity zone (SCSZ) and the snow covered non-sensitivity zone (SCNZ) over North America and Eurasia from April through June for the period 1972-2006. The	

significance level (p -value) was calculated using a two-sided Mann-Kendall trend test. Trend slope (ts) units are $year^{-1}$	107
5.2 Trend analyses for CRU monthly surface air temperature (SAT) in the non-snow covered zone (NSCZ), SCSZ, and SCNZ over North America and Eurasia from April through June for the period 1972-2006. The significance level (p -value) was calculated using a two-sided Mann-Kendall trend test. Ts units are $^{\circ}Cyear^{-1}$	108
5.3 Eighteen soil thermal nodes (STN) and their corresponding depth (m) from the surface. The first STN has a depth of 0 m indicating it is at the surface	113
5.4 Correlation coefficients due to the linear trend and variability for SHC derived from VIC and NOAA-SCE observations in SCSZ and SCNZ over North America and Eurasia from April to June for the period 1972-2006. The significance level (p -value) was calculated using a two-tailed Student t-test with 33 degrees of freedom	120
5.5 Correlation coefficients due to the linear trend and variability for SHC derived from VIC and CRU SAT in NSCZ, SCSZ, and SCNZ over North America and Eurasia from April to June for the period 1972-2006. The significance level (p -value) was calculated using a two-tailed Student t-test with 33 degrees of freedom	121

Acknowledgements

First, I would like to thank my adviser, Professor Dennis P. Lettenmaier, for his invaluable guidance and support throughout my dissertation work. I am very grateful to my other supervisory committee members, Stephen J. Déry of the University of Northern British Columbia, Erkan Istanbuluoglu of the University of Washington, Pavel Ya Groisman of NOAA National Climatic Data Center, Gerard Roe of the University of Washington, James H. Morison of the Applied Physics Laboratory and the University of Washington, and Martin Wild of ETH Zurich, for their thoughtful insights and feedbacks on my dissertation work. Thanks also to Steve Burges of the University of Washington for his teaching of four hydrology classes, Jenny Adam of Washington State University, Qihong Tang and Fengge Su of Chinese Academy of Sciences, Jessica Lundquist of the University of Washington, Huilin Gao of Texas A&M University, Tara J. Troy of Columbia University, and Alan Hamlet of the University of Washington, all of whom provided thoughtful mentoring and advice. Thanks also to the entire Land Surface Hydrology Group at the University of Washington, especially to Ted Bohn for support related to the VIC model, Elizabeth Clark for proof reading my papers, and Chunmei Zhu for help with UNIX. I am also very thankful to all of my friends outside the University, especially from the Global Friends Fellowship, for their friendship and support. I would like to acknowledge the love and unconditional support from my sisters and their spouses.

Dedication

This dissertation is dedicated to my parents, Fuqin Xu (徐福芹) and Chunjiang Shi (史春江), for their love, support and guidance throughout my life.

1. Introduction

Over the pan-Arctic land region, the rise in the surface air temperature (SAT) has been almost twice the global average in recent decades (Serreze et al. 2000; Jones and Moberg 2003; Overland et al. 2004; Hinzman et al. 2005; White et al. 2007; Solomon et al. 2007; Trenberth et al. 2007; Screen and Simmonds 2010). Paleoclimate studies also show that recent temperatures in the pan-Arctic are the highest they have been in the last 400 years (Overpeck et al. 1997). Besides temperatures, many other changes have been observed across the region in recent decades, indicating that the pan-Arctic land area is undergoing a system-wide response to a changing climate (Groisman et al. 1994; Serreze et al. 2000; Peterson et al. 2002; Yang et al. 2003; Smith et al. 2004; Hinzman et al. 2005; McClelland et al. 2006; Adam et al. 2007; Déry and Brown 2007; Rawlins et al. 2010; Shi et al. 2010, 2011; Brown and Robinson 2011).

The physical processes in the pan-Arctic land region differ markedly from the low to mid-latitudes, in part because of the predominance of snow, which is present during much of the year. The presence of snow plays an important role in both the radiation balance and the water cycle due to its high albedo, low thermal conductivity, and high spatial and temporal variability (Liston 1999). For these reasons, snow cover is an important climatic and hydrologic land surface variable, which serves as both an indicator of and a control on climate change over much of the Northern Hemisphere land

area (Gray and Male 1981; Groisman et al. 1994; Frei and Robinson 1999; Robinson and Frei 2000). However, the interpretation of changes in snow cover and its timing is complicated by the low density and poor quality of climate observing stations in Arctic areas for variables such as surface radiative and turbulent fluxes, which affect snow surface energy exchange processes (Cline 1997), as well as other hydroclimate variables (e.g., precipitation and temperature) that also affect snow cover extent (SCE) (Jol et al. 2009). Moreover, observed soil temperatures across the pan-Arctic, which have been used to understand the impact of seasonal snow cover and air temperature on the ground thermal regime in past studies (Osterkamp and Romanovsky 1999; Zhang et al. 2001; Smith et al. 2004; Beltrami et al. 2006; Romanovsky et al. 2002, 2007), are problematic because latent heat effects are neglected which may be significant in regions with frozen soils (Troy 2010).

Satellite data (Stackhouse et al. 2004; Zhang et al. 2004; Robinson et al. 1993) and atmospheric model reanalysis products (Kalnay et al. 1996; Uppala et al. 2005; Simmons et al. 2006; Uppala et al. 2008) provide sources for most or all terms in the surface energy budget and offer the opportunity to investigate the space-time variations in surface radiative and turbulent fluxes. In addition, land surface models (e.g., Liang et al. 1994; Oleson et al. 2004) have improved to the point that they may, in some cases, serve as surrogates for in situ hydroclimatic observations. Off-line runs of these models can provide snowpack energy balance components and offer an opportunity to investigate the nature of spatial and temporal variability of snow cover changes (Betts et al. 2009; Troy

and Wood 2009; Troy et al. 2012; Shi et al. 2010, 2011, 2012). The heat content of the soil column is arguably a better indicator of changes in the land surface energy budget than soil temperatures, because it provides an integrated measure that accounts for changes in temperature, moisture, and latent heat effects (Levitus et al. 2001, 2005; Beltrami et al. 2002, 2006; Hansen et al. 2005; Troy 2010). Recent studies by Troy et al. (2012) have showed that the Variable Infiltration Capacity (VIC) land surface model (Liang et al. 1994; Cherkauer and Lettenmaier 1999) is able to reproduce observed soil temperature profiles and can be used as a surrogate for observations to estimate long-term changes in frozen soil heat content (SHC) at high latitudes.

In this dissertation, my work focuses on the North American and Eurasian portions of the pan-Arctic land region, which include all land areas draining to the Arctic Ocean, as well as those regions draining into Hudson Bay, Hudson Strait, and the Bering Strait. As noted above, this region has some of the largest observed warming trends globally, is particularly sensitive to warming, and has the potential to provide various feedback responses to the global climate system.

The overarching goal of my research is to identify the roles of surface energy fluxes and other hydroclimate indicators in snow cover changes, and to evaluate the impact of snow cover recession on SHC over the pan-Arctic land region by exploring the variability and trends in surface radiative fluxes, SCE and SHC, as well as their corresponding correlations. The specific science questions related to this goal are:

1. To what extent are satellite data, reanalysis products and land surface model simulations consistent with in situ measurements of surface radiative fluxes over the pan-Arctic land region? What is the consistency of dominant temporal and spatial variability of these fluxes at the regional scale? Are there significant trends in these surface radiation fluxes?
2. What are the relative roles of surface energy fluxes in snow cover changes over the pan-Arctic land region? Which are most responsible for the observed spring and summer SCE recession?
3. To what degree can a land surface model reconstruct spatial and temporal changes of SCE compared with corresponding satellite products? What are the relationships between snow cover and hydroclimate changes over each snow cover sensitivity zone for North America and Eurasia?
4. Are there significant trends in SHC over soil profiles? What are the effects of snow cover and air temperature changes on SHC over the pan-Arctic land area?

These questions are addressed in four chapters in this dissertation. **Chapter 2** evaluates the variability and trends of surface radiative fluxes over the pan-Arctic land region using satellite data, reanalysis products, and in situ observations, as well as land surface model simulations, which was published in 2010 in the *Journal of Geophysical Research – Atmospheres*. **Chapter 3** examines the roles of surface radiative and turbulent fluxes in

pan-Arctic snow cover changes during spring and summer, and was published as Shi et al. 2011 in *Environmental Research Letters*. **Chapter 4** (in press, *Journal of Climate*) explores spatial and temporal variations of monthly SCE during the late spring and early summer and their relationships with hydroclimatic variables over each snow cover sensitivity zone (latitude bands) for both North America and Eurasia over the pan-Arctic. **Chapter 5** (in review by the *Journal of Geophysical Research – Atmospheres* as Shi and Lettenmaier, 2012) investigates the effects of snow cover recession and increasing SAT in SHC changes for each study zone over North America and Eurasia by analyzing SHC trends during the late spring and early summer and their correlations with SCE or SAT.

2. Surface Radiative Fluxes over the Pan-Arctic Land Region: Variability and Trends

This chapter was published in the *Journal of Geophysical Research-Atmospheres* as:

Shi, X., M. Wild, and D. P. Lettenmaier, 2010: Surface radiative fluxes over the pan-Arctic land region: Variability and trends. *J. Geophys. Res.*, **115**, D22104, doi:10.1029/2010JD014402.

2.1. Introduction

Variations in surface radiative fluxes have profound climatic and environmental implications, especially for the pan-Arctic, which is one of the most sensitive regions on earth to global climate change (Manabe et al. 1992; Manabe and Stouffer 1994; Miller and Russell 2000). Past studies of the pan-Arctic region (Adam et al. 2007; McClelland et al. 2006; Peterson et al. 2002) have identified changes in land surface hydrological fluxes, but less attention has been placed on the energy inputs to the land system due to the sparse in situ measurements of surface radiative fluxes, which are generally inadequate to reveal spatial and temporal variations.

Recently assembled satellite data (Stackhouse et al. 2004; Zhang et al. 2004) and atmospheric model reanalysis products (Kalnay et al. 1996; Uppala et al. 2005; Simmons et al. 2006; Uppala et al. 2008) have resulted in data sources for most or all terms in the

surface energy budget and offer the opportunity to investigate the space-time variations in surface radiative fluxes. A number of papers have analyzed various aspects of the above data sets globally (e.g. Allan et al. 2004; Betts et al. 2006; Li et al. 1995; Lin et al. 2008; Raschke et al. 2006; Wild et al. 1998), and locally, such as Tibet (Yang et al. 2008); the Arctic Ocean (Liu et al. 2005); northern Eurasia (Troy et al. 2009); and the Mackenzie, Mississippi and Amazon River basins (Betts et al. 2009). However, few have focused on the pan-Arctic land region, despite its importance to the global climate system (ACIA 2005).

In this paper, we attempt to understand the space-time variations in the pan-Arctic land area's surface radiative fluxes based on a suite of satellite, global reanalysis, and temperature index scheme-derived data. In particular, we analyze surface downward shortwave, and longwave radiation and albedo from one satellite dataset, two atmospheric model reanalysis products and a simulation from a temperature index scheme. In addition, we compare diurnal and mean seasonal cycles with in situ measurements from several high quality observation networks. We assess the consistency of dominant spatial, temporal and latitudinal variability of these surface radiative fluxes at the regional scale. Finally, for a small number of stations with records spanning the period from the 1950s and 1960s to post-2000, we analyze long-term trends in downward shortwave radiation. This study contributes to the NASA Energy and Water cycle Studies (NEWS), which are intended to improve estimates of the terrestrial energy budget components for the hydrologic and ecological communities.

2.2. Data Sets

We focused on the pan-Arctic land region, which is defined as all land areas draining to the Arctic Ocean, as well as those regions draining into the Hudson Bay, Hudson Strait, and the Bering Strait as shown in Figure 2.1. We used four data sources: a) in situ observations as shown in Figure 2.1, b) the International Satellite Cloud Climatology Project-Flux Data (ISCCP-FD, abbreviated as ISCCP hereinafter), c) the European Centre for Medium Range Weather Forecast's (ECMWF) ERA-40 and ERA-Interim atmospheric reanalysis products, and d) a Temperature INdex (TIND) scheme. Characteristics of the data sets are summarized in Table 2.1, and are described in the following sections.

Table 2.1 Basic information of surface radiative flux data sets.

Products	Temporal Resolution	Spatial Resolution	Period
GEBA	monthly	N/A (station)	1950-2006
ISCCP	3 hour	2.5° x 2.5°	1984-2006
ERA-40	6 hour	T159	1957-2002
ERA-Interim	12 hour	T255	1989-2009
TIND	3 hour	100-km EASE grid	1979-2007

2.2.1. In Situ Data

Our primary source of observations is the Global Energy Balance Archive (GEBA, Ohmura et al. 1989; Gilgen et al. 1998), which is a central repository for instrumental measurements of surface energy fluxes globally. GEBA is housed at the Institute for Climate and Atmospheric Sciences at Eidgenössische Technische Hochschule (ETH) in Zurich. Currently, GEBA contains 450,000 surface energy flux entries in the form of monthly means from more than 2500 observation sites. Although the GEBA historical radiation data are of variable accuracy depending on the individual station, Gilgen et al. (1998) estimated the relative random error (root mean square error/mean) of downward shortwave radiation data at 5% for monthly means and 2% for annual means. As shown in Figure 1, within the pan-Arctic domain, GEBA sites contain monthly surface downward shortwave radiation (32 sites), longwave radiation (3 sites) and albedo (2 sites) with varying record lengths starting as early as 1950 and ending as late as 2006.

2.2.2. Satellite Data

The satellite surface radiative flux data are from ISCCP (Zhang et al. 2004), which have a spatial resolution of 2.5 degrees at 3-hour time intervals. The period of the ISCCP record is currently from July 1983 through December 2006. The ISCCP data set contains radiative fluxes at the top of atmosphere (TOA), at the surface (SRF), and at three levels (680, 440, and 100 hPa) within the atmosphere. ISCCP uses the NASA Goddard Institute for Space Studies (GISS) radiative transfer model and satellite data from geostationary

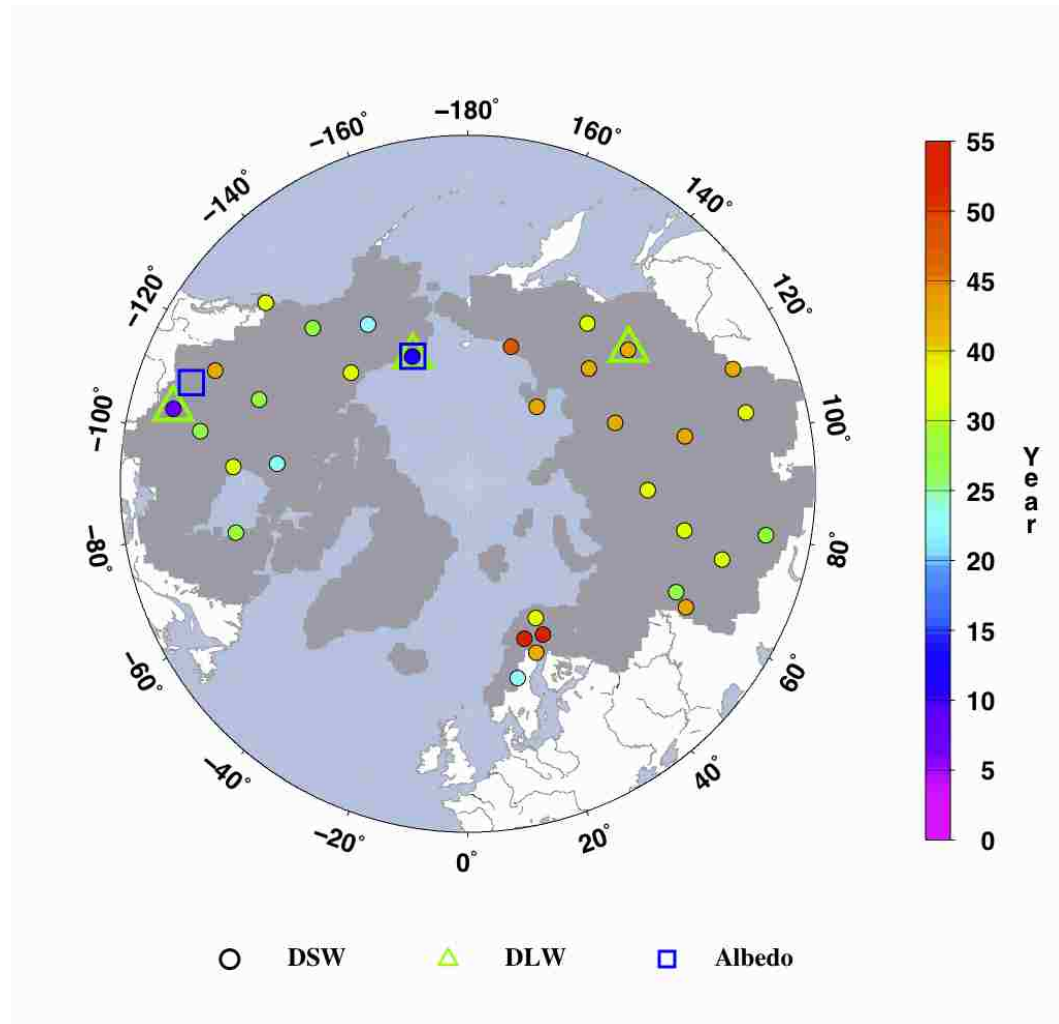


Figure 2.1 Geographical distribution of GEBA observation sites for DSW (32 sites), DLW (3 sites), and albedo (2 sites) over the pan-Arctic land region. The color bar at right indicates the number of archived years of data.

satellites (Meteosat, GOES, GMS, and INSAT) below 55° N latitude, and the NOAA polar orbiters at high latitudes (and when geostationary satellite data are unavailable). All instruments are normalized to a common reference satellite and to remove trends due to instrument drift and changes in instruments and platforms (Rossow et al. 1991; Brest et

al. 1997). More information about the ISCCP products can be found at <http://isccp.giss.nasa.gov/projects/flux.html>.

2.2.3. Reanalysis Data

Two reanalysis products from the ECMWF numerical weather prediction (NWP) model were used. The ERA-40 reanalysis (Uppala et al. 2005) is based on a 3-D variational assimilation system with a spatial resolution of T159 (approximately 125 km) in the horizontal and 60 levels in the vertical, and covers the time period from September 1957 to August 2002 with a 6-hour temporal resolution. ERA-40 has been evaluated and used widely in a variety of studies (Hollingsworth and Pfrang 2005). A new global reanalysis product called ERA-Interim (Simmons et al. 2006) is being produced by ECMWF with data publicly available for the period 1989-2009 with a 12-hour temporal resolution. ERA-Interim is based on a 4-D variational assimilation system at T255 (approximately 80 km) horizontal resolution with the same 60 levels in the vertical as in ERA-40. As compared with ERA-40, the major improvements in ERA-Interim are the variational bias correction of satellite observations, higher spatial resolution, and a more recent cycle of the ECMWF model (Uppala et al. 2008). The NCEP-NCAR reanalysis (Kalnay et al. 1996) is another popular global reanalysis product, which has the advantage of a longer period of record (1948 through near real-time) than either ERA-40 or ERA-Interim. However, previous studies (Brotzge 2004; Sheffield et al. 2006; Troy et al. 2009) have found that it substantially overestimates surface downward shortwave radiation, and for this reason, we chose not to include it in our study.

2.2.4. Temperature Index Scheme

The TIND scheme was used to calculate shortwave and longwave radiative fluxes based on daily temperature range and daily average temperature, which has been widely used in model intercomparison experiments such as the Project for Intercomparison of Land Parameterization Schemes (PILPS) (e.g. Pitman et al. 1999) and others. This temperature index scheme, forced with daily maximum and minimum, has been commonly used by models such as VIC (Liang et al. 1994, 1996; Cherkauer and Lettenmaier 1999, 2003) for long-term simulations in cases when direct observations are not available. The forcing data were at a spatial resolution of 100-km EASE grid, which were constructed using methods outlined in Adam et al. (2007) for the period 1979 to 2007 over the pan-Arctic land region. For shortwave radiation, TIND uses the algorithm of Thornton and Running (1999), described by Maurer et al. (2002). In the calculation of shortwave radiation, a solar geometry model (Gates 1980) was applied first to obtain the total daily shortwave radiation incident at the top of the atmosphere based on the latitude and time of year. Next, the Thornton and Running (1999) model was applied to estimate the daily atmospheric transmittance based on daily maximum and minimum air temperatures. Then, the downward shortwave radiation to ground level was calculated as the product of shortwave radiation incident at the top of the atmosphere and atmospheric transmittance. It should be recognized that the Thornton and Running algorithm does not incorporate any information about diurnal patterns of cloud cover, which may strongly affect the diurnal patterns of shortwave radiation in spring and summer. Downward longwave radiation was estimated using Equations (2.42 and 2.43) from Bras (1990), which are

based on the hourly air temperature (estimated from daily maxima and minima using a sinusoidal fit) and a function for emissivity from TVA (1972). Details are described in Bowling et al. (2003).

2.3. Results

In section 2.3.1, we compare the reanalysis products (ERA-40 and ERA-Interim), satellite product (ISCCP), and temperature index scheme (TIND) with surface observations. In section 2.3.2, we evaluate spatial-temporal patterns and latitudinal variability of downward shortwave radiation (DSW), downward longwave radiation (DLW) and albedo from the different estimates over the entire pan-Arctic domain. In addition, for a few stations with long-term observational DSW records from GEBA, we conduct trend analyses, which are reported in section 2.3.3.

2.3.1. Evaluation of Datasets Using in Situ Observations

For the purposes of our evaluations, the ERA-40, ERA-Interim and ISCCP (gridded) data were interpolated to the 100 km EASE grid from their original spatial projections using the Synagraphic Mapping System (SYMAP) method (Shepard 1984). SYMAP uses inverse distance squared weightings for stations within a pre-defined search radius from the grid-point. Because the ERA-40, ERA-Interim and ISCCP products are already gridded, the selected “stations” are the grid cells surrounding the target (interpolated) point. Because the search radius is constrained (in our case to about 400 km), there is no

influence of grid cells that are far from the target point. Also, the resolution of the interpolated fields is generally lower than the native grid meshes, and the radiation fields generally vary smoothly among surrounding grid cells, therefore effects of local variability on the interpolated fields are small. To compare the gridded products with the in situ data, DSW, DLW, and albedo from the different datasets were extracted for the grid cells in which the surface stations are located.

2.3.1.1 Mean Diurnal Cycle

Comparisons of the DSW mean diurnal cycle anomaly from the ERA-40, ERA-Interim, ISCCP and TIND estimates relative to the observations are shown in Figure 2.2 for winter (DJF), spring (MAM), summer (JJA), and autumn (SON). As mentioned in section 2.2.1, the GEBA data only contain monthly surface radiative fluxes. Therefore, hourly DSW observations for the six index stations that are close to (but generally south of) the pan-Arctic domain were extracted from the archives for four high quality observation networks, specifically: the Asian Automatic Weather Station Network (AAN) for Tiksi and Yakutsk (Russia), the Baseline Surface Radiation Network (BSRN) for Barrow (Alaska, USA), the Boreal Ecosystem-Atmosphere Study (BOREAS) for NSA and SSA (Canada), and the National Solar Radiation Data Base (NSRDB) for Fairbanks (Alaska, USA). Due to different temporal resolutions for the spatial data sets and the station data, we first aggregated the ISCCP, TIND estimates and field measurements from short duration (hourly or 3-hourly) to six-hourly (12-hourly field measurements for ERA-Interim). Because these index stations are from different time zones, we converted all

estimates to local time. Then, the differences from observations were computed by time of day for each season, as shown in Figure 2.2.

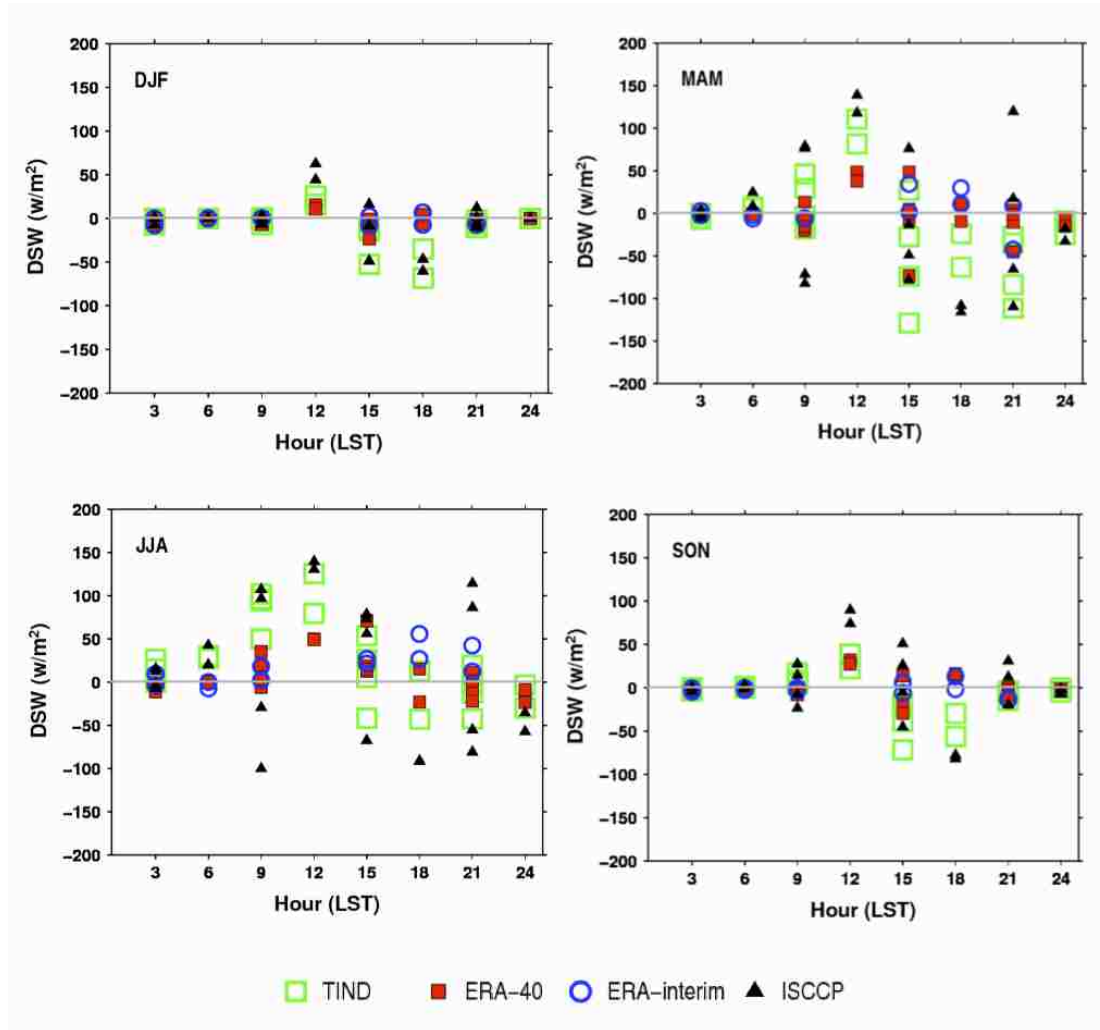


Figure 2.2 The mean diurnal cycle anomaly of DSW from TIND, ERA-40, ERA-Interim and ISCCP relative to the observations for the six index stations over the pan-Arctic for winter (DJF), spring (MAM), summer (JJA), and autumn (SON).

Table 2.2 reports statistics for different data sets including the Mean Bias Error (MBE) and Mean Absolute Error (MAE) of mean diurnal cycle of DSW anomaly to the observed

data, averaged for the six index stations for each season. Comparisons of the MBE and MAE show that ERA-40 and ERA-Interim both have the smallest statistical differences from the station values for almost all seasons. The MAE values for ISCCP and TIND are systematically large and can be greater than 65 W/m^2 in the spring and summer.

However, the ISCCP and TIND estimates show smaller MBE relative to the large MAE values. The differences by time of day in Figure 2.2 for the ISCCP and TIND estimates show a larger variation than ERA-40 and ERA-Interim. The smaller MBE and larger MAE for ISCCP and TIND in Table 2.2 might be related to the large positive and negative biases over the diurnal cycle as shown in Figure 2.2. By contrast, ERA-40 and ERA-Interim generally show smaller biases in Figure 2.2 and Table 2.2 than ISCCP and TIND, which suggest that the reanalysis products have more accurate mean diurnal cycles of DSW than the satellite product and the temperature index scheme simulation.

2.3.1.2 Mean Seasonal Cycle

Figure 2.3(a) compares the mean seasonal DSW variations and biases, averaged over 32 sites across the pan-Arctic land region as shown in Figure 2.1. ERA-40, ERA-Interim, ISCCP, and TIND all have small biases ($\pm 20 \text{ W/m}^2$), compared to the in situ observations. As noted above however, the small biases in ISCCP and TIND actually come about from a cancellation of large positive and negative biases over the diurnal cycle as shown in Figure 2.2. By contrast, the ERA-40 and ERA-Interim products show consistently smaller biases in both Figures 2.2 and 2.3(a). In order to eliminate the

potentially dominating effect of the seasonal cycle, deseasonalized anomalies in the monthly time series were determined by differencing the average in a given month from

Table 2.2 MAE and MBE of DSW mean diurnal cycle anomaly from ERA-40, ERA-Interim, ISCCP, and TIND against the observed data averaged for the six index stations over the pan-Arctic for winter (DJF), spring (MAM), summer (JJA), and autumn (SON). (all units where applicable are W/m^2)

Seasons Products	DJF		MAM		JJA		SON	
	MAE	MBE	MAE	MBE	MAE	MBE	MAE	MBE
ERA-40	4.4	-1.8	16.1	-2.1	17.1	8.1	8.7	1.0
ERA-Interim	3.8	-2.3	12.7	1.9	18.8	17.0	5.5	-2.2
ISCCP	14.4	-2.8	59.0	-3.7	66.3	14.6	25.9	1.4
TIND	11.7	-8.3	39.7	-14.2	39.0	24.4	15.5	-7.3

Table 2.3 Correlations for deseasonalized monthly anomalies of DSW, DLW and albedo between ERA-40, ERA-Interim, ISCCP, TIND, and the GEBA observations.

	ERA-40	ERA-Interim	ISCCP	TIND
DSW	0.88	0.91	0.86	0.76
DLW	0.96	0.97	0.82	0.91
Albedo	0.75	0.79	0.73	0.70

the long-term mean of all years of the same month. Table 2.3 shows the Pearson correlation coefficient (r) for DSW deseasonalized monthly anomalies between different data sets with the GEBA monthly observations. The deseasonalized monthly anomalies from ERA-40, ERA-Interim and ISCCP, relative to the corresponding observed anomalies, yielded relatively high correlation values ($r = 0.88, 0.91$ and 0.86 , respectively) as shown in Table 2.3, while the TIND model ($r = 0.76$) performed slightly worse.

Figure 2.3(b) evaluates the mean seasonal cycles and biases of DLW from the different data sets relative to GEBA field measurements averaged at 3 sites shown in Figure 2.1. Compared to the in situ data, ERA-40, ERA-Interim and TIND all have small biases, which are mostly less than 10 W/m^2 . ISCCP overestimates DLW from November through April, which results in a weak seasonal cycle. Table 2.3 shows that ERA-40, ERA-Interim and TIND DLW deseasonalized monthly anomalies have high correlations ($r = 0.96, 0.97$ and 0.91 , respectively) with GEBA observations whereas the correlation for ISCCP ($r = 0.82$) is somewhat lower.

Figure 2.3(c) compares the mean seasonal cycles and biases of albedo from ERA-40, ERA-Interim, ISCCP, and TIND relative to the GEBA data, averaged at two sites (Barrow, Alaska and Bad Lake, Saskatchewan) in the pan-Arctic. Relatively speaking, TIND matches the observations well except during summer, whereas the reanalysis products do well only for the summer. The ISCCP albedo only shows a good match in

spring. However, as shown by the results in Table 2.3, TIND deseasonalized monthly albedo

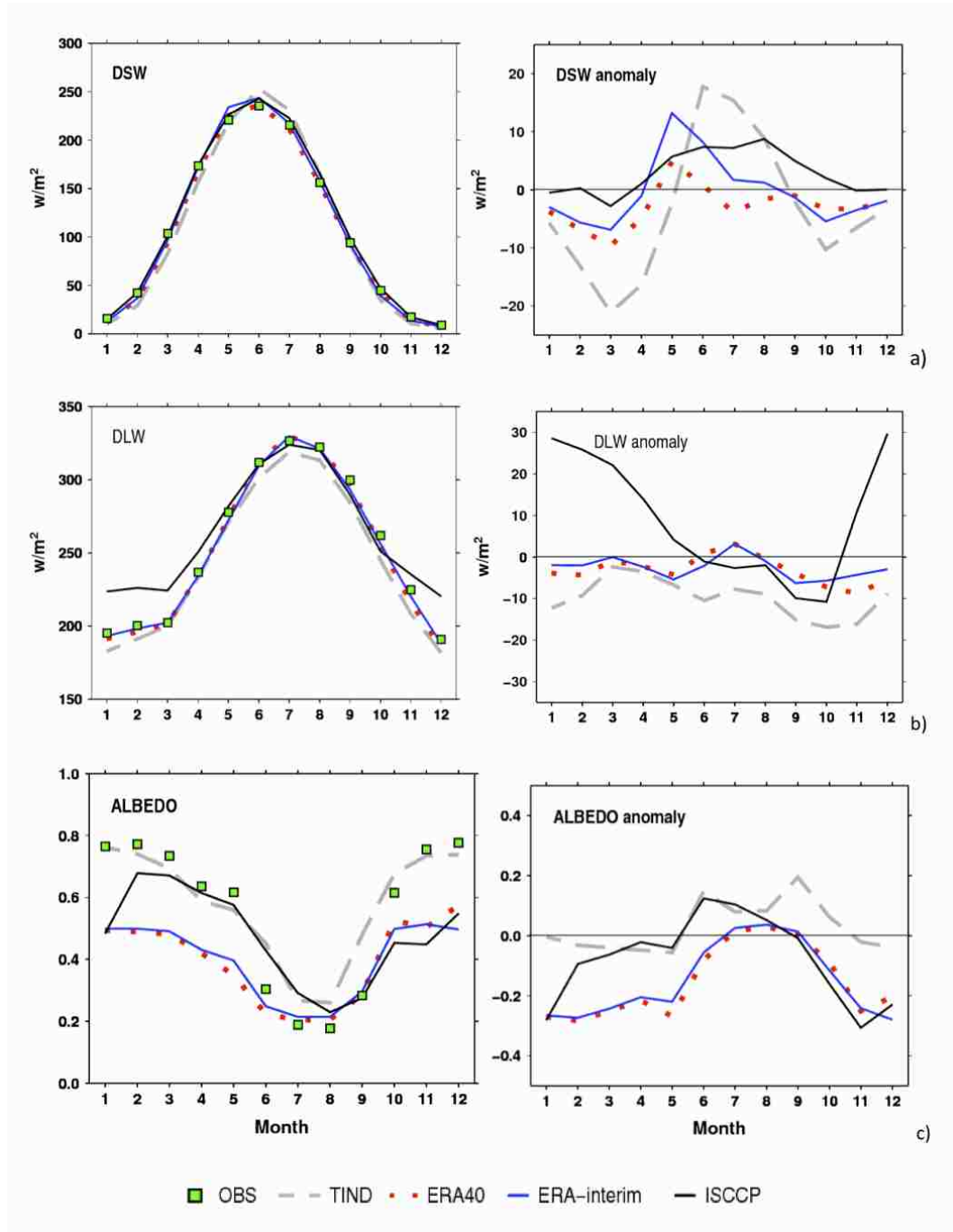


Figure 2.3 Mean seasonal cycles and biases of a) DSW, b) DLW, and c) albedo from TIND, ERA-40, ERA-Interim, and ISCCP with GEBA observations averaged for all the available stations.

anomalies had similar correlations with albedo observations as did ERA-40, ERA-Interim and ISCCP estimates.

Surface radiative fluxes from ERA-40, ERA-Interim, ISCCP, and TIND are all subject to errors from input data and from algorithms in the corresponding radiative transfer models. DSW in the TIND simulations comes from a relationship with the daily temperature range described by Thornton and Running (1999). Based on previous studies (Bowling et al. 2003; Zhu et al. 2007), the differences shown in the mean diurnal cycle of DSW (Figure 2.2) result from bias in the temperature range algorithm. In addition, clouds play an especially important role in estimates of DSW (Sorteberg et al. 2007). ISCCP cloud properties are determined by comparing the observed radiances with a detailed radiative transfer model (Raschke et al. 2005). ISCCP cloud detections are generally less reliable in the polar regions than elsewhere (Rossow and Schiffer 1999). On the other hand, various studies have shown that the cloud fraction is well captured by ERA-40 in the Arctic (Bromwich et al. 2007; Walsh et al. 2009). Therefore, the reanalysis products are expected to provide a more accurate mean diurnal cycle of DSW relative to ISCCP and TIND.

ISCCP DLW is sensitive to air temperature and humidity profiles (Zhang et al. 2006).

Uncertainties in air temperature and humidity result in errors in downward longwave

fluxes. Zhang et al. (2006) found that the surface air temperature has an uncertainty of about 2-4 K (3 K on average), which induces about 15 W/m^2 uncertainty for DLW. The humidity profile comparison suggests an uncertainty of 20–25% for the atmospheric column precipitable water below the 300 hPa level, which results in up to 10 W/m^2 uncertainty for DLW, making it the second largest source of uncertainty. In TIND, DLW is estimated using Equations (2.42 and 2.43) from Bras (1990), which are based on hourly air temperature and a function for emissivity from TVA (1972). The ISCCP surface temperature is retrieved from the clear sky infrared brightness temperature by correcting for atmospheric emission and absorption of radiation, using data for the atmospheric temperature and humidity profiles, and for the fact that the surface infrared emissivity is less than one (Zhang et al. 2004). The reanalysis products calculate model-derived fields (e.g., radiative fluxes, cloud properties) by assimilating atmospheric observations (temperature, pressure, wind, humidity). As for satellite radiances, clear sky infrared radiances are assimilated using a linearized cloud scheme and a radiation scheme that represents cloud effects. Data for cloudy conditions are hence discarded, although these represent a large amount of observations and are situated in meteorologically active areas (McNally, 2002). This is not ideal from the standpoint of the data assimilation system, but it does reduce the danger of circular validation. In addition, radiosonde observations (i.e, the temperature profile) have been assimilated in the reanalyses. Thus it is not surprising that ERA-40 and ERA-Interim better reproduce the temporal variability of DLW relative to ISCCP and TIND.

For TIND, we inferred albedo by taking the ratio of upward to downward shortwave radiation. In TIND, there is a major difference between the snow-free and snow-covered period. For snow-covered conditions, an albedo decay scheme was adapted in VIC (Cherkauer et al. 2003), which imposes a decay process on albedo from the new snow value that is usually 0.85 in the pan-Arctic. This algorithm replaces the surface vegetation-based algorithm that is used for the snow-free period. For the days of year when there is no DSW, snow albedo was set to 0.85, a typical value for new snow. Errors in albedo from ERA-40, ERA-Interim and ISCCP are substantial as described above. ECMWF uses an albedo map, which is from a background yearly climatology with fixed values between 0.07 and 0.80 for land whenever snow occurs, but the albedo for snow-free vegetation is constant throughout the year, based on surface vegetation classification (Gibson et al. 1999). In the ECMWF model, this change in the calculation of albedo over the boreal forests in the presence of snow, which reduces the deep snow albedo from 0.80 to 0.20, greatly affects the albedo estimates in ERA40 and ERA-Interim at high northern latitudes (Viterbo and Betts, 1999). For ISCCP, errors in albedo caused by uncertainties in surface temperature and emissivity are described in Zhang et al. (2007). In making comparisons such as those reported above, it is important to recognize that direct albedo measurements only take into account a very small area (a few square meters below the instrument), and are not necessarily representative for large grid cells, which also include other surface types (e.g. forests).

2.3.2. Regional-Scale Comparisons

2.3.2.1 Temporal Variability

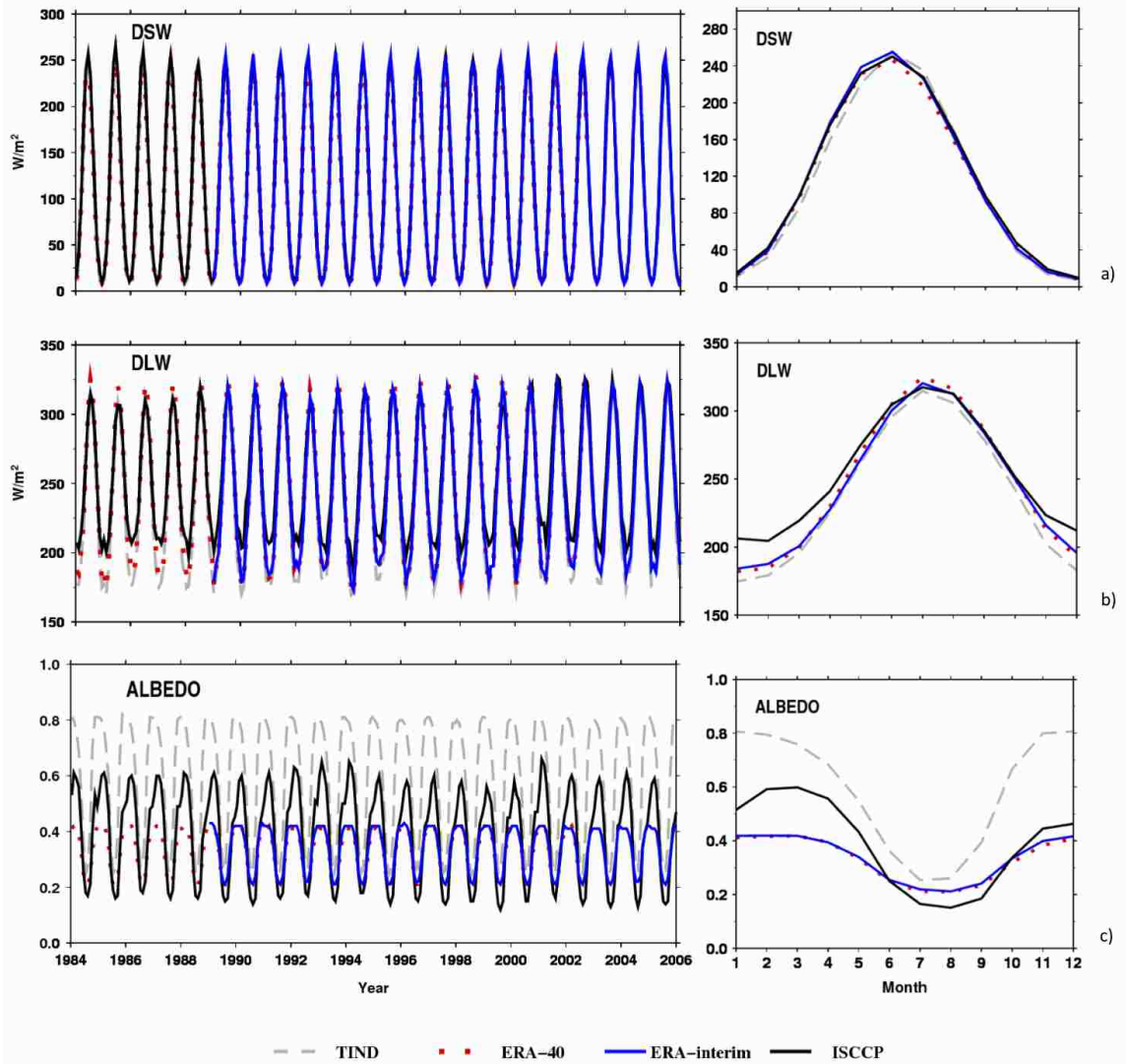


Figure 2.4 Monthly time series (left-hand) and mean seasonal cycle (right-hand) of a) DSW; b) DLW; c) albedo from TIND (dashed), ERA-40 (dotted), ERA-Interim (blue solid), and ISCCP (black solid) for the pan-Arctic land region. All the units where applicable are W/m^2 .

Figure 2.4 shows the monthly time series and mean seasonal cycles of DSW, DLW, and albedo from TIND, ERA-40, ERA-Interim, and ISCCP, averaged across the pan-Arctic land region. The DSW temporal distributions are quite similar in terms of interannual variations (left-hand side of Figure 2.4 (a)). Figure 2.4 (a) (right-hand side) compares the region-wide average seasonal DSW for TIND, ERA-40, ERA-Interim, and ISCCP. The seasonality of DSW is consistently represented by all four data sets.

Figure 2.4 (b) shows the monthly time series and mean seasonal cycle of DLW estimates from TIND, ERA-40, ERA-Interim, and ISCCP. The DLW has similar monthly and seasonal variations among the four estimates, which are low during October to April and peak in July. DLW from ERA-40, ERA-Interim and TIND are more similar to each other than is ISCCP, which is consistently higher than other estimates from November through April for the entire period from 1984 to 2006 (ERA-40, 1984-2002; ERA-Interim, 1989-2006). The overestimation of DLW during the snow season results in a weak mean seasonal cycle for ISCCP.

Monthly time series and seasonal means of albedo from the four datasets in Figure 2.4(c) differ considerably. Albedo values used with TIND are closer to observations over the pan-Arctic area as shown in Figure 2.3(c) except that albedo from June to September is overestimated. Due to the large DSW in this period, the biases in net shortwave radiation from TIND are bigger than other months during the year. In contrast, the ERA-40 and ERA-Interim albedos are much better in the summer time, but they underestimate by up to 0.4 during the snow season as compared to the TIND model. The snow albedo from

ISCCP is higher than the reanalysis products while it is still about 0.1 lower than the TIND values. In addition, the snow albedo from ISCCP for January seems abnormally low as shown in Figure 2.4(c) (right-hand side).

2.3.2.2 Spatial Variability

Given the relatively good performance of the reanalysis products in comparison with in situ observations, we choose ERA-40 as the reference (the choice of ERA-40 relative to ERA-Interim is somewhat arbitrary, as their performances were comparable) to examine the spatial variability of the remaining model and satellite products (ERA-Interim, TIND and ISCCP).

2.3.2.2.1 DSW

Figure 2.5 shows the spatial distribution of seasonal mean DSW from ERA-40, and the difference between ERA-40 and TIND, ERA-Interim and ISCCP for winter (DJF), spring (MAM), summer (JJA), and autumn (SON) averaged over the entire period from 1984 to 2006 (ERA-40, 1984-2002; ERA-Interim, 1989-2006). DSW peaks in summer for all datasets over most land areas, as expected. Because the ERA-40 and ERA-Interim values are both taken from the ECMWF NWP model, the spatial patterns of seasonal average DSW are quite similar for all seasons. Relatively speaking, differences in summer DSW between ERA-Interim and ERA-40 are larger than in other seasons. However, the mean bias is still less than 6% (15 W/m^2) of DSW summer mean. TIND and ISCCP agree reasonably well with the ERA-40 reanalysis both in the timing and magnitude of the

seasonal pattern of DSW. In general, the TIND seasonal mean DSW has larger bias than does ISCCP. In Figure 2.5, spring and summer DSW in TIND is persistently high over eastern and northern Eurasia, northern Alaska and Canada, Hudson Bay, the Canadian Archipelago, and Greenland. DSW in TIND comes from a relationship with the daily temperature range described by Thornton and Running (1999). This may in part be related to issues with the polar day length since the Thornton and Running algorithm assumes that the diurnal temperature variability breaks down during the part of the year when the sun does not set. In addition, this algorithm does not incorporate any information about diurnal patterns of cloud cover, which may strongly affect DSW diurnal patterns in spring and summer. For ISCCP, the area over which DSW is high (relative to ERA-Interim and ERA-40) in spring and summer is similar to that for TIND, but is much smaller in eastern and northern Eurasia. For the rest of the pan-Arctic, spring and summer DSW for TIND and ISCCP is underestimated relative to ERA-40. In winter and autumn, the differences in seasonal means relative to ERA-40 are small for both TIND and ISCCP.

Although the distribution of seasonal mean DSW is generally consistent between ERA-40 and other data sets, significant differences are evident in some areas. TIND, ERA-Interim and ISCCP tend to suggest lower DSW than ERA-40 along the Arctic coast, while they overpredict the seasonal mean DSW in summer and autumn for southern Alaska and Canada and in all seasons for southern and southwestern Eurasia and the Norwegian coast. In Figure 2.5, there is obvious latitude ringing. This may be a result of

the latitudinal gradient in DSW and further enhanced by the coarse spatial resolution of the gridded data sets.

2.3.2.2.2 DLW

The spatial distributions of seasonal average DLW from ERA-40, and the difference between ERA-40 and TIND, ERA-Interim and ISCCP are shown in Figure 2.6. In general,

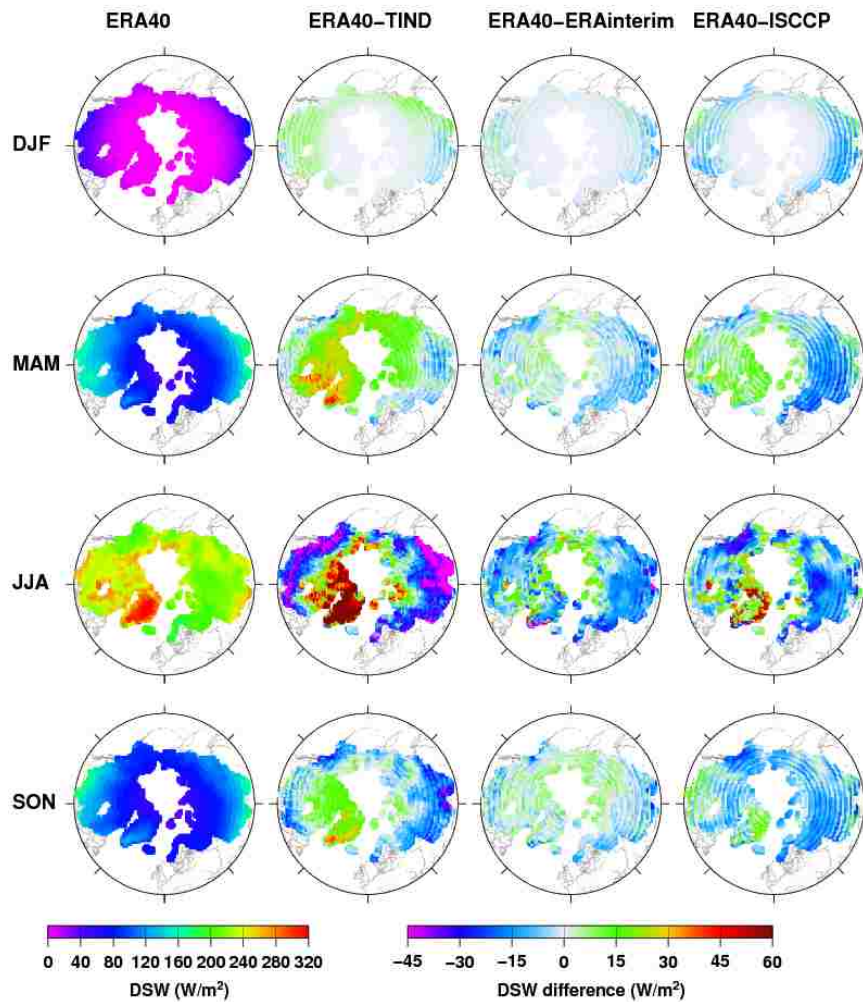


Figure 2.5 Spatial distribution of seasonal mean DSW from ERA-40, and the difference between ERA-40 and TIND, ERA-Interim, and ISCCP for the pan-Arctic land area.

the DLW bias in the winter and spring for TIND, ERA-Interim and ISCCP is higher than in summer and autumn over most land areas of the pan-Arctic. Similar to DSW, the spatial pattern of seasonal mean DLW between ERA-40 and ERA-Interim is also consistent through all the seasons. TIND and ISCCP agree reasonably well with ERA-40 but show different behaviors. For TIND, winter and spring DLW is persistently higher than ERA-40 over the most southern Eurasia, Hudson Bay, the Canadian Archipelago and Greenland. For the rest of the land areas, TIND always underestimates DLW compared to ERA-40. In the summer and autumn, differences between ERA-40 and TIND are positive over the entire pan-Arctic except Greenland. For ISCCP, the overestimation areas in the summer and autumn are similar to TIND, but are relatively larger, especially in Greenland. It should be noted that winter and spring DLW from ISCCP is significantly higher than from ERA-40 for almost all the land areas except southwestern Eurasia and the Norwegian coast. This is consistent with our findings in section 2.3.1.

2.3.2.2.3 Albedo

The spatial distribution of seasonal mean albedo from ERA-40, and the differences between ERA-40 and TIND, ERA-Interim and ISCCP are shown in Figure 2.7. Similar to

DSW and DLW, differences in mean seasonal albedo between ERA-40 and ERA-Interim are small while the positive and negative biases are evenly distributed over the entire pan-Arctic through all the seasons. In general, the bias of autumn, winter and spring albedo

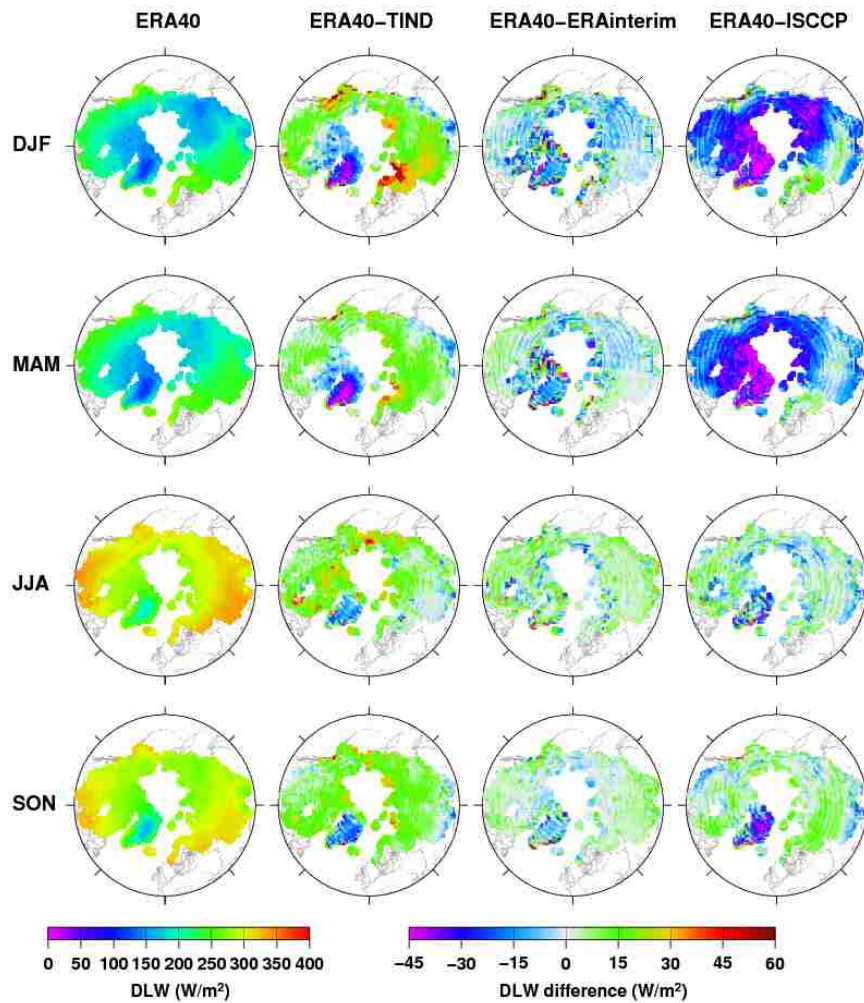


Figure 2.6 Spatial distribution of seasonal mean DLW from ERA-40, and the difference between ERA-40 and TIND, ERA-Interim, and ISCCP for the pan-Arctic land area.

for TIND and ISCCP is higher than in summer over most land areas due to the effect of snow. As described in section 2.3.1, TIND matches observed albedo well except in

summer, while the reanalysis products do well only for the summertime. For TIND, autumn, winter and spring albedo is persistently higher than for ERA-40 over most of the pan-Arctic domain, with maximum bias up to 0.8 in the mountains of Eurasia and North America. In the summertime, the difference between ERA-40 and TIND is much smaller. As shown in section 2.3.1, ISCCP albedo only shows a good match with the others in spring. For ISCCP, the overestimation areas in winter and spring are similar to the TIND, but relatively smaller.

2.3.2.3 Latitudinal Variability

Figure 2.8 shows the annual means of DSW, DLW, and albedo as a function of latitude for the pan-Arctic from TIND, ERA-40, ERA-Interim and ISCCP. The annual mean DSW from TIND, ERA-40, ERA-Interim and ISCCP shows similar latitudinal patterns, which in general are at a maximum in the 45-50°N band, and then decreases sharply with latitude poleward. Based on comparisons with in situ observations in section 2.3.1, the reanalysis products (ERA-40 and ERA-Interim) are more accurate than the others over the pan-Arctic. In Figure 2.8 (a), the TIND model shows a similar pattern to the reanalysis products. However, it overestimates the annual mean DSW relative to the reanalyses at the lowest latitudes up to 60-65°N, where they are almost equal, and then underestimates it at higher latitudes. For ISCCP, DSW is much closer to the reanalysis products with biases, which are mostly less than 10 W/m².

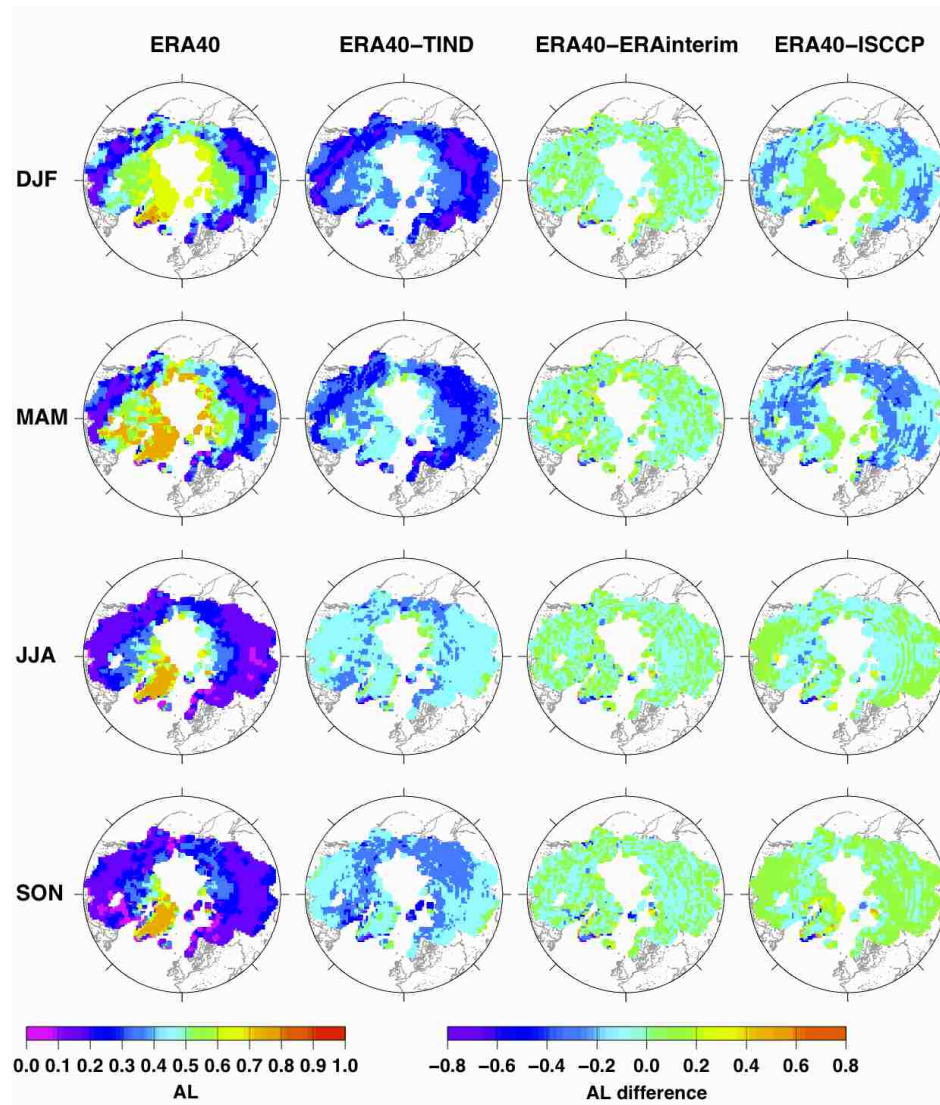


Figure 2.7 Spatial distribution of seasonal mean albedo from ERA-40, and the difference between ERA-40 and TIND, ERA-Interim, and ISCCP for the pan-Arctic land area.

As shown in Figure 2.8 (b), the annual mean of DLW from different datasets decreases gradually with latitude from 45-50°N to 80-85°N. TIND is mostly consistent with the reanalysis products with differences less than 10 W/m². Although ISCCP follows similar patterns to the other three estimates, it considerably overestimates annual mean DLW and

the bias relative to the other three data sets generally increases (at least in a relative sense) with latitude.

Figure 2.8 (c) shows that the annual mean albedo from TIND, ERA-40, ERA-Interim and ISCCP increases with poleward latitude. Based on the comparisons with point observations in section 2.3.1, the albedo from the TIND off-line simulation is more accurate than the other estimates. From 45-50° N to 60-65° N, the annual mean albedo from the reanalysis products (ERA-40 and ERA-Interim) has large differences relative to TIND and ISCCP. The biases are up to 0.3 compared to TIND and 0.2 compared to ISCCP. However, the annual mean albedo from ERA-40 and ERA-Interim is almost equal to ISCCP and the difference between TIND and the reanalysis products is much smaller from 65-70° N. This suggests that the need to improve the albedo for ERA-40 and ERA-Interim is greatest for latitudes from 45° N to 65° N.

2.3.3 Trend Analysis

To examine long-term trends in observed DSW, we used the non-parametric Mann-Kendall trend test (Mann 1945) for trend significance, and the Hirsch et al. (1982) method to estimate trend slope. Trend tests were performed for annual and seasonal

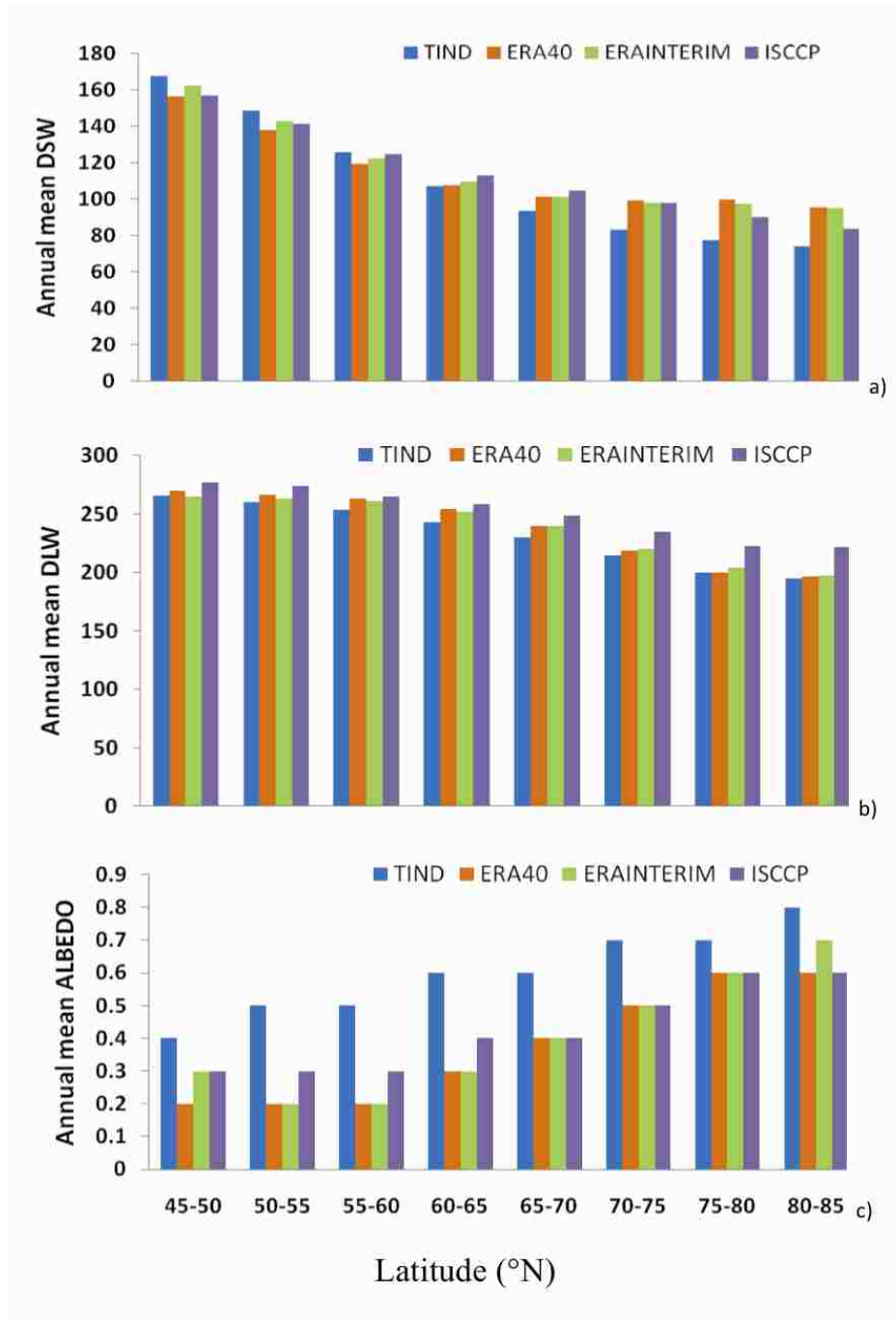


Figure 2.8 Annual mean a) DSW, b) DLW, and c) albedo versus latitude from TIND, ERA40, ERA-Interim, and ISCCP for the pan-Arctic.

(Winter: DJF, Spring: MAM, Summer: JJA, Fall: SON) DSW at 12 GEBA stations with records spanning the period from the 1950s and 1960s to post-2000. A 95% significance level (two-sided test) was specified. Table 2.4 shows that eight stations have decreasing trends of which four are significant, while three stations have increasing trends and two of them are significant for annual DSW.

Station 1413 (Lulea, Sweden) with the longest record from 1965 to 2006 has no statistically significant trend. Here we tested DSW trend significance and slope for a range of start and end years using the method described in Adam and Lettenmaier (2008). The periods were selected systematically: for the start year 1965, a set of end years was selected between 1986 and 2005. Therefore, trends were tested for the following periods: 1965-1986, 1965-1987, 1965-1988, ..., 1965-2002, 1965-2003, 1965-2004, and 1965-2005. For the start year 1986, a set of end years was also selected between 1995 and 2006. Therefore, trends were tested for the following periods: 1986-1995, 1986-1996, ..., 1986-2004, and 1986-2006. As shown in Figure 2.9 (a), the periods from 1965 to 1986 through 2005 predominantly show decreasing trends while increasing trends dominate in the periods from 1986 to 1995 through 2006. Thus, the absence of trend for station 1413 for 1965-2006 results from cancellation of upward and downward trends.

Similar trend tests were applied to the other stations. Figure 2.9 (b) shows that DSW increases significantly at station 2104 (Oestersund, Sweden) for the period from 1983 to

Table 2.4 Trend analysis details for GEBA annual and seasonal DSW at 12 stations over the pan-Arctic land region. The significance level (p -value) achieved by two-sided Mann-Kendall test.

GEBA ID	Station Name	Start Year	End Year	Annual		Winter		Spring		Summer		Fall	
				p	Trend	p	Trend	p	Trend	p	Trend	p	Trend
396	Edmonton	1950	1987	<0.05	-0.16	<0.01	-0.20	---	-0.40	---	-0.15	<0.05	-0.27
442	Whitehorse	1971	1987	<0.01	-0.47	<0.05	-0.25	<0.01	-0.83	---	-0.67	---	-0.15
1413	Lulea	1965	2006	---	0.00	---	-0.01	---	-0.07	---	-0.11	---	0.05
2104	Oestersund	1983	2005	<0.01	0.38	---	0.00	---	0.32	---	0.62	---	0.27
2492	Ekaterinburg	1964	1994	<0.05	-0.21	---	-0.03	---	-0.21	---	-0.44	---	-0.23
930	Turukhansk	1964	1995	---	-0.04	---	-0.04	<0.05	-0.44	---	0.29	---	0.03
931	Olimyakon	1964	1992	<0.01	-0.36	---	-0.02	---	-0.41	<0.01	-0.95	---	-0.06
932	Yakutsk	1964	1991	---	-0.07	---	-0.05	---	-0.25	---	-0.08	---	0.10
933	Aleksandrovskoe	1964	1993	<0.05	0.30	---	0.00	---	0.17	<0.05	0.72	---	-0.07
936	Sverdlovsk	1964	1990	---	-0.01	---	0.00	---	-0.30	---	0.14	---	-0.18
937	Omsk	1964	1995	---	0.04	---	0.00	---	0.13	---	0.13	---	0.03
940	Irkutsk	1964	1993	<0.1	-0.23	---	0.00	---	-0.33	---	-0.61	---	-0.18

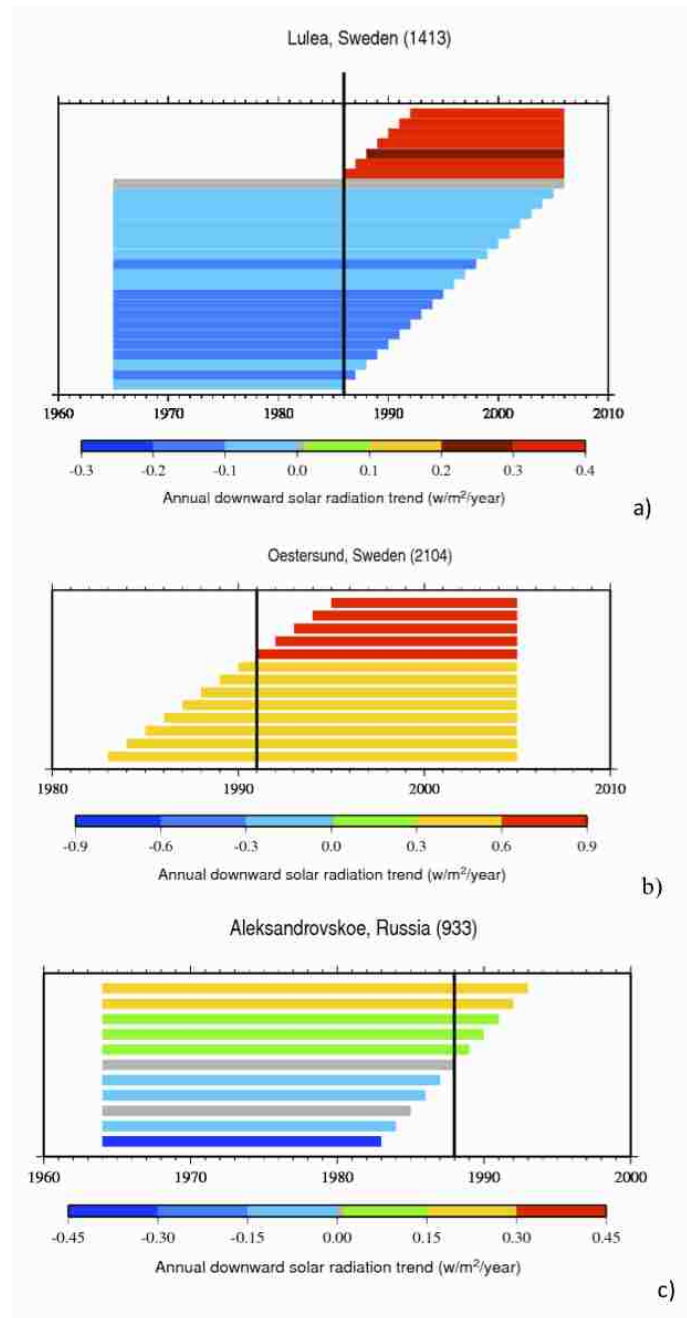


Figure 2.9 GEBA annual DSW trend plots for all periods with trends significant at 95% using the Mann-Kendall non-parametric test at a) Lulea, Sweden, b) Oestersund, Sweden, and c) Aleksandrovskoe, Russia. Each line represents a period for which the trend slope is given by the color of the line and the period length is given by the length of the line (starting and ending at the start and end of the period, respectively).

2005, and that this trend increases significantly after 1991. In addition, for station 933 (Aleksandrovskoe, Russia), the decreasing trends start to shift to increasing trends when extending the time series beyond 1988 as shown in Figure 2.9 (c). Trend slopes as shown in Figure 2.9 (statistical significance not shown, though all trend values plotted are significant to the 95% confidence level) taken over a range of start and end dates showed that there is a turning point between 1985 and 1990 at these stations. Before that, a dimming period exists, whereas brightening occurred thereafter, in line with the other recent studies (e.g. Wild 2009).

To get a sense of whether the above data sets could reproduce the GEBA trends, we analyzed DSW values from TIND, ERA-40, ERA-Interim and ISCCP for the same grid cells within which the GEBA observations lie. Due to data limitations, we only analyzed trends for the station 1413 and station 2104 grid cells. To produce a full record for the reanalysis products, we merged ERA-40 and ERA-Interim into a new time series called ERA-40-Interim by adjusting the segments (2002-2009) by the ratio of the long-term monthly means in the overlap period. As shown in Table 2.5, all products show similar brightening trends with the observed data at Station 1413 for the period 1984-2006 although they are not statistically significant. At station 2104, there are slightly positive trends with no significance from ERA-40 and ERA-40-Interim but a strong positive trend ($p < 0.025$) from the observations over the period of 1984–2005, while all the other products had negative trends.

Since DSW is a major energy source for the melt processes of snow cover in the pan-Arctic, a potential consequence of the solar dimming/brightening phenomenon might be evidenced by changes in snow cover extent. According to the recent Intergovernmental Panel on Climate Change's (IPCC's) Fourth Assessment Report (AR4; Solomon et al. 2007), Northern Hemisphere snow cover extent underwent no major changes between the 1930s and 1980s, but then sharply declined from the 1980s to 2000 (Brown 2000). The observed changes in DSW are consistent with the decline in Northern Hemisphere snow cover since the late 1980s (Wild 2009).

Table 2.5 DSW trend tests at Lulea (1413), Oestersund (2104) and corresponding grid cells from TIND, ISCCP, ERA-40, ERA-Interim, and ERA-40-Interim. The significance level (p -value) achieved by two-sided Mann-Kendall test.

Products \ Stations	Lulea (1413)			Oestersund (2104)		
	Years	p	Trend	Years	p	Trend
OBS	1984-2006	<0.025	0.32	1984-2005	<0.025	0.32
TIND	1984-2006	---	0.02	1984-2005	---	-0.03
ISCCP	1984-2006	---	0.01	1984-2005	---	-0.16
ERA-40	1984-2001	---	0.14	1984-2001	---	0.08
ERA-Interim	1989-2006	---	0.01	1989-2005	---	-0.19
ERA-40-Interim	1984-2006	---	0.16	1984-2005	---	0.03

2.4. Summary and Conclusions

We have evaluated different surface radiative flux data sets over the pan-Arctic land region, with a focus on variability and trends. More specifically, DSW, DLW and albedo were analyzed from a temperature index scheme (TIND), a satellite product (ISCCP), and two global reanalysis products (ERA-40 and ERA-Interim). Our main findings are:

As compared with the in situ measurements, the reanalysis products provide better estimates of the DSW diurnal cycle than do the satellite product and temperature index scheme simulation. All data sets agree quite closely with the observations in terms of the mean seasonal cycles of surface DSW and DLW except ISCCP, which consistently overestimates DLW in winter and spring, and has larger MAE (up to 50 W/m²) in DSW. The TIND mean seasonal cycle of albedo matches the observations well except during summer, while the reanalysis products do well only for the summertime and ISCCP only shows a good match in spring.

At the regional scale, all data sets have similar temporal patterns except for DLW in ISCCP and snow season albedo. In terms of dominant spatial variability, DSW and DLW fluxes show a similar latitudinal gradient for all data sets. However, the difference in albedo suggests a need of improvement for the reanalysis products.

Relative to the reanalysis products and satellite data, the VIC model is capable of providing surrogates for observations of surface energy fluxes, which offer the opportunity to investigate the roles of surface energy fluxes in snow cover changes. In

addition, a turning point was found in long-term trends at some GEBA stations in the mid-1980s. Before that, a dimming period exists with decreasing trends, whereas brightening occurred thereafter, which is consistent with the other recent studies (e.g., Wild, 2009). More work is needed to understand the corresponding impact on land surface hydrological fluxes, such as snow cover extent, however observed trends in high latitude snow cover extent appear to be at least approximately consistent with the DSW trends.

3. The Role of Surface Energy Fluxes in Pan-Arctic Snow Cover Changes

This chapter was published in *Environmental Research Letters* as:

Shi, X., P. Y. Groisman, S. J. Déry, and D. P. Lettenmaier, 2011: The role of surface energy fluxes in pan-Arctic snow cover changes. *Environ. Res. Lett.*, **6**, 035204.

3.1. Introduction

The pan-Arctic domain is one of the most sensitive regions on Earth to global climate change (Manabe and Stouffer 1994; Miller and Russell 2000; Holland and Bitz 2003; Serreze et al. 2009). As the largest single component of the cryosphere in terms of spatial extent (Armstrong and Brodzik 2001), snow cover variations in space and time have resulted in significant changes in the surface energy and water budgets over the pan-Arctic land region (Serreze et al. 2000; Peterson et al. 2002; Serreze et al. 2003; Yang et al. 2003; McClelland et al. 2006; Adam et al. 2007; Shiklomanov et al. 2007; Rawlins et al. 2010). However, the interpretation of changes in the areal extent of snow cover and its timing is complicated by the sparseness of in situ observations of surface radiative and turbulent fluxes, which are the most important variables affecting snow surface energy exchange processes (Cline 1997).

Previous studies have attempted to track energy balance changes associated with snow cover variations at the point scale in Finland (Kuusisto 1986; Koivusalo and Kokkonen 2002); New Zealand (Prowse and Owens 1982; Moore and Owens 1983); the southern Sierra Nevada region of California in the western United States (Marks and Dozier 1992), and at the basin scale in two regions of Alaska (Robinson 1986); the Red River Valley of North Dakota and Minnesota (Dyer and Mote 2002); Trail Valley Creek of northern Canada (Marsh and Pomeroy 1996; Pohl and Marsh 2006). However, few studies have examined the large-scale factors that would provide better understanding of the relative importance of snow surface energy balance components (Male and Granger 1981; Cline 1997; Leathers et al. 2004), in large scale snow cover changes, especially for the pan-Arctic land area. On the other hand, land surface models (e.g. Liang et al. 1994) have improved to the point that they may, in some cases, serve as surrogates for in situ observations. Off-line runs of these models provide sources for most or all terms in the snow surface energy balance and offer the opportunity to investigate the nature of the space-time variability of the snow surface energy budget (Betts et al. 2009; Troy et al. 2009; Shi et al. 2010).

In this paper, our main objective is to identify the individual role of surface energy fluxes in the snow surface energy balance and determine which are most responsible for observed changes in snow cover extent (SCE) of the pan-Arctic land region as shown in Figure 3.1. First, monotonic trends in satellite snow cover observations and

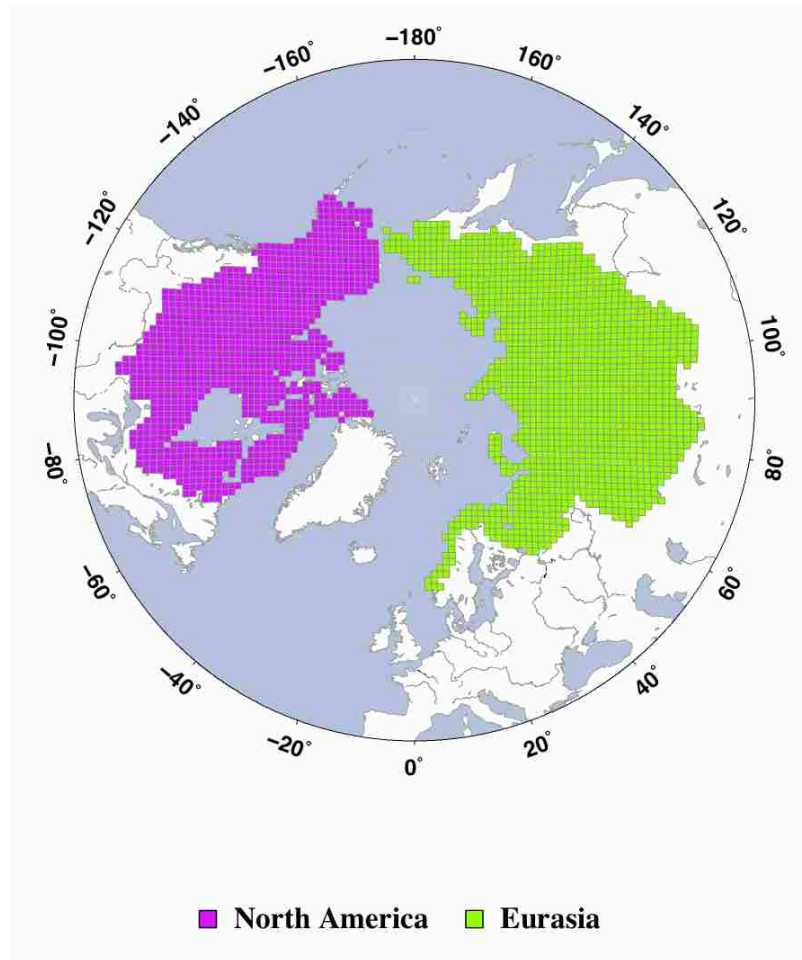


Figure 3.1. Study domain with 100 km resolution EASE grid mesh.

corresponding reconstructions generated by a land surface model are analyzed using a non-parametric trend test. Subsequently, the relationships between observed SCE and modeled surface radiative and turbulent fluxes are examined. In the final part of the paper, the relative importance of each component in the snow surface energy balance is estimated.

3.2. Data Sets

3.2.1. Snow Cover Extent Data

Observed seasonal values of SCE were extracted from the weekly snow cover and sea ice extent version 3 product for the Northern Hemisphere maintained at the National Snow and Ice Data Center (NSIDC), which combines snow cover and sea ice extent for the period from October 1966 through June 2007 (Armstrong and Brodzik 2007). The data set is based on weekly maps of continental SCE produced by the National Oceanic and Atmospheric Administration's (NOAA) National Environmental Satellite Data and Information Service (NESDIS) (Robinson et al. 1993; Frei and Robinson 1999), which were derived from digitized versions of manual interpretations of Advanced Very High Resolution Radiometer (AVHRR), Geostationary Operational Environmental Satellite (GOES), and other visible band satellite data. This satellite-based data set has been regridded to the NSIDC EASE-grid with a spatial resolution of 25 km. Our study is restricted to the period 1972-2006 because there are some missing charts between 1967 and 1971 (Robinson 2000). Although ending the time series in 2006 leaves out some exceptionally low Arctic spring SCE values in recent years (e.g. 2008-2010), the nonparametric statistical method we used (section 3.3.1) is robust to modest changes in the length of the record analyzed. In addition, Greenland is not included in the analyses as its snow cover is mainly perennial in nature (Déry and Brown 2007). Brown et al. (2010) have assessed this SCE record (commonly referred to as the NOAA weekly SCE record) in comparison to other available Arctic snow cover data sets. In general, their study, and others (Wiesnet et al. 1987; Robinson et al. 1993) have found that the NOAA

weekly SCE data set is reliable for continental-scale studies of snow cover variability. It has become a widely used tool for deriving trends in climate-related studies (Groisman et al. 1994; Déry and Brown 2007; Flanner et al. 2009; Derksen et al. 2010; Derksen and Brown 2011), notwithstanding uncertainties in some parts of the domain for certain times of the year, especially during springtime over northern Canada (Wang et al. 2005). A more recent update to the data set we used (NOAA snow chart climate data record (CDR)) is now available (Brown and Robinson 2011), but the differences between the new CDR and the data set we used at the pan-Arctic scale are small.

In this study, simulated SCE was reconstructed from 1972 to 2006 using the Variable Infiltration Capacity (VIC) model, which is a macroscale hydrologic model that solves the energy and water balance and represents ephemeral snow cover over a gridded domain (Liang et al. 1994, 1996). The off-line simulations from VIC used here are at a three-hour time step in full energy balance mode (meaning that the model closes its surface energy budget), forced with daily precipitation, maximum and minimum temperatures and wind speed through 2007 at a spatial resolution (EASE grid) of 100-km, constructed using methods outlined by Adam and Lettenmaier (2008). Precipitation and temperature were from gridded observations (Willmott and Matsuura 2009) and wind speed was from the NCEP/NCAR reanalysis (Kalnay et al. 1996). Precipitation was adjusted for gauge undercatch and orographic effects as described by Adam and Lettenmaier (2003) and Adam et al. (2006). The snow parameterization in VIC represents snow accumulation and ablation processes using a two-layer energy and mass balance

approach (Cherkauer and Lettenmaier 2003) and a canopy snow interception algorithm (Storck et al. 2002; Andreadis et al. 2009) when an overstory is present. In the VIC model, each grid cell is partitioned into five elevation (snow) bands, which can include multiple land cover types (tiles). The snow model is then applied to each tile separately. When snow water equivalent is greater than 3 mm, VIC assumes that snow fully covers the tile. For each grid cell, the simulated snow cover extent is calculated as the area averages of the tiles.

3.2.2. Surface Energy Fluxes Data

Surface energy fluxes including downward shortwave radiation (DSW) and downward longwave radiation (DLW) were calculated by using a Temperature INDEX (TIND) scheme (Kimball et al. 1997; Thornton and Running 1999; Shi et al. 2010) wherein DSW and DLW are estimated based on relationships with the daily temperature range and daily average temperature, respectively. TIND has been commonly used in model intercomparison experiments such as the Project for Intercomparison of Land Parameterization Schemes (PILPS) (e.g. Pitman et al. 1999) and land surface models, such as VIC, for long-term simulations in cases when direct observations of energy fluxes are not available. Shi et al. (2010) evaluated DSW, DLW, and albedo computed in an off-line simulation of VIC embedded with TIND along with satellite data and global reanalysis products in comparison with in situ observations from the Global Energy Balance Archive (GEBA, Ohmura et al. 1989) and showed that these estimates compared well with observations over the pan-Arctic land region. Compared to the in situ

observations, the mean seasonal DSW from the European Centre for Medium-Range Weather Forecast (ECMWF) 40-Year Reanalysis (ERA-40), the ECMWF Interim Reanalysis (ERA-Interim), the International Satellite Cloud Climatology Project-Flux Data (ISCCP-FD), and the TIND-based scheme all have small biases ($\pm 20 \text{ Wm}^{-2}$). ERA-40, ERA-Interim and VIC DLW deseasonalized monthly anomalies had high correlations ($r = 0.96, 0.97$ and 0.91 , respectively) with GEBA observations whereas the correlation for the satellite-based (ISCCP-FD) product was somewhat lower. VIC deseasonalized monthly albedo had similar anomaly correlations with GEBA observations as did ERA-40, ERA-Interim and ISCCP-FD estimates.

Surface net radiation (SNR) was obtained as the sum of net shortwave (SW) and longwave radiative (LW) fluxes. SW at the snow surface is a measure of the difference between DSW and upward shortwave radiation (USW). USW is the product of DSW and snow surface albedo that is assumed to decay with age based on relationships published by the US Army Corps of Engineers (1956). LW is the sum of DLW emitted by the atmosphere and the fluxes emitted upward by a melting snow surface. DLW was estimated using Equations (2.42 and 2.43) from Bras (1990), which are based on air temperature and a function for emissivity from Tennessee Valley Authority (1972). The turbulent fluxes (sensible heat (SH) and latent heat (LH)) near the snow surface were produced using VIC's bulk aerodynamic approach, which is described in Andreadis et al. (2009). The algorithm requires snow surface temperature, which is calculated by VIC's snow algorithm, wind speed, surface air temperature, and relative humidity, the last three

of which are taken from the forcing data. Bulk transfer coefficients for momentum, heat, and water vapor were calculated initially for a neutral condition (Price and Dune 1976). Subsequently, the aerodynamic resistance in the presence of snow cover was corrected using the bulk Richardson's number for stable or unstable atmospheric conditions (Anderson 1976) as implemented in the VIC snow model (Andreadis et al. 2009). A similar approach has been successfully applied in various settings in Arctic environments (e.g. Hinzman et al. 1991; Woo et al. 1999; Boike et al. 2003). Other energy fluxes in the snow surface energy balance, such as ground heat and advective fluxes were also generated by VIC. VIC's energy flux convention is that surface energy fluxes towards the snow surface are defined as positive.

3.3. Results

3.3.1. Temporal Analyses of SCE and Surface Energy Fluxes

We defined April and May as spring, consistent with Groisman et al. (1994), and a three-month window centered on July was defined as summer. Observed and simulated SCE in spring and summer expressed as a snow-covered fraction were calculated for the Eurasia and North America study domains (Figure 3.1). Figure 3.2 shows North American and Eurasian snow cover fraction (SCF) during spring and summer from VIC and NOAA observations for the period of 1972-2006. The VIC simulations match the observed SCF over both North America and Eurasia quite well, with a mean absolute bias of 4.5% in spring and 0.6% for summer.

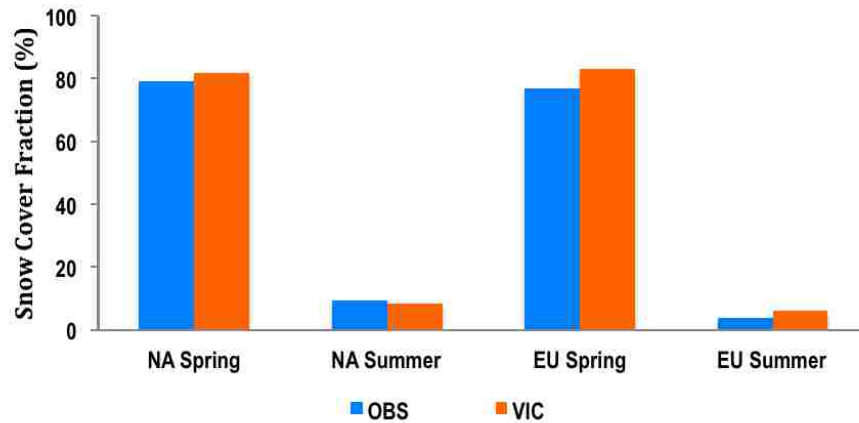


Figure 3.2. Spring and summer SCF over the pan-Arctic land areas in North America and Eurasia from VIC and satellite observations for the period of 1972-2006.

To examine long-term trends in SCE and surface energy fluxes, we used the non-parametric Mann-Kendall trend test (Mann 1945) for trend significance, and the Sen method (Sen 1968) to estimate trend slope. A 5% significance level (two-sided test) was specified. Trend tests were performed for seasonal SCE from VIC and satellite observations, and modeled radiative and turbulent fluxes averaged over the snow-covered portions of Eurasia and North America, respectively.

Table 3.1 summarizes trend test results for spring and summer SCE over North America and Eurasia from VIC and satellite observations. Strong negative trends were found in the NOAA satellite observations, during spring and summer in both North American and Eurasian sectors of the Arctic, which are statistically significant ($p < 0.025$) except that for Eurasia in spring the significance level is $p < 0.10$. VIC reproduces the same trend directions, with similar significance levels as compared with the satellite observations,

Table 3.1. Monotonic trends in spring and summer SCE over North America and Eurasia from the VIC model and satellite observations (OBS) in the pan-Arctic land region. The significance level (p -value) was calculated by two-sided Mann-Kendall test. (the unit of trend slope is in year⁻¹)

		VIC		OBS	
		$p <$	Slope	$p <$	Slope
North America	Spring	0.005	-0.0023	0.005	-0.0023
	Summer	0.025	-0.0012	0.005	-0.0037
Eurasia	Spring	0.10	-0.0006	0.10	-0.0011
	Summer	0.025	-0.0006	0.005	-0.0015

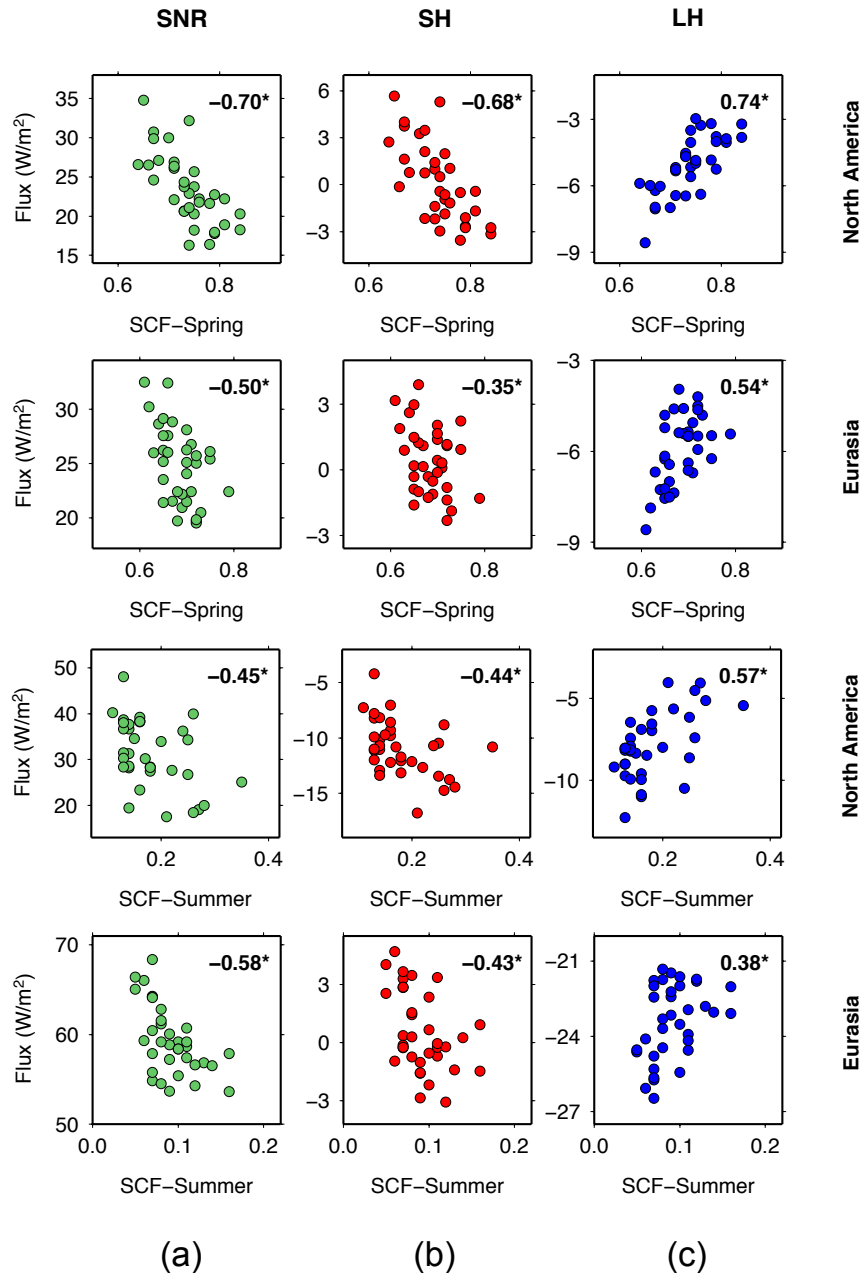


Figure 3.3. Scatterplots of surface energy fluxes: (a) SNR, (b) SH, and (c) LH versus satellite SCF over North America and Eurasia during spring and summer. The sign of star means that the correlation has a significance level $p < 0.025$.

for both continents in spring and summer. However, the VIC and observed trend slope magnitudes differ somewhat, especially in summer. The simulated trend slope in summer is about one third of that observed in North America, and 40% of that observed in Eurasia in summer. This discrepancy may be related to uncertainties in the NOAA SCE data set in July and August for both continents (Déry and Brown 2007) and in May and June for North America (Wang et al. 2005). Because the trend directions and statistical significances are consistent, we chose to include July and August to maintain completeness of the summer period.

The non-parametric Mann-Kendall trend test was also applied to the surface energy inputs to the snow surface, including SNR, SH and LH. Table 3.2 summarizes their trends over both continents during spring and summer. Trends were computed for seasonal mean fluxes over the snow-covered portion of the regions. Strong positive trends were found in SNR during spring and summer in North America and Eurasia. Similarly, SH fluxes also had statistically significant upward trends, except for Eurasia in spring for which the direction of change was positive, but the trend was not significant at $p < 0.10$. LH changes were mostly negative in spring to summer, but were statistically significant at $p < 0.10$ for North America in summer and Eurasia in spring.

3.3.2. Correlations between Observed SCE and Modeled Surface Energy Fluxes

The Pearson's product-moment correlation coefficient was used to assess relationships between satellite SCE and VIC-simulated surface energy fluxes. Figure 3.3 shows scatterplots of the surface energy fluxes (a) SNR, (b) SH, and (c) LH from VIC against

Table 3.2. Trend analyses for the terms related with SNR during spring and summer over snow-covered North America and Eurasia generated from VIC. The significance level (p -value) was calculated by two-sided Mann-Kendall trend test. (the unit of total change during the 35-year period for fluxes is W/m^2 ; the unit for T_{min} and T_{max} is $^{\circ}C$; no unit for Albedo and RH)

		SW		DSW		Albedo		DLW		Tmin		Tmax		RH	
		$p <$	Δ	$p <$	Δ	$p <$	Δ	$p <$	Δ	$p <$	Δ	$p <$	Δ	$p <$	Δ
North America	Spring	0.025	7.98	0.01	-3.83	0.01	-0.04	0.05	5.68	0.05	1.48	0.05	1.27	0.025	-2.41
	Summer	0.05	9.45	--	0.42	0.025	-0.06	0.005	2.86	0.025	0.72	0.20	0.46	--	0.96
Eurasia	Spring	0.05	5.50	--	0.16	0.025	-0.03	0.025	4.83	0.05	1.06	0.05	1.30	0.01	2.56
	Summer	0.005	8.31	--	0.12	0.005	-0.04	0.005	3.92	0.005	0.74	0.005	0.90	0.005	3.50

observed SCF over North America and Eurasia in spring and summer. The correlations of surface energy fluxes with SCF as shown in Figure 3.3 are all statistically significant at $p < 0.025$ (two sided test). The negative sign indicates that SNR and SH have opposite change directions with SCF. SNR has a relatively stronger relationship with SCF than SH, especially in Eurasia. For LH, the correlations are positive and are stronger in North America than in Eurasia.

3.3.3. Role of Surface Energy Fluxes in Snow Cover Changes

In general, the energy balance at a snow surface includes net radiative fluxes, sensible and latent heat fluxes, ground heat fluxes, and the energy transfer due to rain on snow. Over the pan-Arctic, the ground heat flux is a small component of the energy balance of a melting snowpack compared with radiative and turbulent heat fluxes. Therefore, its effects on total snowmelt can safely be ignored (Gray and Prowse 1993). Similarly, rain on snow has an important influence on the water retention characteristics of snow and water movement in the pack but is of minor importance compared with other energy fluxes (Male and Granger 1981). Surface energy fluxes towards the snow surface are defined as positive, therefore the net radiative and sensible heat fluxes usually have positive sign and supply the energy available for snowmelt. Latent heat fluxes are directed away from the snow surface and reduce the melt energy. However, it was not clear which individual component(s) of the snow surface energy budget dominates the significant spring and summer SCE recession since 1972 as shown in Table 3.1. Therefore, we

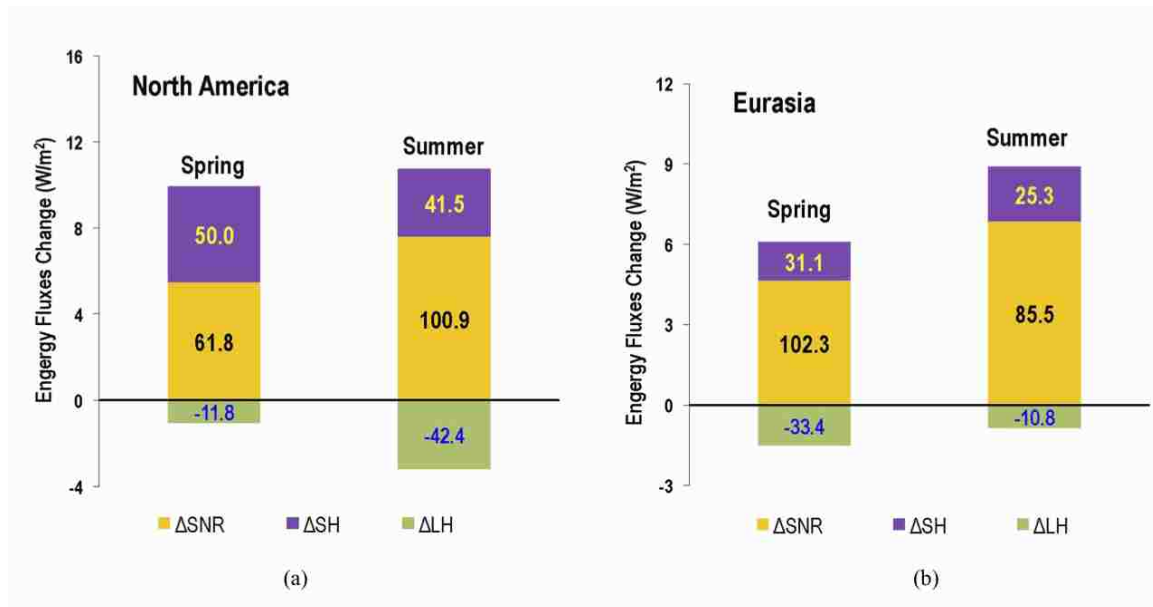


Figure 3.4. Relative role of spring and summer surface energy fluxes averaged only over snow-covered (a) North America and (b) Eurasia.

calculated the increment due to monotonic trends in SNR, SH and LH over the 35-year period as ΔSNR , ΔSH and ΔLH in order to determine the role of each term in the observed downward trends of SCE.

Figure 3.4 shows the relative role of surface energy fluxes averaged over the snow-covered portions of North America and Eurasia in spring and summer. It is apparent that ΔSNR is the dominant energy source in both spring and summer, accounting for between 61.8% and 102.3% of the energy available for snow cover changes. The contribution of ΔSH plays a secondary role (from 25.3% to 50.0%). ΔLH is always opposite in sign with ΔSH and ΔSNR and almost completely cancels ΔSH in North America during summer and Eurasia in spring. However, ΔLH has a smaller absolute value than ΔSH at other

times, such as in North America during spring (-11.8%) and Eurasia in summer (-10.8%). Therefore, we conclude that ΔLH has a minor influence on pan-Arctic snow cover changes compared with ΔSNR and ΔSH .

Figure 3.5 summarizes the latitudinal variations in spring and summer surface energy fluxes over North America and Eurasia. Basically, ΔSNR has a latitudinal pattern, which in general is at a maximum in the lower latitudinal band, and then decreases with latitude poleward. Compared with ΔSNR , ΔLH shows a similar pattern with a negative sign in most cases. However, it sharply decreases to zero at higher latitudes. In Eurasia during summer, it even has a positive sign for the bands 70-75° N and 75-80° N.

Corresponding to the patterns in ΔSNR and ΔLH , ΔSH is variable depending on the seasons and latitudinal bands. As shown in Figure 3.5(a), the contribution of ΔSH is much larger than ΔSNR for the 45-50° N latitudinal band in North America, reaching 78% of the total energy attributable to SCE changes. Thereafter, this contribution decreases gradually with latitude to the 70-75° N band. At 75-80° N and 80-85° N, ΔSH turns negative. In summer, ΔSH over North America is effectively canceled by ΔLH with a negative residual from 55-60° N to 70-75° N and a positive one for 75-80° N and 80-85° N. For Eurasia, ΔSH does not follow the same pattern as for North America. Although ΔSH in Eurasia is about half of ΔSNR for the latitudinal bands 45-50° N and 50-55° N during spring, its effect over the entire domain as shown in Figure 3.4(b) is small because of the small contribution between 55-60° N and 65-70° N. In summer, the pattern was

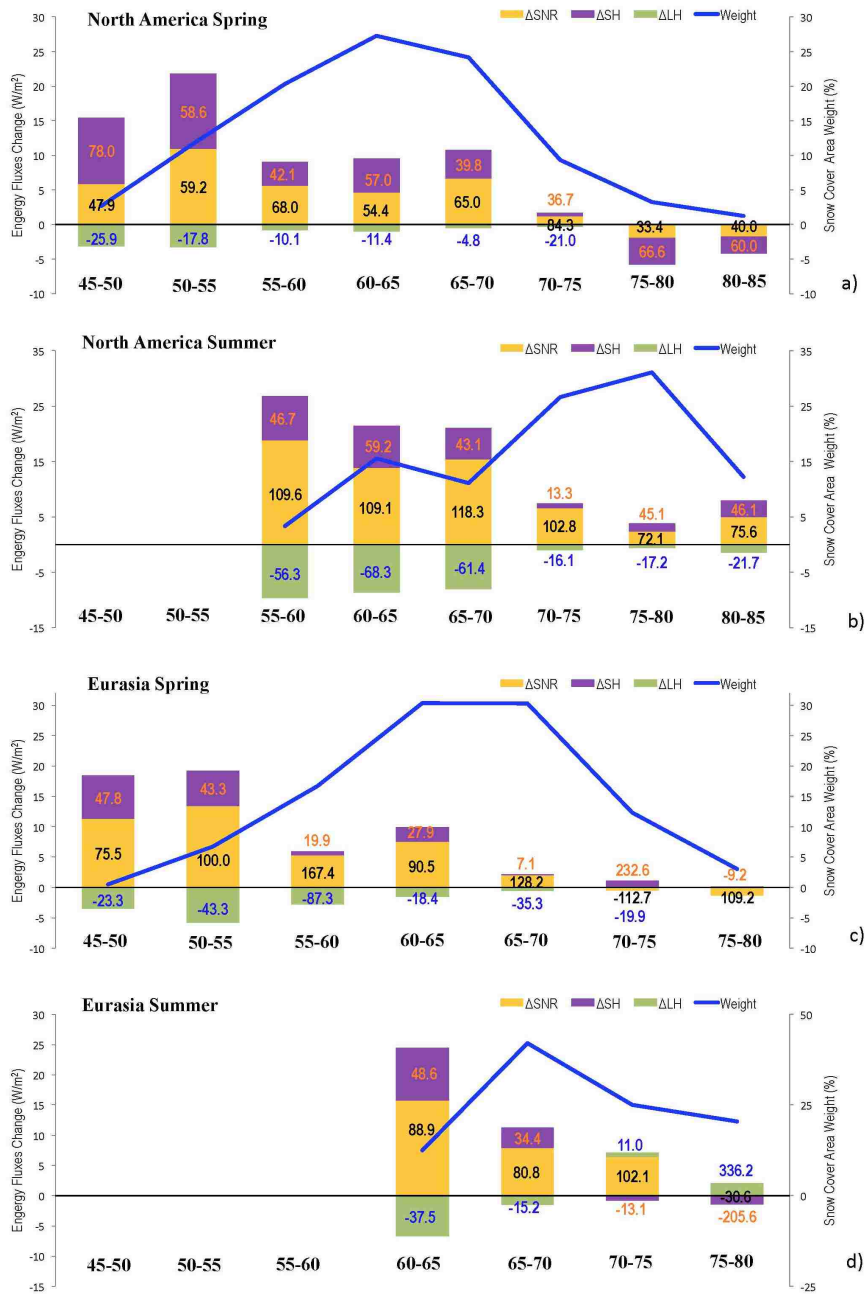


Figure 3.5. Latitudinal profiles of the changes in spring and summer surface energy fluxes over North America and Eurasia snow covered areas. The blue line shows the weight (fraction of snow cover in each latitudinal band).

mainly dominated by the 65-70° N latitudinal band in Figure 3.5(d) because of its area weight (up to 47.4%).

3.4. Summary and Discussion

By exploring long-term trends in satellite observations of SCE, we have shown that North American and Eurasian snow cover over the pan-Arctic declined significantly in spring and summer for the period 1972-2006. Furthermore, long-term means of seasonal SCE and their trend directions are reproduced by the VIC model, which allowed us to diagnose the causes of the observed trends. We have also shown that surface radiative and turbulent heat fluxes simulated in VIC have strong correlations with observed SCE. We find that positive trends in SNR are mostly associated with the observed and model-derived SCE trends. Modeled LH and SH trends associated with warming mostly cancel, except for North America in spring, and to a lesser extent for Eurasia in summer, when the SH contribution to the SCE trends remains substantial. Our results indicate that Δ SNR is the primary energy source and Δ SH plays a secondary role in changes of SCE. Compared with Δ SNR and Δ SH, Δ LH only has a minor influence on pan-Arctic snow cover changes.

Changes in sensible and latent heat fluxes are mostly dominated by increases in pan-Arctic surface air temperature, which have risen at a rate almost twice as large as the global average in recent decades (Lugina et al. 2006; Serreze and Francis 2006; Bekryaev et al. 2010). As shown in Table 3.3, the increases in SNR are mainly associated with increased SW and increased DLW due to warmer atmospheric temperature, whereas

Table 3.3. Trend analyses for the terms related with SNR during spring and summer over snow-covered North America and Eurasia generated from VIC. The significance level (p -value) was calculated by two-sided Mann-Kendall trend test. (the unit of total change during the 35-year period for fluxes is W/m^2 ; the unit for T_{min} and T_{max} is $^{\circ}C$; no unit for Albedo and RH)

		SW		DSW		Albedo		DLW		Tmin		Tmax		RH	
		$p <$	Δ	$p <$	Δ	$p <$	Δ	$p <$	Δ	$p <$	Δ	$p <$	Δ	$p <$	Δ
North America	Spring	0.025	7.98	0.01	-3.83	0.01	-0.04	0.05	5.68	0.05	1.48	0.05	1.27	0.025	-2.41
	Summer	0.05	9.45	--	0.42	0.025	-0.06	0.005	2.86	0.025	0.72	0.20	0.46	--	0.96
Eurasia	Spring	0.05	5.50	--	0.16	0.025	-0.03	0.025	4.83	0.05	1.06	0.05	1.30	0.01	2.56
	Summer	0.005	8.31	--	0.12	0.005	-0.04	0.005	3.92	0.005	0.74	0.005	0.90	0.005	3.50

emitted upward longwave fluxes do not change much as the snowpack temperature is mostly isothermal during the melt period. Strong upward trends in SW mostly result from statistically significant decreasing trends in snow surface albedo, while the contribution from increased DSW trends is minor (<5%) except for North America during spring when DSW decreases. VIC was forced by DSW calculated using the method of Thornton and Running (1999) based on the daily temperature range and vapor pressure. Therefore, there is a decreasing DSW trend in Table 3.3 for North America during spring because daily minimum temperature (T_{\min}) has increased more rapidly than daily maximum temperature (T_{\max}) and the relative humidity (RH) has decreased in the mean time.

4. Relationships between Recent Pan-Arctic Snow Cover and Hydroclimate Trends

This chapter is in press in the *Journal of Climate* as:

Shi, X., S. J. Déry, P. Y. Groisman, and D. P. Lettenmaier, 2012: Relationships between recent pan-Arctic snow cover and hydroclimate trends. *J. Climate* (in press).

4.1. Introduction

Snow cover is an important climatic and hydrologic land surface variable. Its long-term variations serve as both indicators and controls of climate change over much of the Northern Hemisphere land area (Gray and Male 1981; Groisman et al. 1994; Frei and Robinson 1999; Robinson and Frei 2000). Therefore, spatial and temporal variations of snow cover across the Northern Hemisphere have attracted considerable scientific attention. Many studies have used the visible satellite imagery produced by the National Oceanic and Atmospheric Administration (NOAA) (Robinson 1993; Groisman et al. 1994; Frei and Robinson 1999; Serreze et al. 2000; Dye 2002; Stone et al. 2002; Brown et al. 2007; Déry and Brown 2007; Brown and Mote 2009; Zhao and Fernandes 2009; Brown et al. 2010; Choi et al. 2010; Derksen et al. 2010; Brown and Robinson 2011; Derksen and Brown 2011; Liston and Hiemstra 2011). Variations in snow cover extent (SCE) have been shown to have a significant effect on surface energy and mass

exchanges over the pan-Arctic land region (Serreze et al. 2000; Peterson et al. 2002; Serreze et al. 2003; Yang et al. 2003; McClelland et al. 2006; Adam et al. 2007; Shiklomanov et al. 2007; Rawlins et al. 2010). However, the interpretation of changes in SCE and its timing is complicated by the sparseness of in situ observations of key variables, such as surface radiative and turbulent fluxes, which affect snow surface energy exchange processes (Cline 1997), as well as other hydroclimate variables (e.g., precipitation and temperature) that also affect SCE (Jol et al. 2009).

Numerous studies have been conducted in an attempt to understand the relationships between SCE observations and the other hydroclimatic variables, such as surface radiation, precipitation, temperature, and river discharge. These studies have focused on a range of spatial scales, including the local scale at individual meteorological stations (Baker et al. 1992; Koivusalo and Kokkonen 2002; Stieglitz et al. 2003; Shi et al. 2009; Westermann et al. 2009), the regional scale over areas such as the Red River Valley of North Dakota and Minnesota (Dyer and Mote 2002) and Trail Valley Creek of northern Canada (Marsh and Pomeroy 1996; Pohl and Marsh 2006), and continental scale studies over North America or Eurasia (Voeikov 1889; Karl et al. 1993; Groisman et al. 1994; Clark et al. 1999; Déry et al. 2005; Bulygina et al. 2009; Tan et al. 2011). Few studies, however, have examined the large-scale factors that control the relative importance of snow surface energy balance components and help to diagnose the direct or indirect causes in large-scale snow cover changes (Male and Granger 1981; Cline 1997; Leathers et al. 2004; Dyer and Mote 2007; Shi et al. 2011), especially for the pan-Arctic land area.

Land surface models (e.g., Liang et al. 1994; Oleson et al. 2004) have improved to the point that they may, in some cases, serve as surrogates for in situ hydroclimatic observations. Off-line runs of these models can provide snow surface energy balance components and offer an opportunity to investigate the nature of spatial and temporal variability of snow cover changes (Betts et al. 2009; Troy et al. 2009; Shi et al. 2010, 2011).

In this paper, we follow three steps in our assessment of the relationships between recent pan-Arctic snow cover and hydroclimate trends during the late spring and early summer (April-June) period:

- 1) We evaluate whether a land surface model is able to reconstruct spatial and temporal changes of observed snow cover across the pan-Arctic land area;
- 2) We identify the individual role of modeled surface energy fluxes in the snow surface energy budget and determine which flux is most responsible for observed pan-Arctic snow cover changes; and,
- 3) We assess the relationships between snow cover observations and hydroclimatic indicators, and identify possible causes of snow cover changes over the pan-Arctic.

This work is an extension of Shi et al. (2011), in which a preliminary assessment was conducted on the role of surface radiative and turbulent fluxes in pan-Arctic snow cover changes during spring and summer. In section 4.2 of this paper, we describe observed and

modeled data sets on which the subsequent analyses are based. In section 4.3, we (a) use a non-parametric trend test to analyze monotonic trends in the satellite snow cover observations and in corresponding reconstructions generated by the land surface model; (b) examine correlations between SCE observations and surface energy fluxes generated from the land surface model; and (c) estimate the relative importance of each component in the snow surface energy balance. Section 4.3 ends with a discussion of possible causes of snow cover changes over the pan-Arctic. Concluding remarks are in section 4.4.

4.2. Data Sets

4.2.1. Observed and Modeled Snow Cover Extent Data

Observed monthly values of SCE were extracted from the weekly snow cover and sea ice extent version 3.1 product for the Northern Hemisphere (<http://nsidc.org/data/nsidc-0046.html>) maintained at the National Snow and Ice Data Center (NSIDC), which combines snow cover and sea ice extent for the period from October 1966 through June 2007 (Armstrong and Brodzik 2007). The data set is based on weekly maps of continental SCE produced by the NOAA's National Environmental Satellite Data and Information Service (NESDIS) (Robinson et al. 1993; Frei and Robinson 1999), which were derived from digitized versions of manual interpretations of Advanced Very High Resolution Radiometer (AVHRR), Geostationary Operational Environmental Satellite (GOES), and other visible band satellite data. This satellite-based data set has been regridded to the NSIDC EASE grid with a spatial resolution of 25 km by Armstrong and Brodzik (2007).

The SCE monthly means for each grid cell contain a binary value (one or zero). A one indicates 50% or greater probability of occurrence of snow, whereas zero means probability of occurrence was less than 50%. Our study is restricted to the period after 1972 since there are some missing charts between 1967 and 1971 (Robinson 2000). Although ending the time series in 2006 leaves out some exceptionally low Arctic spring SCE values in recent years (e.g., 2008-2010), the non-parametric statistical method we used (section 4.3.1) is robust to modest changes in the length of the record analyzed. In addition, we did not include Greenland in the analyses since its snow cover is mainly perennial in nature. Brown et al. (2010) have assessed this SCE record (commonly referred to as the NOAA weekly SCE record) in comparison to other available Arctic snow cover data sets. In general, their study and others (e.g., Wiesnet et al. 1987; Robinson et al. 1993) have found that the NOAA weekly SCE data set is reliable for continental-scale studies of snow cover variability. It has become a widely used tool for deriving trends in climate-related studies (Groisman et al. 1994; Déry and Brown 2007; Flanner et al. 2009; Derksen et al. 2010; Derksen and Brown 2011), notwithstanding uncertainties in some parts of the domain for certain times of the year, especially during summertime over northern Canada (Wang et al. 2005). A more recent update to the data set we used (NOAA snow chart climate data record, CDR) is now available (Brown and Robinson 2011), but the differences between the new CDR and the data set we used at the pan-Arctic scale are small (Shi et al. 2011).

We reconstructed SCE from 1972 to 2006 using the variable infiltration capacity (VIC) model, which is a macroscale land surface hydrologic model that solves the energy and water balance and represents ephemeral snow cover over a gridded domain (Liang et al. 1994, 1996). The off-line simulations from VIC used here were at a three-hour time step in full energy balance mode (meaning that the model closes its surface energy budget) forced with daily precipitation, maximum and minimum temperatures, and wind speed through 2007 at a spatial resolution (EASE grid) of 100 km. The forcing data were constructed using methods outlined by Adam and Lettenmaier (2008; hereafter AL2008) as described in section 4.2.2. The model simulations used calibrated parameters, such as soil depths and infiltration characteristics, from Su et al. (2005) for the period of 1979 to 1999 over the pan-Arctic drainage basins. The snow parameterization in VIC represents snow accumulation and ablation processes using a two-layer energy and mass balance approach (Andreadis et al. 2009) and a canopy snow interception algorithm (Storck et al. 2002) when an overstory is present. In the VIC model, each grid cell is partitioned into five elevation (snow) bands, which can include multiple land cover types (tiles). The snow model is then applied to each tile separately. When snow water equivalent is greater than 3 mm, VIC assumes that snow fully covers the tile. The 3 mm threshold was adopted from Su et al. (2005) and Adam and Lettenmaier (2008). For each grid cell, the simulated SCE is calculated as the area averages of the tiles. To set the initial conditions in VIC, we initialized the model with a 10-year (1962-1971) spin-up simulation.

4.2.2. Hydroclimatic Forcing Data

We forced VIC with the University of Washington (UW) extended gridded precipitation product (AL2008) for the period 1972-2006 over the pan-Arctic land region. Monthly precipitation in AL2008 was derived from the Arctic land surface precipitation gridded monthly time series version 1.03 from the University of Delaware (UDel), which is interpolated from in situ stations (see Willmott and Matsuura 2009). The sources of the station data include the Global Historical Climatology Network, the Atmospheric Environment Service in Environment Canada, the Russian Institute for Hydrometeorological Information, the Greenland Climate Network, the Automatic Weather Station Project, and the Global Surface Summary of Day. To improve the monthly precipitation estimates, the UDel product was adjusted by AL2008 to account for gauge undercatch since gauge-measured precipitation data may underestimate solid precipitation in winter by 10%-50% (Adam and Lettenmaier 2003). Furthermore, the Adam et al. (2006) corrections for orographic effects were applied. Finally, daily time series of precipitation were produced by rescaling the updated product of Sheffield et al. (2004) to match the monthly time series of precipitation from AL2008.

Monthly average maximum and minimum temperatures were created using observed monthly mean time series from the UDel product and the monthly diurnal temperature range from the Climatic Research Unit (CRU, Brohan et al. 2006) (CRUTEM3 dataset from <http://www.cru.uea.ac.uk/cru/data/temperature/>). As with the precipitation product, daily disaggregation for temperatures was performed using the method of AL2008. In addition, surface air temperature (SAT) anomaly data were also derived from CRU,

which are based on anomalies from the long-term mean temperature for the period 1961-1990 and are available for each month since 1850. The wind speed was obtained from the National Centers for Environmental Prediction–National Center for Atmospheric Research (NCEP–NCAR) reanalysis (Kalnay et al. 1996). Finally, all these data were regridded to the 100 km EASE grid using an inverse distance interpolation as implemented in Su et al. (2005) including the NOAA SCE observations that were aggregated from the 25 km product. The monthly mean time series of daily maximum temperature (T_{\max}), daily minimum temperature (T_{\min}) and wind speed (WS) were derived for the study domains similar to the precipitation field.

Surface radiative fluxes were calculated by using a Temperature INdex (TIND) scheme (Kimball et al. 1997; Thornton and Running 1999; Shi et al. 2010) wherein downward shortwave radiation (DSW) and downward longwave radiation (DLW) are estimated based on relationships with the diurnal temperature range (DTR) and daily average temperature, respectively. DLW is dependent on atmospheric water vapor pressure (VP), and cloud cover (CC) is also used in the calculation. TIND has been commonly used in model intercomparison experiments such as the Project for Intercomparison of Land Parameterization Schemes (PILPS) (e.g., Pitman et al. 1999) and to force land surface models, such as VIC, for long-term simulations in cases when direct observations of radiation fluxes are not available. In VIC, the snow surface albedo is assumed to decay with age based on relationships published by the US Army Corps of Engineers (1956). Shi et al. (2010) evaluated DSW, DLW, and albedo computed in an off-line simulation of

VIC embedded with TIND along with satellite data and global reanalysis products in comparison with in situ observations from the Global Energy Balance Archive (GEBA, Ohmura et al. 1989) and showed that TIND-based estimates compared well with observations over the pan-Arctic land region. Compared to in situ observations, the mean seasonal DSW from the European Centre for Medium-Range Weather Forecast (ECMWF) 40-Year Reanalysis (ERA-40), the ECMWF Interim Reanalysis (ERA-Interim), the International Satellite Cloud Climatology Project-Flux Data (ISCCP-FD), and the TIND-based scheme in VIC all have small to moderate (up to $\pm 20 \text{ W m}^{-2}$) biases. ERA-40, ERA-Interim and VIC DLW deseasonalized monthly anomalies had high correlations ($r = 0.96, 0.97$ and 0.91 , respectively) with GEBA observations whereas the correlation for the satellite-based (ISCCP-FD) product was somewhat lower. VIC deseasonalized monthly albedo had similar anomaly correlations with GEBA observations as did ERA-40, ERA-Interim and ISCCP-FD estimates (Shi et al. 2010).

Surface net radiation (SNR) was obtained as the sum of net shortwave (SW) and longwave (LW) radiative fluxes. SW at the snow surface is a measure of the difference between DSW and upward shortwave radiation (USW). USW is the product of DSW and snow surface albedo (ALB), which is assumed to decay with age as described by US Army Corps of Engineers (1956). LW is the sum of DLW emitted by the atmosphere and the fluxes emitted upward by a snow surface. DLW was estimated using Eq. (2.42) from Bras (1990), which is based on air temperature and a function for emissivity from Tennessee Valley Authority (1972). The turbulent fluxes (sensible heat, SH, and latent

heat, LH) near the snow surface were estimated using VIC's bulk aerodynamic approach, which is described in Andreadis et al. (2009). In this algorithm, bulk transfer coefficients for momentum, heat, and water vapor are calculated initially for neutral atmospheric boundary surface layer conditions (Price and Dunne 1976). Subsequently, the aerodynamic resistance in the presence of snow cover is corrected using the bulk Richardson's number for stable and/or unstable atmospheric conditions (Anderson 1976) as implemented in the VIC snow model (Andreadis et al. 2009). A similar approach has been successfully applied in various Arctic settings (e.g., Hinzman et al. 1991; Woo et al. 1999; Boike et al. 2003). Other surface energy-related variables, such as CC, DTR, and VP, were generated using TIND. The energy flux convention is that surface energy fluxes towards the snow surface are defined as positive.

4.3. Results and Discussion

Recent studies have shown that SCE over northern Canada becomes decoupled with air temperature anomalies in July (Wang et al. 2005; Brown et al. 2007). These results along with the recent findings of Robinson (personal communication) suggest that July and August snow cover time series may not be suitable for trend analysis (Déry and Brown 2007). Moreover, comparisons of the NOAA satellite snow cover observations in July and August with the Global Land Ice Monitoring System (GLIMS) database (<http://nsidc.org/glims/>) suggest that most of the July and August SCE in fact is associated with glaciers. Therefore, we focus on the period April through June.

4.3.1. Spatial and Temporal Variability of SCE

The spatial distribution of monthly mean SCE from April through June for 1972-2006 is shown in Figure 4.1 for North America and Eurasia. Observed and simulated long-term means of SCE expressed as area fractions were calculated for each month. The percentages on the map show the snow cover area fractions from VIC and the NOAA SCE data (hereafter NOAA) for each month over the 35-year period. From April through June, the VIC estimates are always higher than NOAA for both continents. The overestimation for Eurasia is somewhat larger than for North America. In April, VIC agrees reasonably well not only in representing the observed spatial patterns of SCE but also the magnitudes of snow cover area fraction over the pan-Arctic. The difference between observed and simulated snow cover area fraction is quite small (1.3% for Eurasia and 1.9% for North America). In June, the patterns are similar, with a VIC bias of 2.6% for both continents. Although the SCE spatial distributions from VIC and NOAA are quite close in June, differences are nonetheless evident in some areas, such as northeastern Eurasia, which are likely related to the lower surface air temperatures over this mountainous region in the forcing of VIC as described in Su et al. (2006). The most significant difference between observations and simulations is in May when the snow cover area fraction bias is 3.1% for North America and 6.6% in Eurasia. Overall, the match of VIC estimates with NOAA observations is quite good, with mean absolute bias over both continents equal to 1.6% in April, 4.9% for May, and 2% in June.

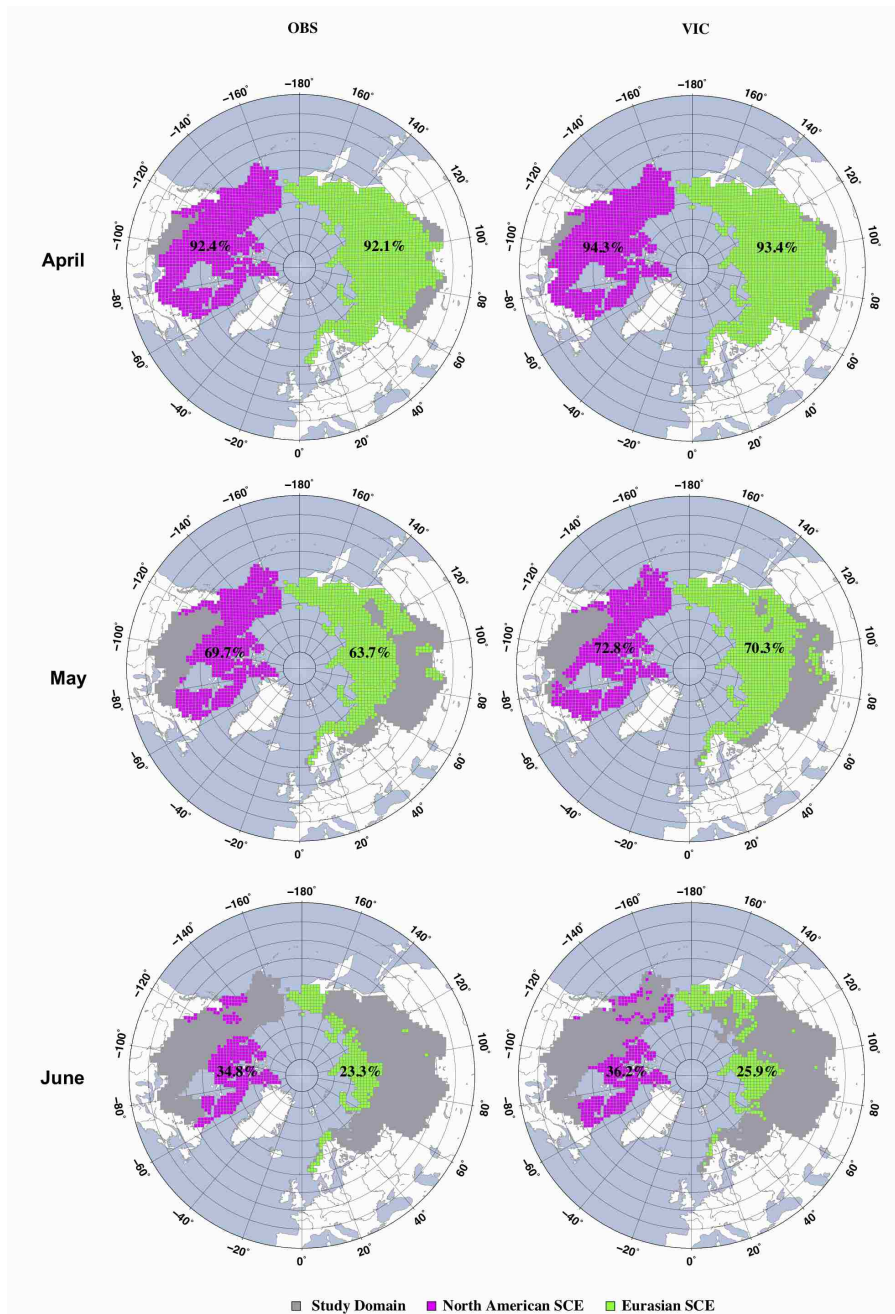


Figure 4.1 Spatial distribution of monthly mean SCE from the VIC model (VIC) and NOAA satellite observations (OBS) over North America and Eurasia from April through June for the period 1972-2006. The percentages on the map show the snow cover area fractions from VIC and NOAA for each month over the 35-year period of analysis.

To examine long-term trends in the SCE time series, we used the non-parametric Mann-Kendall trend test (Mann 1945) for trend significance, and the Sen method (Sen 1968) to estimate their slopes. A 5% significance level (two-sided test) was selected in the trend significance tests. For both VIC and NOAA, trend tests were performed on the monthly SCE time series area-averaged over the snow-covered portions of Eurasia and North America. Figure 4.2 shows these results for April through June for VIC and NOAA. Strong negative trends were detected in NOAA in both North American and Eurasian sectors of the pan-Arctic, which are statistically significant ($p < 0.025$) except for Eurasia in April. Negative SCE trends with similar significance levels were reproduced by VIC for both continents from April through June. However, the trend slope magnitudes for NOAA and VIC differ somewhat, especially in Eurasia, where the simulated trend slope from VIC is about 60% of that from NOAA in May, and 50% of the NOAA magnitude for June. This discrepancy is likely related to uncertainties in the NOAA weekly SCE data set (Wang et al. 2005; Déry and Brown 2007) and the VIC forcings, which generally are of higher quality in North America than Eurasia because of the availability of a denser observational network (Niu and Yang 2007). Table 4.1 summarizes correlation coefficients due to the linear trend and the variability between VIC and NOAA SCE time series over North America and Eurasia from April to June for the period 1972-2006. The significance level (p -value) is based on a two-tailed Student t -test with 33 degrees of freedom. The VIC and NOAA SCE time series are correlated with a very high significance level, not only for the secular trend ($p < 0.0001$) but also for the variability ($p < 0.03$).

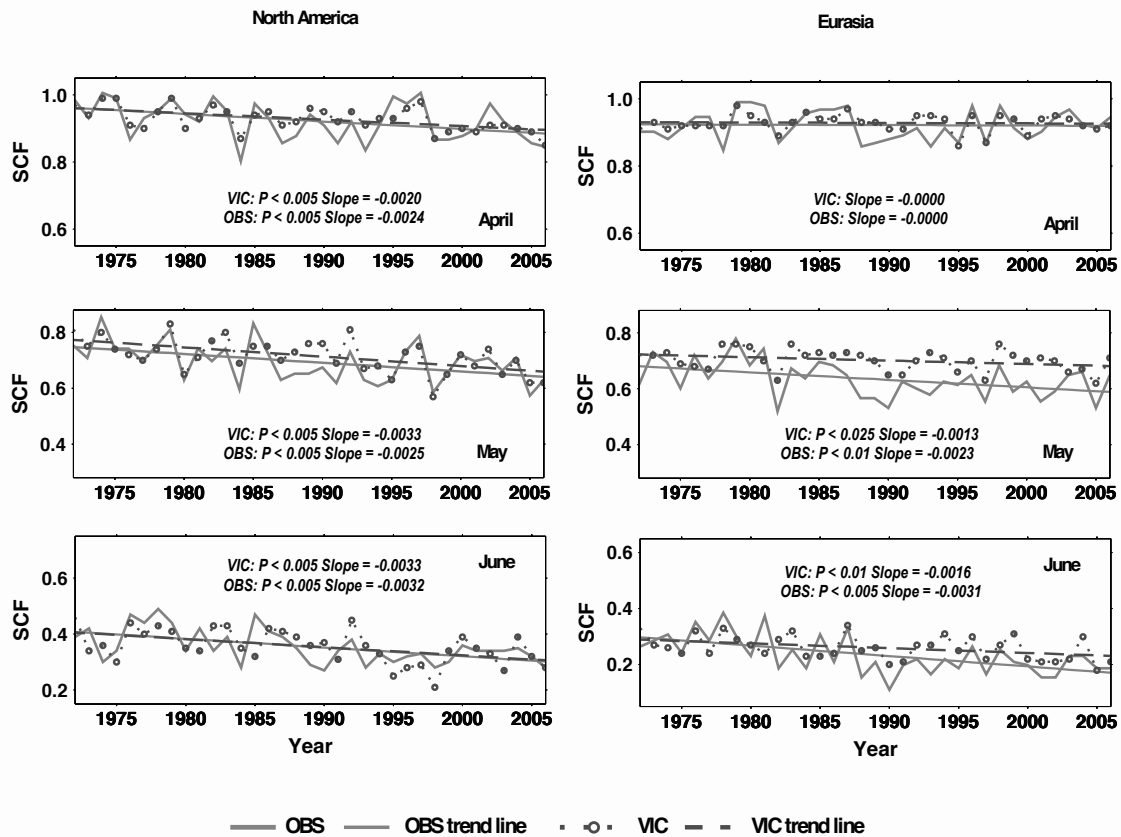


Figure 4.2 Monthly time series of snow cover fraction (SCF) and their trends (the unit of trend slope is in $year^{-1}$) derived from the VIC model (VIC, dashed lines) and NOAA observations (OBS, solid lines) for the period 1972-2006 for North America and Eurasia over the pan-Arctic land area.

Figures 4.1 and 4.2 show that biases both in mean reconstructed SCE and in simulated trend slopes for Eurasia are relatively larger than for North America. These biases in the model reconstructions could have several causes. We believe the most likely is errors in

Table 4.1 Correlation coefficients due to the linear trend and the variability for the monthly time series (from April to June) of SCE derived from VIC and NOAA observations in the North American and Eurasian SCSZs for the period 1972-2006. The significance level (p -value) was calculated using a two-tailed Student t-test with 33 degrees of freedom.

		April		May		June	
		$p <$	r	$p <$	r	$p <$	r
Correlation (Trend)	North America	0.0001	1.00	0.0001	1.00	0.0001	1.00
	Eurasia	0.0001	0.95	0.0001	1.00	0.0001	1.00
Correlation (Variability)	North America	0.0001	0.78	0.0001	0.68	0.029	0.37
	Eurasia	0.0001	0.64	0.002	0.51	0.012	0.42

the model meteorological forcings, due especially to the sparseness of the gauge network, changes in observing instruments and protocols, and similar issues (e.g., Adam and Lettenmaier 2008). Model structural errors (e.g., Wagener et al. 2001), and model parameter estimates (e.g., Shi et al. 2008) could also be causes. Model parameter errors were reduced through a process of calibration following methods similar to those reported by Troy et al. (2011).

Figure 4.3 shows the latitudinal variations of SCE trends and their area fractions from VIC and NOAA from April through June. The percentage under each bar chart is the trend significance at each 5° of latitude (expressed as a confidence level). Figure 4.3 shows that the snow cover area fraction for each month has a latitudinal pattern, which in general is at a minimum in the lowest latitude band, and then increases with latitude poleward. The figure clearly shows that VIC lags behind NOAA for the snowmelt during April and May, especially in the lower latitude bands, while SCE in June shows remarkable consistency between VIC and NOAA observations. The trend slopes have a negative sign nearly everywhere but without latitudinal patterns. Although the trend slope generally decreases to zero at higher latitudes, it is positive in April for the band 55-60°N over Eurasia. Most importantly, VIC shows a strong ability to reproduce the NOAA SCE trends for almost all the latitudinal bands over North America and Eurasia, not only in direction but also in their statistical significance. The magnitude of the VIC trend slopes agrees well with NOAA for most latitude bands.

From April through June, snow mostly covers latitude bands north of 45°N over the pan-Arctic land area, which are denoted as the snow covered zone (SCZ) in Figure 4.3. We selected only those latitudinal bands within which SCE trends were statistically

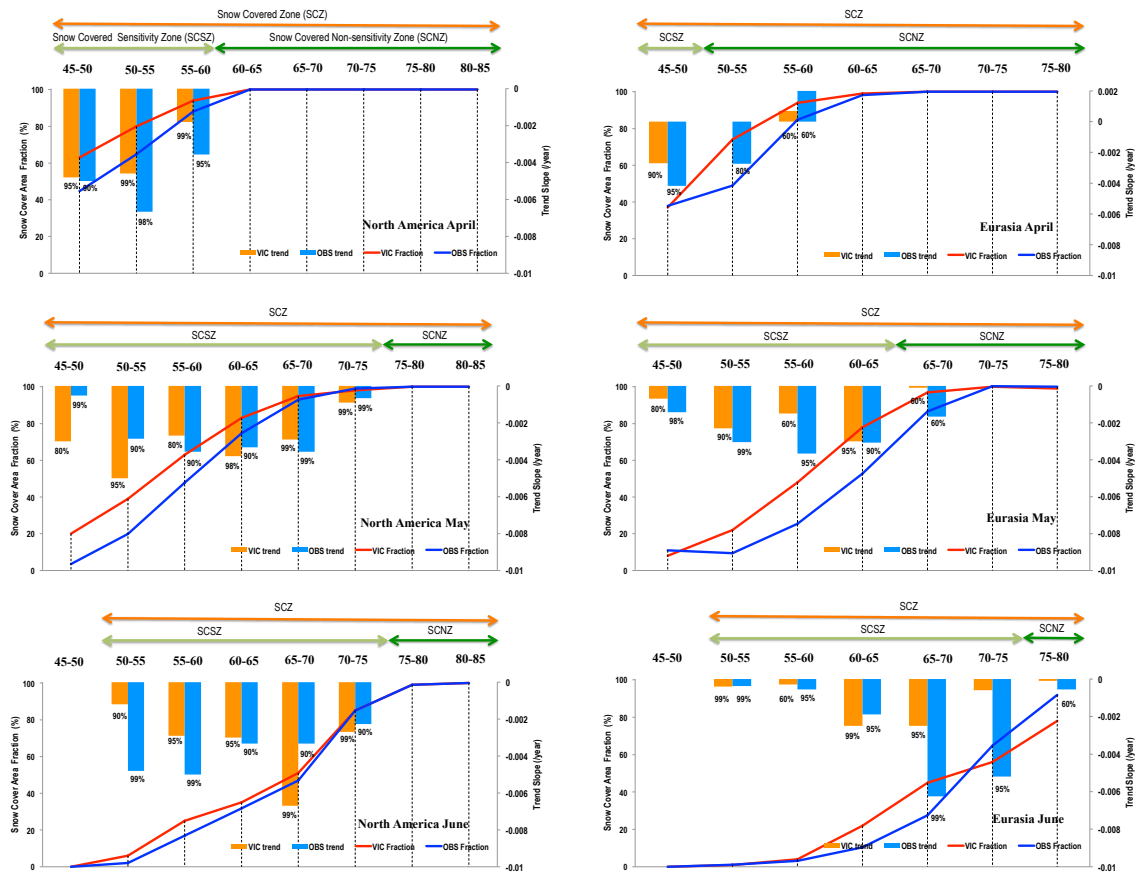


Figure 4.3 Latitudinal variations of the SCE trends and their area fractions derived from the VIC model (VIC) and NOAA satellite observations (OBS) over (a) North American and (b) Eurasian Snow Covered Zones (SCZs), including the Snow Covered Sensitivity Zones (SCSZs) and Snow Covered Non-sensitivity Zones (SCNZs) as indicated by the arrows, from April through June for the period 1972-2006. The percentage under each bar chart is the trend significance for each 5° (N) of latitude (expressed as a confidence level).

significant at the 90% confidence level for further analyses. For each month, we name these bands the snow cover sensitivity zone (SCSZ). In Figure 4.3, the North American and Eurasian SCZs including the SCSZs and Snow Covered Non-sensitivity Zones (SCNZs) are highlighted by different gray-shaded arrows. For example, the SCSZ in May for North America has six latitude bands from 45-50°N to 70-75°N, whereas there is only one band (45-50°N) for the Eurasian SCSZ in April. In the future as warming continues, the SCSZ zone can be expected to shift northward, and may require a somewhat different analysis approach. In addition, the discrepancy of snow cover area fraction between VIC and NOAA for each SCSZ is generally greater at the lower latitudes than at the higher latitudes. However, the importance of these differences is reduced because the weights for the lower latitude bands are relatively small as indicated in Figure 4.4.

4.3.2. Temporal Analyses of Surface Energy Fluxes

The energy balance at a snow surface includes net radiative fluxes, sensible and latent heat fluxes, ground heat fluxes, and the energy transfer due to rain on snow. Over the pan-Arctic, ground heat flux is a small component of the energy balance of melting snowpack compared with radiative and turbulent heat fluxes. Therefore, its effects on total snowmelt can safely be ignored (Gray and Prowse 1993). Similarly, rain on snow has an important influence on the water retention characteristics of snow and water movement in the pack but is of minor importance compared with other energy fluxes (Male and Granger 1981). For these reasons, our trend analysis using the non-parametric

Table 4.2 Trend analyses for three surface energy fluxes (surface net radiation (SNR), sensible heat (SH), and latent heat (LH)) from April to June for 1972-2006 in the North American and Eurasian SCSZs generated from VIC. The significance level (p -value) was calculated using a two-sided Mann-Kendall trend test. Trend slope units are $W m^{-2} year^{-1}$.

		SNR		SH		LH	
		$p <$	Slope	$p <$	Slope	$p <$	Slope
North America	April	0.05	0.217	0.01	0.188	0.10	-0.033
	May	0.025	0.270	0.005	0.230	0.025	-0.046
	June	0.025	0.549	0.005	0.384	0.005	-0.152
Eurasia	April	--	0.220	--	0.173	0.10	-0.029
	May	0.005	0.493	0.10	0.135	0.01	-0.122
	June	0.005	0.593	0.005	0.225	0.05	-0.104

Mann-Kendall trend test was applied only to the surface energy inputs at the snow surface, i.e., to SNR, SH and LH. Table 4.2 summarizes their monotonic trends over North America and Eurasia from April through June for the period 1972-2006. Trends were computed for monthly means of surface energy fluxes over SCSZs for both continents.

Strong positive trends were found in SNR in the North American and Eurasian SCSZs, except for Eurasia where the trend was not statistically significant in April. As with SNR, the SH fluxes also did not have a statistically significant trend in April for Eurasia, whereas they had statistically significant upward trends for other SCSZs. The changes in LH are mostly negative, and statistically significant at $p < 0.025$ for the North American SCSZ in May and June, and at $p < 0.01$ for the Eurasian SCSZ only in May.

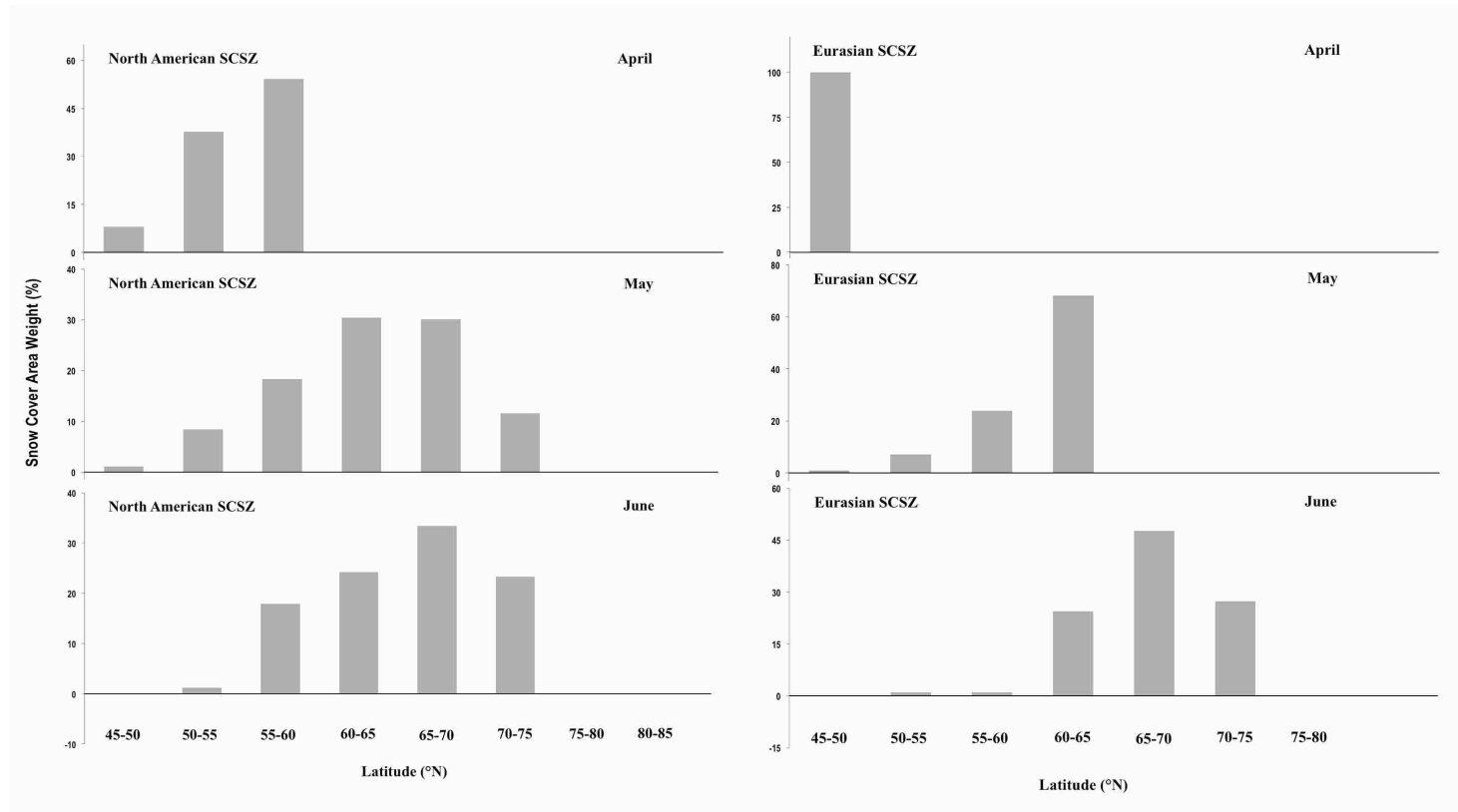


Figure 4.4 Snow cover area weights (the fraction of snow-covered area falling within each 5° (N) latitude band) for North American and Eurasian SCSZs from April through June for the period 1972-2006.

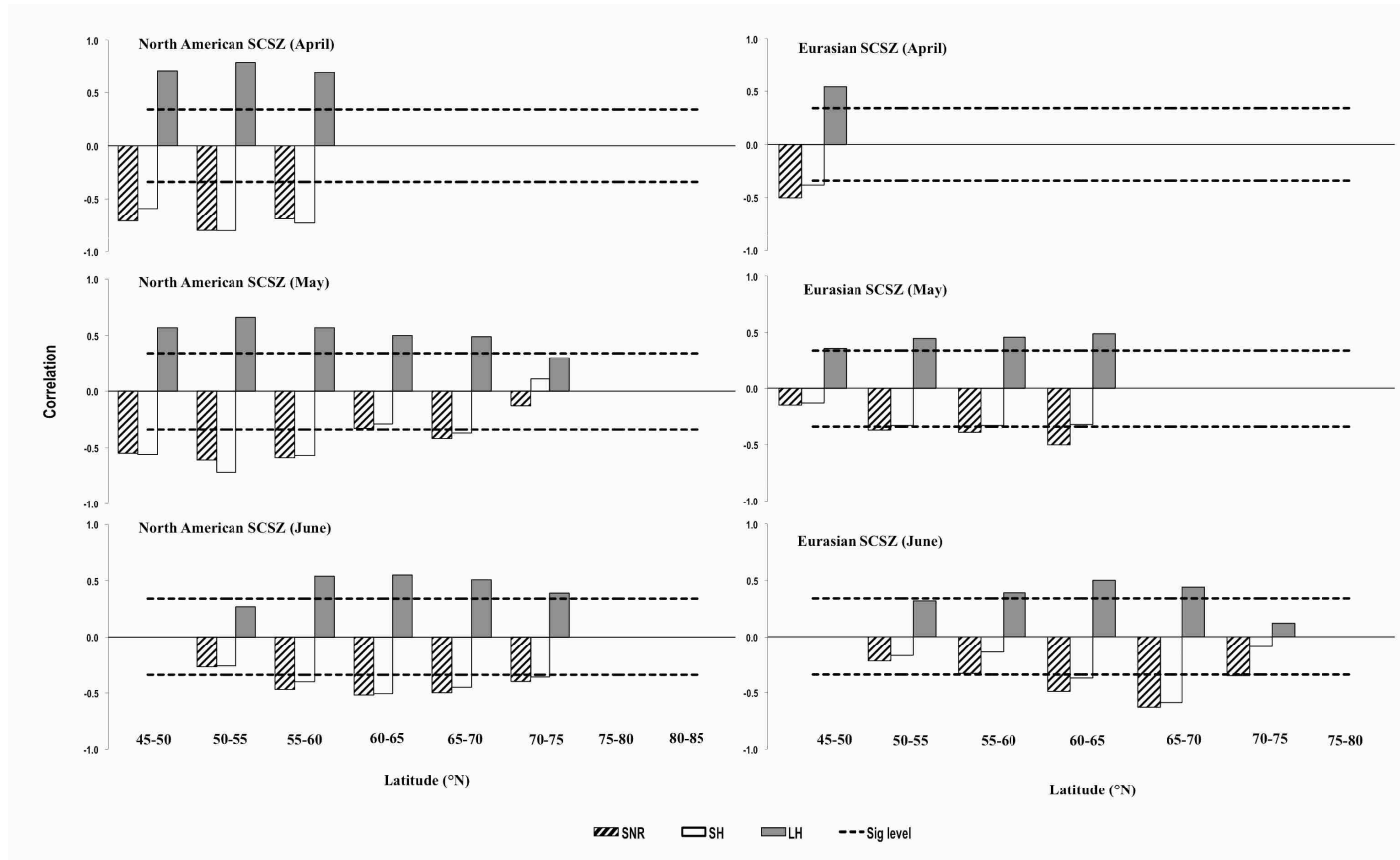


Figure 4.5 Correlations between three surface energy fluxes: SNR, SH, and LH versus NOAA satellite SCE observations for each latitude band in the North American and Eurasian SCSZs for April, May and June. The significance level of $p < 0.025$ (dashed line) was calculated by the Student t-test.

4.3.3. Correlations between Observed SCE and Modeled Surface Energy Fluxes

The Pearson's product-moment correlation coefficient was used to assess relationships between NOAA SCE and VIC-simulated surface energy fluxes for each 5° latitude band over the North American and Eurasian SCSZs from April through June (Figure 4.5). The correlations in April are all statistically significant at $p < 0.025$ (two sided test) for each latitude band in the SCSZs over both continents. For May, SNR and SH have non-significant relationships with NOAA SCE from 60-65°N to 70-75°N in North America, as well as for the 45-50°N latitude band over Eurasia. Additionally, the correlation between SH and SCE is positive for 70-75°N in North America. For June, the latitude bands 45-50°N over the North American SCSZ and 50-60°N and 70-75°N over the Eurasian SCSZ have non-significant correlations with SNR and SH. The negative correlations indicate that SNR and SH have opposite trend directions with observed SCE. Generally speaking, SNR has a relatively stronger relationship with NOAA SCE than does SH, especially in Eurasia. For LH, the correlations are always positive and much stronger in North America than that in Eurasia.

4.3.4. Role of Surface Energy Fluxes in Snow Cover Changes

In VIC, surface energy fluxes towards the snow surface are defined as positive; therefore, the net radiative and sensible heat fluxes usually have positive signs and supply the energy available for snowmelt. Latent heat fluxes are directed away from the snow surface and reduce the snowmelt energy. However, it was not clear which component(s)

of the snow surface energy budget dominate the SCE recession from April through June depicted in Figure 4.2. In order to determine the role of each component in the observed downward trends in SCE, we calculated the increment due to monotonic trends in SNR, SH and LH over the 35-year period (Δ SNR, Δ SH and Δ LH) for each month for the North American and Eurasian SCSZs. Figure 4.6 summarizes the latitudinal variations of these increments from April through June by latitude band. Δ SNR has an obvious latitudinal pattern, which is generally large in the lowest latitude bands (e.g., 45-50°N and 50-55°N), and then decreases with latitude poleward. Compared with Δ SNR, Δ LH shows a similar pattern with a negative sign in most cases. However, it sharply decreases at the higher latitudes, and sometimes is close to zero. In June over Eurasia, Δ LH even has a positive sign for the 70-75°N band. Corresponding to the patterns in Δ SNR and Δ LH, Δ SH is variable depending upon the months and latitude bands. As shown in Figure 4.6, the contribution of Δ SH in April is less than Δ SNR except for the latitude band 50-55°N in the North American SCSZ where it is slightly larger than Δ SNR (53.5% of the total energy attributable to snow cover changes). In May, Δ SH is much larger than Δ SNR for the 45-50°N band in North America, reaching 75.5% of the total energy associated with snow cover changes. Thereafter, its contribution decreases gradually with latitude to the 70-75°N band. Δ SNR had a larger contribution in the Eurasian SCSZ than in the North American SCSZ in May and June. From April to June, Δ LH increases significantly with rising surface air temperature. Since Δ LH has a negative sign in the snow surface energy balance, it is effectively canceled by Δ SH with a positive residual in each SCSZ, except

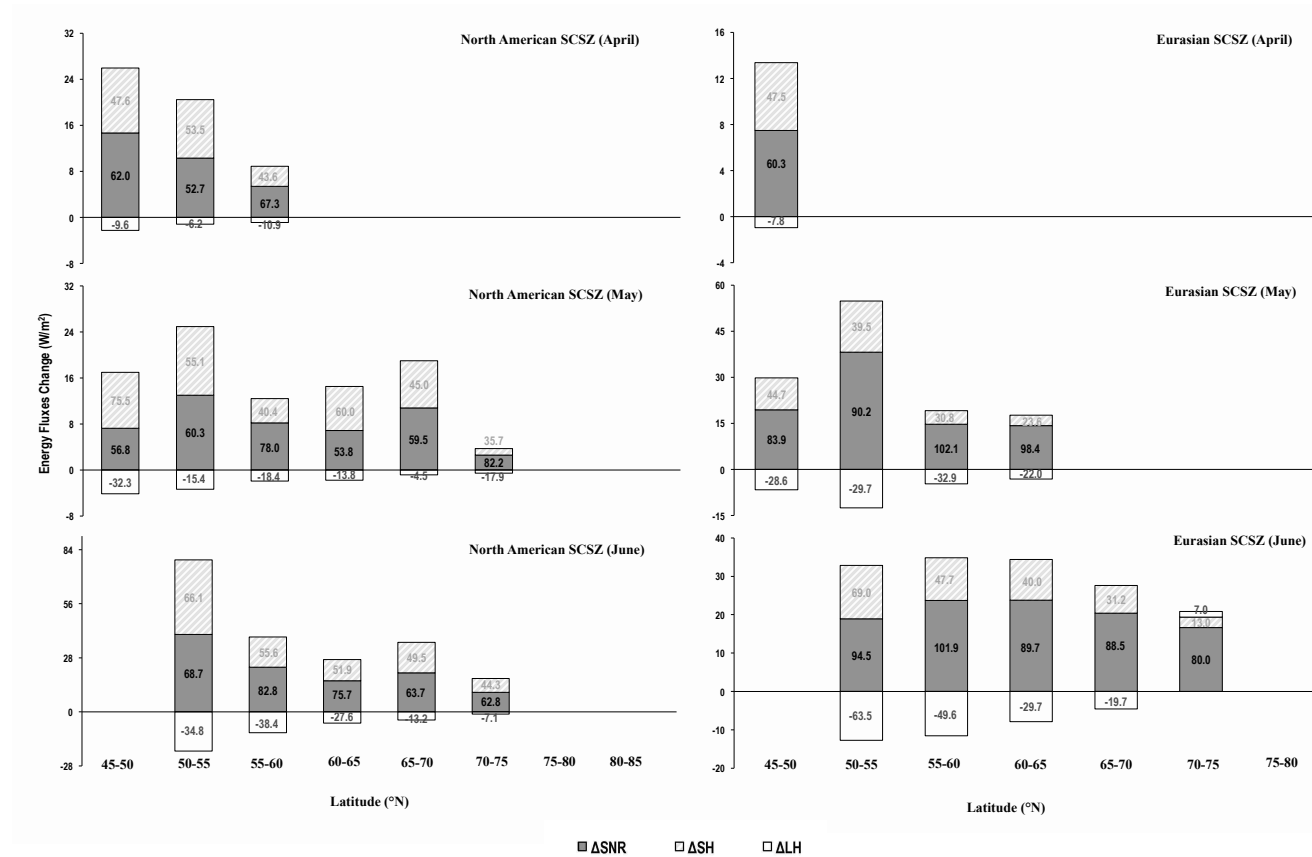


Figure 4.6 Latitudinal variations in the changes of surface energy fluxes in the North American and Eurasian SCSZs from April through June for the period 1972-2006 by 5° latitude band. The number in each bar denotes the relative role of the total energy attributable to snow cover changes.

in May and June for the Eurasian SCSZ. As shown in the middle and lower plots of Figure 4.6 for Eurasia, the contribution of ΔLH is even larger than ΔSH with an opposite sign at 55-60°N in May and June. For Eurasia, ΔSH does not follow the same pattern as in North America. Although ΔSH in the lower latitudinal bands has a significant contribution compared with ΔSNR , its impact over the entire SCSZ is smaller due to the small SCSZ weights of these bands as shown in Figure 4.4.

Figure 4.7 shows the relative role of the three surface energy fluxes from April through June averaged over each SCSZ in North America and Eurasia. It is apparent that ΔSNR is the dominant energy source in both continents, accounting for between 58.4% and 97.4% of the energy available for snow cover changes. The contribution of ΔSH plays a secondary role (from 26.7% to 50.7%) and ΔSNR has a larger contribution than ΔSH in Eurasia compared to North America. ΔLH is always opposite in sign with ΔSH and ΔSNR and almost completely cancels ΔSH in May over Eurasia. However, ΔLH has a smaller absolute value than ΔSH in all other cases, such as in April when it comprises only -8.8% and -7.8% of the energy available for snow cover changes over the North American and Eurasian SCSZs respectively. Therefore, we conclude that ΔLH has a minor influence on pan-Arctic snow cover changes compared to ΔSNR and ΔSH .

4.3.5. Causes of Pan-Arctic Snow Cover Changes

We have shown above that (1) the time series of continental-scale, late spring and early summer snow cover over the pan-Arctic have statistically significant negative trends

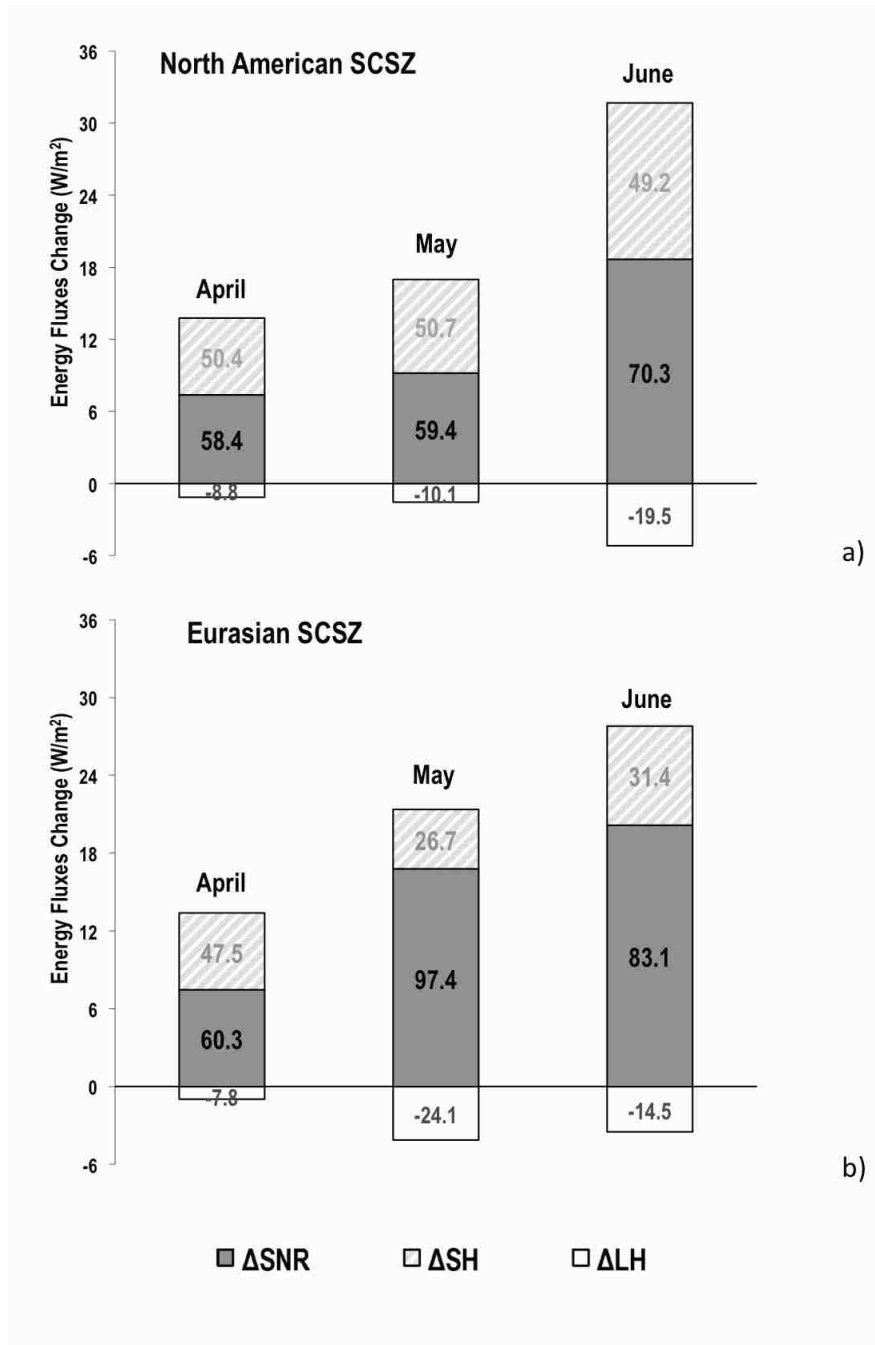


Figure 4.7 Relative role of three surface energy fluxes' changes during the April to June part of the year area-averaged over each SCSZ for (a) North America and (b) Eurasia for the period 1972-2006. The number in each bar denotes the contribution of the total energy attributable to snow cover changes.

from April to June for the period 1972-2006, and (2) VIC has the ability to reproduce spatial and temporal variations in the NOAA SCE time series. This offers an opportunity to diagnose the causes of observed snow cover changes. In addition to the surface radiative and turbulent fluxes, we also investigated other hydroclimatic indicators that might be related to SCE. Figure 4.8 shows correlations between NOAA SCE and fifteen hydroclimatic indicators over the North American and Eurasian SCSZs from April through June. Apparently, the changes of SCE over the study domains have statistically significant correlations with surface energy fluxes (SNR, SH, LH, SW, and DLW), ALB, and VP, as well as with temperatures (SAT, T_{\max} , and T_{\min}). For each of these variables, the absolute values of correlation coefficients are greater than 0.34 at a significance level of $p < 0.025$. However, other hydroclimatic indicators (DSW, P, DTR, WS, and CC) show non-significant relationships with SCE for both continents.

Table 4.3 reports changes, which were aggregated based on the Mann-Kendall trend slope from 1972 to 2006, for a number of hydroclimatic indicators potentially related to pan-Arctic SCE changes from April to June over the North American and Eurasian SCSZs. It shows that the increases in SNR are mainly associated with increased SW and increased DLW, whereas emitted upward longwave fluxes do not change much (probably because the snowpack temperature is mostly isothermal during the melt period). Strong upward trends in SW mostly result from statistically significant decreasing trends in ALB, while the contribution from increased DSW trends over Eurasia is minor. Over

North America DSW decreases. In TIND, DSW is calculated by the method of Thornton and Running (1999) which depends upon DTR and VP. Therefore, a decreasing DSW trend over North America is explained by a more rapid increase of T_{\min} compared to that of T_{\max} as well as by an increase of VP. As noted above, DLW from TIND also depends upon DTR and VP. Changes in sensible and latent heat fluxes are mostly dominated by increases in SAT over much of the pan-arctic region (Table 4.3; see also Lugina et al. 2005; Serreze and Francis 2006; Bekryaev et al. 2010). For P, the downward trends in the North American SCSZ are statistically significant. However, they are variable in the Eurasian SCSZ, where there is a downward trend in April and increasing trends in May and June, all of which are statistically insignificant. The correlations between CC and SCE as well as between WS and SCE are statistically insignificant in each month from April through June.

We conclude that SNR provides the primary energy source and SH plays a secondary role in changes of SCE. Compared to SNR and SH, LH has only a minor influence on pan-Arctic snow cover changes. The changes in snow surface energy fluxes resulting in the pan-Arctic snow cover recession are associated with statistically significant decreased ALB, increased surface air temperatures, and increased VP. All these changes are occurring in concert with feedbacks to each other. They cannot be considered in a cause-consequence relationship at the time scale used in this study (months). For example, the

Table 4.3 Total changes for twelve pan-Arctic hydroclimatic characteristics from April to June during the period 1972-2006 in the North American and Eurasian SCSZs. The significance level (p -value) was calculated using a two-sided Mann-Kendall trend test. The unit of total change for radiation fluxes (net shortwave radiation (SW), downward shortwave radiation (DSW), and downward longwave radiation (DLW)) is $W m^{-2}$. Units for diurnal temperature range (DTR), surface air temperature (SAT), daily maximum temperature (T_{max}), and daily minimum temperature (T_{min}) are $^{\circ}C$; for atmospheric water vapor pressure (VP) hPa ; for precipitation (P) mm ; and for wind speed (WS) $m s^{-1}$. Snow surface albedo (ALB) and cloud cover (CC) are dimensionless

		SW		ALB		DSW		DTR		VP		DLW	
		$p <$	Δ	$p <$	Δ	$p <$	Δ	$p <$	Δ	$p <$	Δ	$p <$	Δ
North America	April	0.025	12.82	0.05	-0.041	0.005	-8.72	--	-0.14	0.10	0.034	0.10	4.67
	May	0.01	11.51	0.005	-0.044	0.005	-9.80	0.025	-0.32	0.20	0.020	0.005	7.82
	June	0.01	25.26	0.01	-0.092	0.10	-5.00	--	-0.12	0.10	0.041	0.20	3.41
Eurasia	April	0.20	9.40	--	-0.037	--	1.48	--	0.00	0.20	0.027	--	1.02
	May	0.01	17.90	0.005	-0.075	0.20	1.81	--	0.20	0.005	0.075	0.10	4.59
	June	0.005	22.30	0.005	-0.085	0.01	6.93	0.20	-0.16	0.005	0.082	0.005	7.64

(Table 4.3 continuation)

		CC		P		SAT		T _{min}		T _{max}		WS	
		<i>p</i> <	Δ	<i>p</i> <	Δ	<i>p</i> <	Δ	<i>p</i> <	Δ	<i>p</i> <	Δ	<i>p</i> <	Δ
North America	April	0.20	4.9×10^{-4}	0.005	-0.45	0.10	1.36	0.05	1.38	0.10	1.19	0.20	-0.031
	May	0.10	1.4×10^{-2}	0.025	-0.20	0.10	0.83	0.20	0.58	--	0.41	--	0.000
	June	--	0×10^0	0.005	-0.27	0.005	1.41	0.10	0.87	0.20	0.68	--	0.000
Eurasia	April	0.10	-2×10^{-2}	--	-0.13	--	0.49	--	0.29	--	0.87	0.025	0.228
	May	0.10	3.5×10^{-4}	--	0.07	0.005	1.7	0.005	1.79	0.005	2.12	--	0.000
	June	0.20	3.0×10^{-4}	--	0.05	0.005	1.88	0.005	1.54	0.005	1.45	--	-0.017

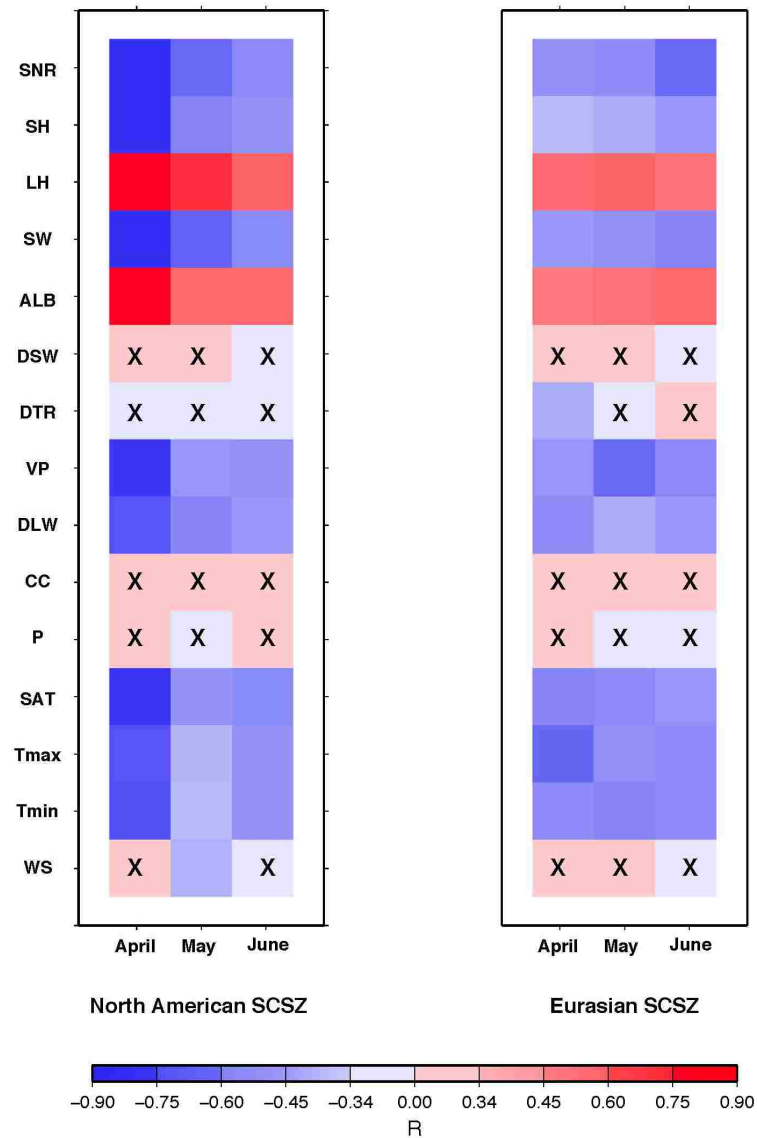


Figure 4.8 Correlations between NOAA SCE observations and fifteen hydroclimatic characteristics in the North American and Eurasian SCSZs from April to June for the period 1972-2006. The correlation is statistically significant at a level of $p < 0.025$ when its absolute value is greater than 0.34. X denotes that the correlation is not significant. The abbreviations for the hydroclimate variables are defined as follows: surface net radiation (SNR), sensible heat (SH), latent heat (LH), net shortwave radiation (SW), snow surface albedo (ALB), downward shortwave radiation (DSW), diurnal temperature

range (DTR), atmospheric water vapor pressure (VP), downward longwave radiation (DLW), cloud cover (CC), precipitation (P), surface air temperature (SAT), daily maximum temperature (T_{\max}), daily minimum temperature (T_{\min}), and wind speed (WS).

SNR increase “causes” the SCE retreat that decreases ALB, which in turn, “causes” the SNR increase. However, we can quantify the relative role of the surface energy fluxes in the SCE changes (Figure 4.7).

Although surface observations over the pan-Arctic domain are brief and sparse, our findings are consistent with a variety of evidence. For instance, recent studies have shown that the most significant and strongest Arctic warming occurred in the most recent 40 years with warming at nearly double the global rate (Serreze et al. 2000; Overland et al. 2004; Chapin et al. 2005; Hinzman et al. 2005; White et al. 2007; Solomon et al. 2007). Furthermore, increasing VP trends were found in previous work that examined data collected mainly in the latter decades of the twentieth century (Dai 2006; Vincent et al. 2007; Santer et al. 2007), which is important as water vapor is itself a greenhouse gas (Held and Soden 2000). Most recently, Isaac and Wijngaarden (2012) detected larger trends for both VP and SAT during 1981-2010 after examining 309 stations located across North America.

In addition to the surface data, satellite data provide a unique opportunity to gain knowledge of environmental and climate change in the Arctic, as well as the climate model. Enhancement of poleward atmospheric moisture transport in a warmer climate was found to be responsible for amplified Arctic warming in idealized experiments

without surface albedo feedback (Graversen and Wang 2009). Also, increasing oceanic moisture transport is correlated with Arctic warming and the amount of sea ice loss (Holland et al. 2006; Wang et al. 2010; Mahlstein and Knutti 2011). Moreover, increasing greenness is occurring in the northern high latitudes (Sturm et al. 2001; Stow et al. 2004; Chapin et al. 2005). An increase in vegetation coverage reduces snow-covered surface albedo (due to the effects of vegetation protruding through relative thin snow cover), causing a noticeable increase in absorbed surface solar radiation and amplifying the feedback among snow cover, surface albedo, and absorbed solar radiation (Zhang and Walsh 2007). Overall, our findings provide a link to these recent studies and fit into the bigger picture of Arctic system-wide change.

4.4. Conclusions

Following our pilot study of the role of surface radiative and turbulent fluxes in aggregate changes of SCE for the entire North American and Eurasian land area over the pan-Arctic (Shi et al. 2011), we focused in this paper on spatial and temporal variations of monthly SCE during the late spring and early summer and their relationships with a number of hydroclimatic variables over each SCSZ (latitude bands) for both continents. By exploring long-term monotonic trends in NOAA SCE observations and their relationships with surface energy fluxes and associated variables predicted by the VIC land surface model, we conclude that:

- 1) North American and Eurasian late spring and early summer (from April through June)

snow cover over the pan-Arctic have declined significantly for the period 1972-2006.

Spatial distribution of monthly SCE and the pattern of its trends (trend signs, rates of changes, and statistical significance levels) are reproduced well by the VIC model.

2) Surface radiative and turbulent heat fluxes generated by VIC are strongly correlated with observed SCE in the North American and Eurasian SCSZs. SNR supplies the primary energy source for the pan-Arctic late spring and early summer snow recession and SH plays a secondary role in these snow cover changes. Relative to SNR and SH, LH has a minor influence on the changes of SCE.

3) Correlation analyses of fifteen hydroclimatic characteristics and NOAA SCE observations in each SCSZ over North America and Eurasia reveal that the changes in surface energy fluxes resulting in the pan-Arctic late spring and early summer snow cover recession are mainly associated with statistically significant decreased ALB, increased air temperatures (SAT, T_{\max} , and T_{\min}), and increased VP, while other hydroclimatic variables (DSW, P, DTR, WS, and CC) have less impact on observed SCE changes in SCSZs for both continents.

5. The Effects of Pan-Arctic Snow Cover and Air Temperature Changes on Frozen Soil Heat Content

This is in review by the *Journal of Geophysical Research-Atmospheres* as:

Shi, X., and D. P. Lettenmaier, 2012: The effects of pan-Arctic snow cover and air temperature changes on frozen soil heat content. *J. Geophys. Res.* (in review).

5.1. Introduction

Over the pan-Arctic region (for purposes of this paper, defined as the land area draining to the Arctic Ocean), the rise in surface air temperature (SAT) has been almost twice as large as the global average in recent decades (Serreze et al. 2000; Jones and Moberg 2003; Overland et al. 2004; Hinzman et al. 2005; White et al. 2007; Solomon et al. 2007; Trenberth et al. 2007; Screen and Simmonds 2010). Increases in SAT have been accompanied by increasing soil temperatures with deeper active layer thickness across permafrost regions and decreasing frozen soil depths in the seasonally frozen ground regions (Hinzman and Kane 1992; Frauenfeld et al. 2004; Romanovsky et al. 2007). Given the potential for releases of soil carbon to the atmosphere at warmer temperatures, warming of the land surface at high latitudes has attracted considerable scientific attention (Stieglitz et al. 2003; Heimann and Reichstein 2008).

Observed soil temperatures across the pan-Arctic have been used as an indicator of climate change in past studies (Osterkamp and Romanovsky 1999; Zhang et al. 2001; Smith et al. 2004; Beltrami et al. 2006; Romanovsky et al. 2002, 2007). However, in situ soil temperatures are problematic because latent heat effects, which may be significant in regions with frozen soils (Troy 2010), are neglected. Arguably, the heat content of the soil column is a better indicator of changes in the land surface energy budget because it provides an integrated measure that accounts for changes in temperature, moisture, and latent heat effects. For this reason, it has been used in various studies to document how the land surface responds to atmospheric changes (Levitus et al. 2001, 2005; Beltrami et al. 2002, 2006; Hansen et al. 2005; Troy 2010). For instance, using the Variable Infiltration Capacity (VIC) land surface model (Liang et al. 1994; Cherkauer and Lettenmaier 1999), Troy et al. (2012) showed that modeled soil temperature profiles and soil heat content (SHC) trends reproduced observed trends at high latitudes. Following these previous studies, we evaluate SHC trends and their causes, with particular attention to the pan-Arctic land region.

Because snow is a strong insulator, it limits the efficient transport of heat between the atmosphere and the ground, and thus plays an important role in determining how air temperature signals propagate into the soil column (Gold 1963; Goodrich 1982; Osterkamp and Romanovsky 1996; Stieglitz et al. 2003; Zhang 2005; Bartlett et al. 2005; Iwata et al. 2008; Lawrence and Slater 2010). In general, seasonal snow cover tends to

result in relatively higher mean annual ground temperatures, especially at high latitudes where stable snow cover lasts from a few weeks to several months (Zhang 2005).

In the visible satellite imagery produced by the National Oceanic and Atmospheric Administration (NOAA) (Robinson et al. 1993; Frei and Robinson 1999), a substantial retreat of snow cover extent (SCE) has been observed during late spring and early summer in recent decades (Groisman et al. 1994; Déry and Brown 2007; Brown et al. 2010; Shi et al. 2011, 2012). Moreover, these negative SCE trends are well reproduced for both North America and Eurasia by simulations using the VIC model (Shi et al. 2012).

Recent studies have attempted to explain the impact of seasonal snow cover and air temperature on the ground thermal regime over the pan-Arctic by using soil temperature as an index (e.g., Zhang et al. 1997; Zhang and Stamnes 1998; Romanovsky et al. 2002; Bartlett et al. 2004, 2005; Lawrence and Slater 2010). However, the interpretation of relationships between seasonal snow cover and air temperature on the ground thermal regime is complicated because surface temperature is affected by multiple variables. An alternative approach is to use SHC as an indicator of changes in the ground thermal regime because it can provide a complete understanding of high latitude land surface warming.

In this paper, we explore the effects of snow cover recession and increases in SAT on SHC over the pan-Arctic, with particular emphasis on trends and variability during the late spring and early summer. In section 5.2, we describe the observations and model-

derived data sets on which our analyses are based. In section 5.3, we explore trends in SHC and examine correlations between SCE, SAT, and SHC and the relative roles of snow cover recession and increasing SAT on SHC changes.

5.2. Data sets

5.2.1. Observed SCE and SAT Data

Observed monthly values of SCE were extracted from the weekly snow cover and sea ice extent version 3.1 product for the Northern Hemisphere (<http://nsidc.org/data/nsidc-0046.html>), maintained at the National Snow and Ice Data Center (NSIDC). These data span the period October 1966 through June 2007 (Armstrong and Brodzik 2007). The data set is based on weekly maps of continental SCE produced by NOAA's National Environmental Satellite Data and Information Service (NESDIS) (Robinson et al. 1993; Frei and Robinson 1999), which were derived from digitized versions of manual interpretations of Advanced Very High Resolution Radiometer (AVHRR), Geostationary Operational Environmental Satellite (GOES), and other visible band satellite data. We used a version of the data that has been regridded to the NSIDC EASE grid with a spatial resolution of 25 km by Armstrong and Brodzik (2007). Our study is restricted to the period from 1972 on since some charts between 1967 and 1971 are missing (Robinson, 2000). Although ending the time series in 2006 leaves out some exceptionally low Arctic spring SCE values in recent years (e.g., 2008-2010) (Derksen and Brown 2012), the non-parametric statistical method we used (section 5.3.2) is robust to modest changes in the

length of the record analyzed. We did not include Greenland in the analyses since its snow cover is mainly perennial in nature. Brown et al. (2010) have compared this SCE record (commonly referred to as the NOAA weekly SCE record) with other available Arctic snow cover data sets. In general, their study and others (e.g., Wiesnet et al. 1987; Robinson et al. 1993) have found that the NOAA weekly SCE data are reliable for continental-scale studies of snow cover variability. They have become a widely used tool for deriving trends in climate-related studies (Groisman et al. 1994; Déry and Brown 2007; Flanner et al. 2009; Derksen et al. 2010; Derksen and Brown 2011; Shi et al. 2011, 2012), notwithstanding uncertainties in some parts of the domain for certain times of the year, such as summertime over northern Canada (Wang et al. 2005). A more recent update to the data set we used (NOAA snow chart climate data record, CDR) is now available (Brown and Robinson, 2011), but the differences between the new CDR and the data set we used at the pan-Arctic scale are small (Shi et al. 2011).

Monthly SAT anomaly data were derived from the Climatic Research Unit (CRU, Brohan et al. 2006) (CRUTEM3 data set from <http://www.cru.uea.ac.uk/cru/data/temperature/>), which are based on anomalies from the long-term mean temperature for the period 1961-1990 and are available for each month since 1850. The land-based monthly data are on a regular 0.5° by 0.5° global grid. We regridded these data, including the NOAA SCE observations that were aggregated from the 25-km product, to the 100-km EASE grid using an inverse distance interpolation as implemented in Shi et al. (2012).

5.2.2. Modeled SHC

The version of VIC used for this study is 4.1.2, which includes some updates to the model's algorithms for cold land processes. For instance, the model includes a snow parameterization that represents snow accumulation and ablation processes using a two-layer energy and mass balance approach (Andreadis et al. 2009), a canopy snow interception algorithm when an overstory is present (Storck et al. 2002), a finite-difference frozen soils algorithm (Cherkauer and Lettenmaier 1999) with sub-grid frost variability (Cherkauer and Lettenmaier 2003), and an algorithm for the sublimation and redistribution of blowing snow (Bowling et al. 2004), as well as a lakes and wetlands model (Bowling and Lettenmaier 2010). In our implementation of the VIC model, each grid cell is partitioned into five elevation (snow) bands, which can include multiple land cover types (tiles). The snow model is then applied to each tile separately. The current version of the frozen soils algorithm uses a finite difference solution in the algorithm that dates to the work of Cherkauer and Lettenmaier (1999). To improve spring peak flow predictions, a parameterization of the spatial distribution of soil frost was developed (Cherkauer and Lettenmaier 2003). Adam (2007) described some significant modifications to the frozen soils algorithm, including the bottom boundary specification using the observed soil temperature datasets of Zhang et al. (2001), the exponential thermal node distribution, the implicit solver using the Newton-Raphson method, and an excess ground ice and ground subsidence algorithm in VIC 4.1.2. In order to model permafrost properly, our implementation used a depth of 15 m with 18 thermal nodes

exponentially distributed with depth and a no flux bottom boundary condition (Jennifer Adam, personal communication), which is similar to Troy et al. (2012).

We used the same study domain as documented in Shi et al. (2012), which is defined as all land areas draining into the Arctic Ocean, as well as those regions draining into the Hudson Bay, Hudson Strait, and the Bering Strait, but excluding Greenland (because its snow cover is mainly perennial in nature). The model simulations used calibrated parameters, such as soil depths and infiltration characteristics, from Su et al. (2005). The off-line VIC runs are at a three-hour time step in full energy balance mode (meaning that the model closes a full surface energy budget by iterating for the effective surface temperature, as contrasted with water balance mode, in which the surface temperature is assumed to equal the surface air temperature) forced with daily precipitation, maximum and minimum temperatures, and wind speed at a spatial resolution (EASE grid) of 100 km. The forcing data were constructed from 1948 through 2006 using methods outlined by Adam and Lettenmaier (2008), as described in Shi et al. (2012). To set the initial conditions including the thermal state in VIC, we initialized the model with a 100-year climatology created by randomly sampling years from the 1948-1969 meteorological forcings. Using VIC 4.1.2, we reconstructed SHC from 1970 to 2006 for the pan-Arctic land area.

5.3. Results

5.3.1. Definition of Study Zones

The NOAA weekly SCE data (hereafter NOAA-SCE) were analyzed to determine whether or not there are regions with significant changes of NOAA-SCE in North America and Eurasia. On the basis of the SCE trends derived from NOAA-SCE in 5° latitude bands from April through June for the period 1972-2006 as described in Shi et al. (2012), we defined a snow covered sensitivity zone (SCSZ), a snow covered non-sensitivity zone (SCNZ), and a non-snow covered zone (NSCZ) for North America and Eurasia, respectively.

Figure 5.1(a) shows the spatial distribution of long-term monthly means of SCE from NOAA-SCE from April through June for the 35-year period over North American and Eurasian pan-Arctic domains. Figures 5.1 (b) and (c) illustrate the latitudinal variations of SCE trends and their area fractions over the North American and Eurasian study domains from April through June. The percentage under each bar chart is the trend significance expressed as a confidence level for each 5° of latitude, while the solid line shows the latitudinal patterns in the snow cover area fractions for each month, which in general are at a minimum for the lowest latitude band, and then increase with latitude poleward.

Based on the latitudinal changes of NOAA-SCE as shown in Figure 5.1, we identified different study zones for North America and Eurasia. From April through June, snow mostly covers latitude bands north of 45°N over the pan-Arctic land area, which are denoted as snow covered zones (SCZs) in Figure 5.1. The rest of the study domains were denoted as non-snow covered zones (NSCZs) (see Figure 5.1(a) for North America and Eurasia, respectively). Within the SCZs, we selected only those latitudinal bands within

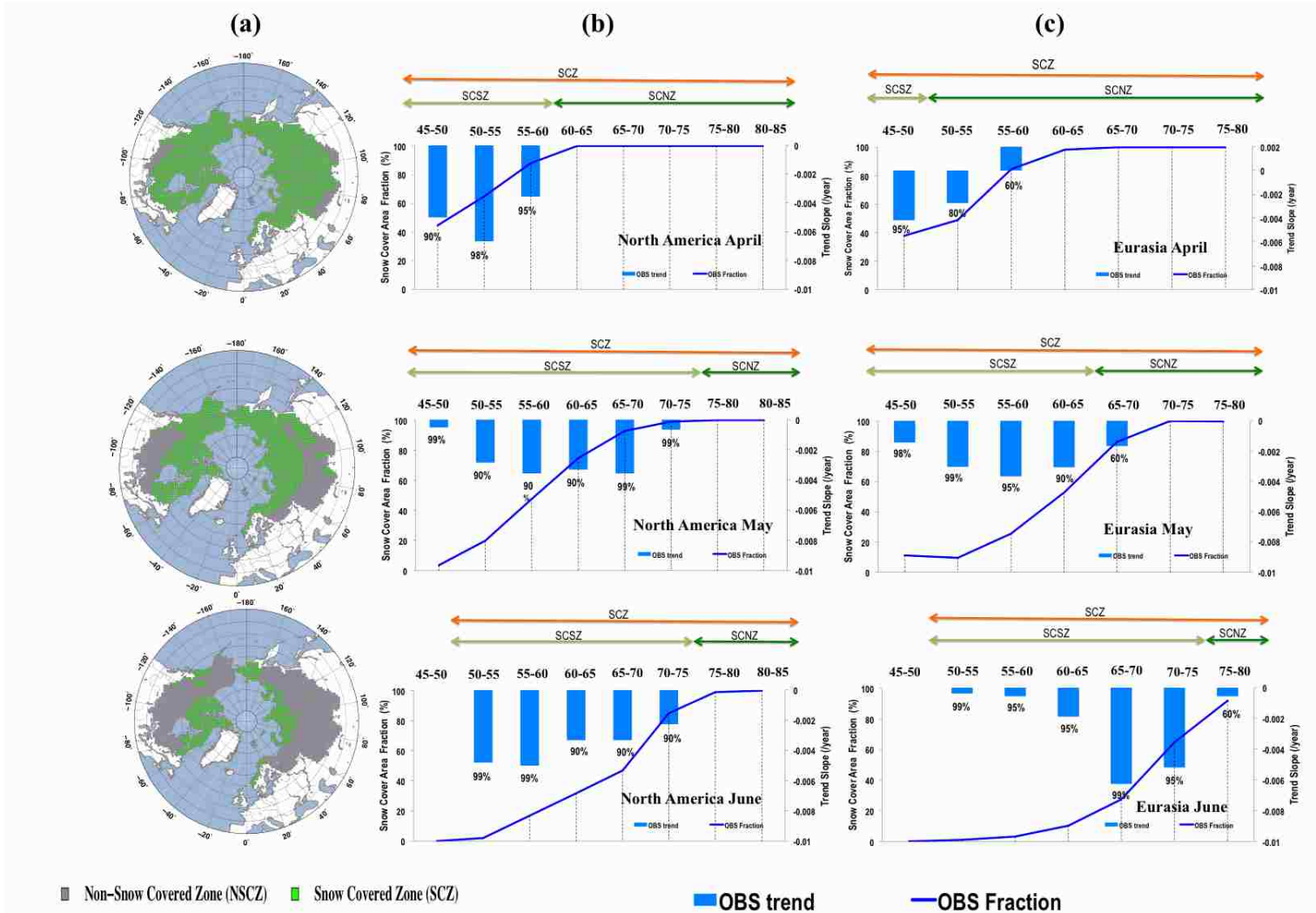


Figure 5.1. (a) Spatial distribution of monthly mean snow cover extent (SCE) from NOAA satellite observations (OBS) over North America and Eurasia in the pan-Arctic land region (non-snow covered zone (NSCZ) and snow covered zone (SCZ)) from April through June for the period 1972-2006. The SCE trends in 5° (N) latitude bands and their area fractions over (b) North American and (c) Eurasian SCZ, including the snow covered sensitivity zone (SCSZ) and snow covered non-sensitivity zones (SCNZ) as indicated by the arrows. The percentage under each bar chart is the trend significance for each 5° (N) of latitude (expressed as a confidence level (CL)).

which SCE trends were statistically significant for further analyses. For each month, we denoted these bands as snow cover sensitivity zones (SCSZs). For the remaining bands in the SCZs, there is no significant snow cover recession, and these bands are defined as snow covered non-sensitivity zones (SCNZs). In Figures 5.1(b) and 5.1(c), we use different gray-shaded arrows to highlight the North American and Eurasian SCZs, which include the SCSZs and SCNZs. For example, the SCSZ for May in North America has six latitude bands from $45-50^{\circ}\text{N}$ to $70-75^{\circ}\text{N}$, whereas there is only one band ($45-50^{\circ}\text{N}$) for the Eurasian SCSZ in April.

5.3.2. Experimental Design Based on SCE and SAT Trends

Trend tests were performed on the monthly time series of SCE and SAT area-averaged over the North America and Eurasia study zones. We used the non-parametric Mann-Kendall trend test (Mann 1945) for trend significance, and the Sen method (Sen 1968) to estimate their slopes. A 5% significance level (two-tailed test) was used. Tables 5.1 and 5.2 summarize the SCE and SAT trends and their significance levels in NSCZ, SCSZ,

and SCNZ for both continents from April through June for the entire study period (1972-2006). Table 5.1 shows that strong statistically significant ($p < 0.025$) negative trends were detected in SCE for both North American and Eurasian SCSZs, as found in many previous studies. In SCNZ, the decreasing trends in SCE are all non-significant, and the absolute values of trend slopes are much smaller than that in SCSZ. As reported in Table 5.2, increasing SAT trends were detected for both continents except for North America in May. For June in North America and for May and June in Eurasia, these SAT trends are statistically significant in NSCZ, SCSZ, and SCNZ. In SCNZ, increasing SAT trends are all statistically significant for both continents except for Eurasia in April.

Based on the above long-term trends in SCE and SAT for NSCZ, SCSZ, and SCNZ, it is clear that the impact of increasing SAT on SHC changes can be isolated in NSCZ as there is no presence of snow. In SCSZ, the effects of both SCE and SAT changes on SHC can be compared as indicated in Figure 5.2. By comparing SCSZ and SCNZ, we can investigate the effect of snow cover recession on SHC changes, as there is snow cover recession in SCSZ but none in SCNZ. In addition, it should be emphasized that the sizes of the rectangles in Figure 5.2 are not exactly proportional to the areas of each zone, but rather are variable for each month. Figure 5.3 shows the area percentages for NSCZ, SCSZ and SCNZ in North America and Eurasia from April through June. In Eurasia, the SCNZ dominates in April as there is no significant snow cover recession for most portions of the study domain. When snow cover retreats, the SCSZ and NSCZ in Eurasia expands significantly in May and June. Over North America, the NOAA-SCE

Table 5.1. Trend analyses for observed snow cover extent (SCE) in the snow covered sensitivity zone (SCSZ) and the snow covered non-sensitivity zone (SCNZ) over North America and Eurasia from April through June for the period 1972-2006. The significance level (p -value) was calculated using a two-sided Mann-Kendall trend test. Trend slope (ts) units are year⁻¹.

	North America						Eurasia					
	April		May		June		April		May		June	
	$p <$	ts	$p <$	ts	$p <$	ts	$p <$	ts	$p <$	ts	$p <$	ts
SCE-SCSZ	0.025	-0.0052	0.01	-0.0026	0.01	-0.0029	0.025	-0.0042	0.01	-0.0035	0.005	-0.0034
SCE-SCNZ	--	-0.0002	--	-0.0000	--	-0.0000	--	0.0003	--	-0.0010	--	-0.0006

Table 5.2. Trend analyses for CRU monthly surface air temperature (SAT) in the non-snow covered zone (NSCZ), SCSZ, and SCNZ over North America and Eurasia from April through June for the period 1972-2006. The significance level (p -value) was calculated using a two-sided Mann-Kendall trend test. Ts units are $^{\circ}\text{C year}^{-1}$.

	North America						Eurasia					
	April		May		June		April		May		June	
	$p <$	ts	$p <$	ts	$p <$	ts	$p <$	ts	$p <$	ts	$p <$	ts
SAT-NSCZ	--	0.0345	--	-0.0243	0.005	0.0323	--	0.0531	0.005	0.0663	0.005	0.0412
SAT-SCSZ	--	0.0400	--	0.0243	0.005	0.0415	--	0.0143	0.005	0.0500	0.005	0.0552
SAT-SCNZ	0.005	0.0657	0.005	0.0806	0.01	0.0467	--	0.0044	0.005	0.0435	0.005	0.0471

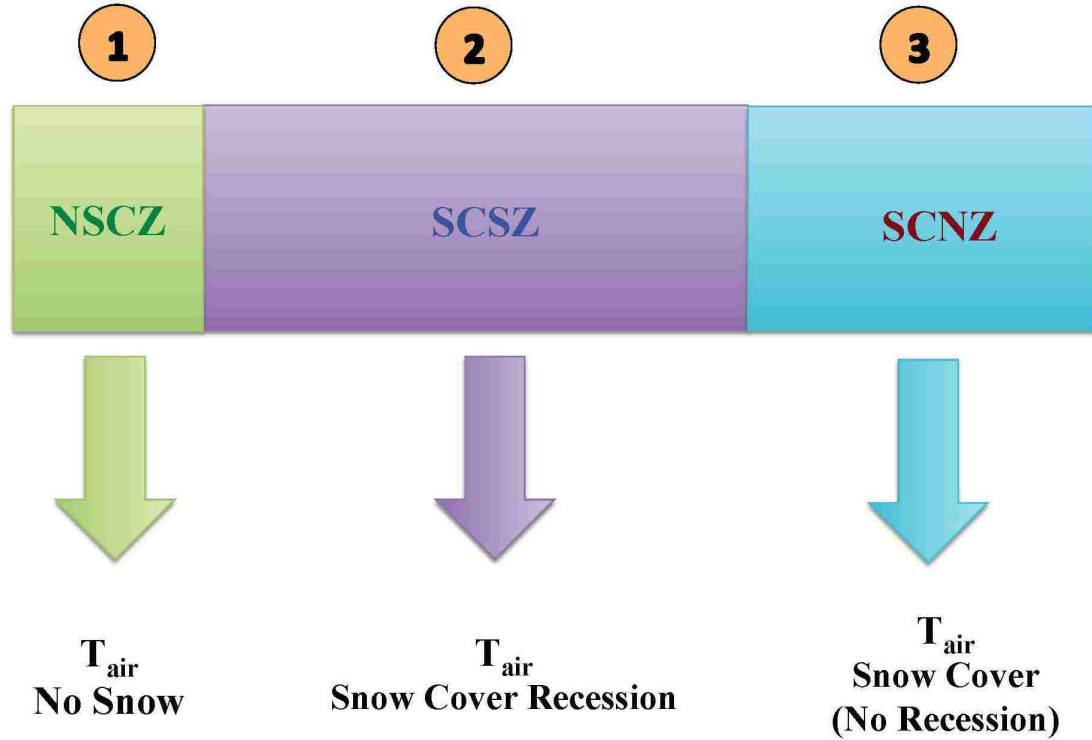


Figure 5.2. Experimental design for assessing the effects of pan-Arctic snow cover and air temperature changes on soil heat content (SHC) in NSCZ, SCSZ, and SCNZ over North America and Eurasia from April through June for the period 1972-2006.

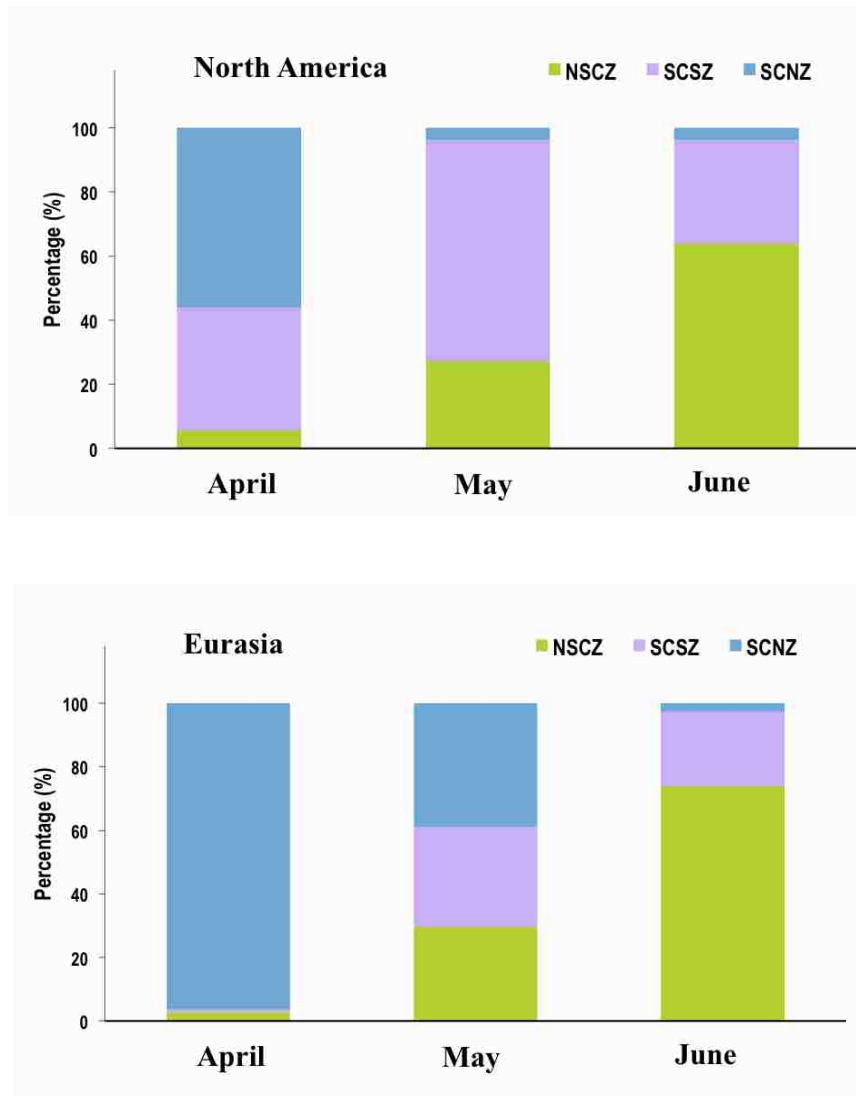


Figure 5.3. Area comparisons of NSCZ, SCSZ, and SCNZ in North America and Eurasia from April through June for the period 1972-2006.

recession occurs earlier than in Eurasia. Especially for May, most regions in North America have snow cover recession. In June, Figure 5.3 clearly illustrates that SCE is already gone for most portions of Eurasia.

5.3.3. SHC Trends

Recent studies by Troy et al. (2012) have shown that the VIC model is able to reproduce soil temperature profiles and can be used as a surrogate for (scarce) observations to estimate long-term changes in SHC. To maximize computational efficiency, the spacing of soil thermal nodes in the frozen soils framework in VIC should reflect the variability in soil temperature (Adam, 2007). Because the greatest variability in soil temperature occurs near the surface, it is preferable to have tighter node spacings near the surface and wider node spacings near the bottom boundary where temperature variability is reduced. Therefore, we used eighteen soil thermal nodes (STNs) distributed exponentially with depth as indicated in Table 5.3.

The SHC for each STN in the soil column was calculated for each model time step (three hours) and then aggregated for each month from April through June. Along the soil profile from the top to the bottom, the first STN was named as STN0 with a depth of 0 m indicating it is at the surface, while the deepest one is STN17 with a depth of 15 m. The SHC for STN17 represents an averaged thermal value for the soil profile. To simplify the analyses, we used the mean monthly SHC in 1970 as zero because the change in soil heat is relative to the datum chosen as described in Troy (2010). All monthly SHC values are relative to this datum. In addition, monthly SHC anomalies were calculated on the basis

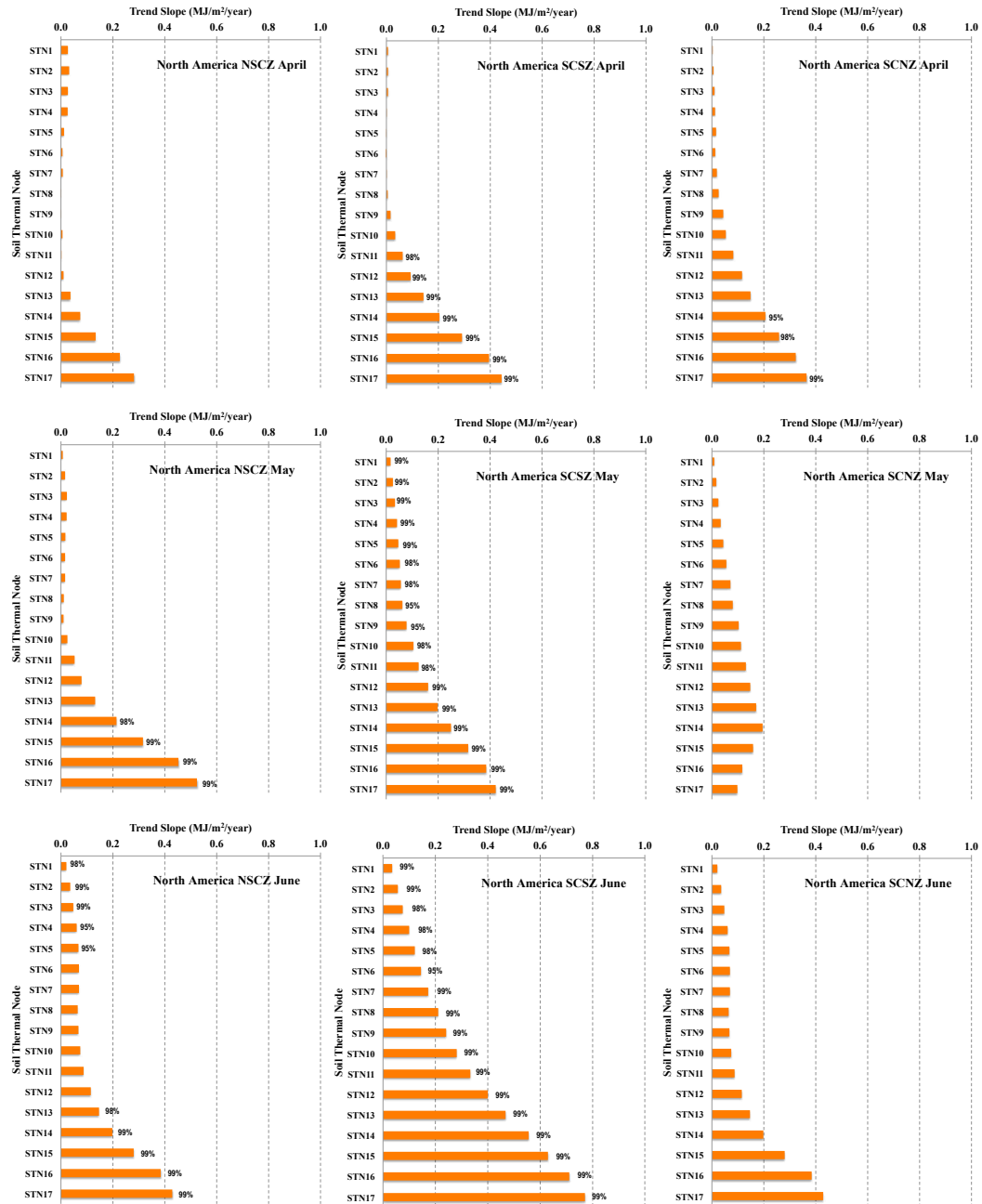
of monthly means averaged over each NSCZ, SCSZ and SCNZ of North America and Eurasia by removing the 1981-1990 mean. To examine long-term trends in the time series of monthly SHC anomalies, the Mann-Kendall trend test (significance level $p < 0.025$, two-sided test) and the Sen method as described above were applied. For each study zone, monotonic trend tests were performed on the monthly SHC anomalies averaged over each study zone for each soil thermal node.

Figure 5.4 shows the trends and significance levels of the VIC-derived SHC for each STN in NSCZ, SCSZ and SCNZ over North America and Eurasia from April through June. Figures 5.4a and 5.4b show that there are obvious differences for trends and significance levels between North America and Eurasia. For North America (Figure 5.4a), the SHC in SCSZ increases significantly from the top thermal nodes to the deeper ones, whereas in NSCZ and SCNZ, most thermal nodes have increasing trends, which are not statistically significant. Over Eurasia, this is quite different. In Figure 5.4b, almost all the thermal nodes in NSCZ, SCSZ, and SCNZ over Eurasia from April through June show statistically significant increasing trends in SHC, indicating that there are different effects of snow cover recession and increasing SAT on SHC changes between Eurasia and North America.

Table 5.3. Eighteen soil thermal nodes (STN) and their corresponding depth (m) from the surface. The first STN has a depth of 0 m indicating it is at the surface.

Soil Thermal Node	Depth (m)
STN0	0.0
STN1	0.2
STN2	0.4
STN3	0.6
STN4	0.9
STN5	1.3
STN6	1.7
STN7	2.1
STN8	2.7
STN9	3.3
STN10	4.1
STN11	5.1
STN12	6.1
STN13	7.3
STN14	8.8
STN15	10.6
STN16	12.6
STN17	15.0

(a)



(b)

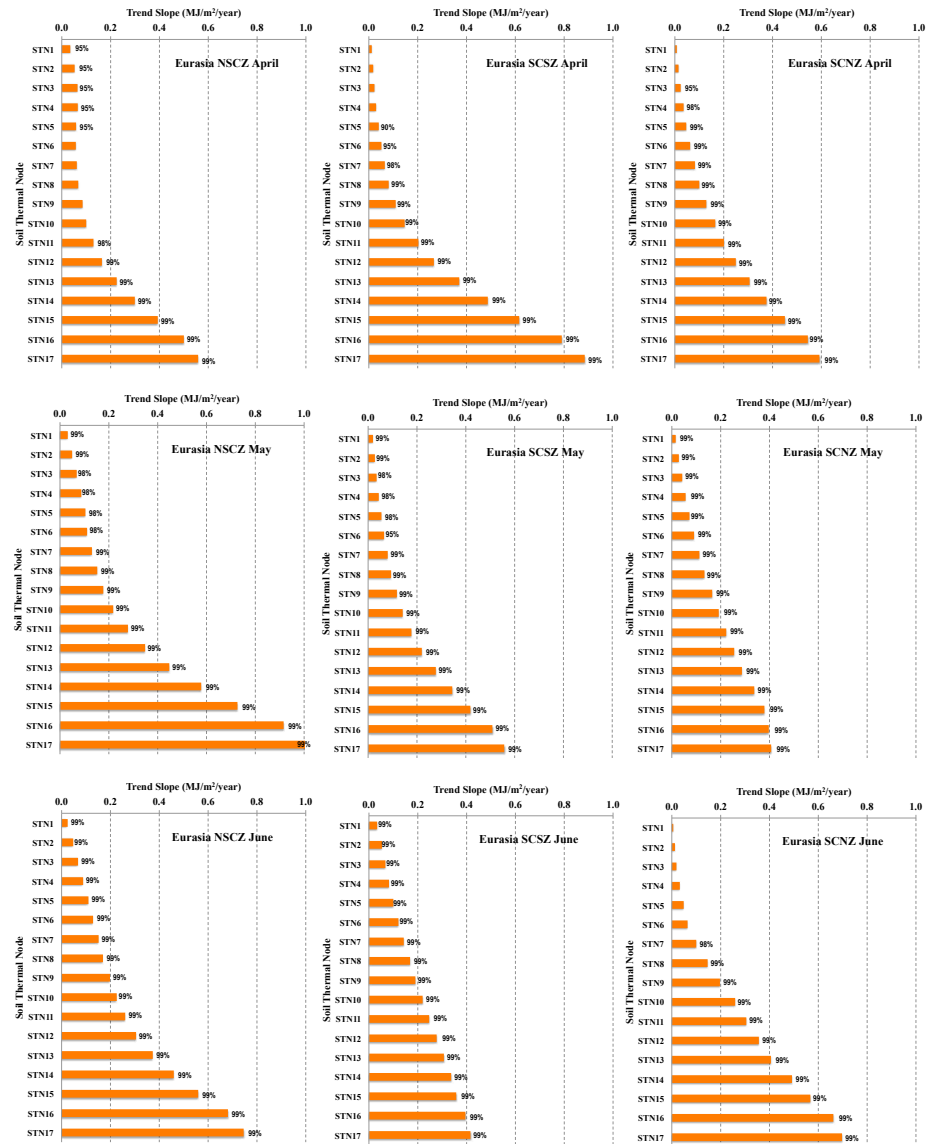


Figure 5.4. SHC trend results for time series averaged over thermal profiles from the surface to the depth indicated (soil thermal nodes) in NSCZ, SCSZ, and SCNZ over (a) North America and (b) Eurasia from April through June for the period 1972-2006. The significance level (expressed as a CL) was calculated using a two-sided Mann-Kendall trend test. Trend slope (ts) units are $\text{mJ m}^{-2} \text{year}^{-1}$.

5.3.4. Effects of SCE and SAT Changes on SHC

In order to identify the relative roles of snow cover recession and increasing SAT on pan-Arctic SHC changes, we examined the correlations among SHC, SCE, and SAT over NSCZ, SCSZ and SCNZ for both North America and Eurasia. The Pearson's product-moment correlation coefficient was computed separately for each study zone from April through June. Given the 35-year record, correlations are statistically significant at a level of $p < 0.025$ (two-sided) when the absolute value of the sample correlation is greater than 0.34 based on the Student t-test with 33 degrees of freedom. Figure 5.5 shows correlations between observed SCE and VIC-derived SHC in NSCZ, SCSZ, and SCNZ over North America and Eurasia from April through June. In SCSZ, the correlations between SHC and SCE are all statistically significant over both continents from April through June. Over SCNZ, however, the correlations are much smaller and have no statistical significance. These results imply that the static snow cover insulation in SCNZ has a non-significant impact on SHC changes over the pan-Arctic. Additionally, no correlation exists between SHC and SCE in NSCZ. Furthermore, the implied impact of snow cover changes on SHC is similar for North America and Eurasia.

Figure 5.6 shows correlations between observed SAT and simulated SHC monthly time series in NSCZ, SCSZ, and SCNZ over North America and Eurasia from April through June. Overall, the results indicate that SAT has a significant impact on SHC changes in

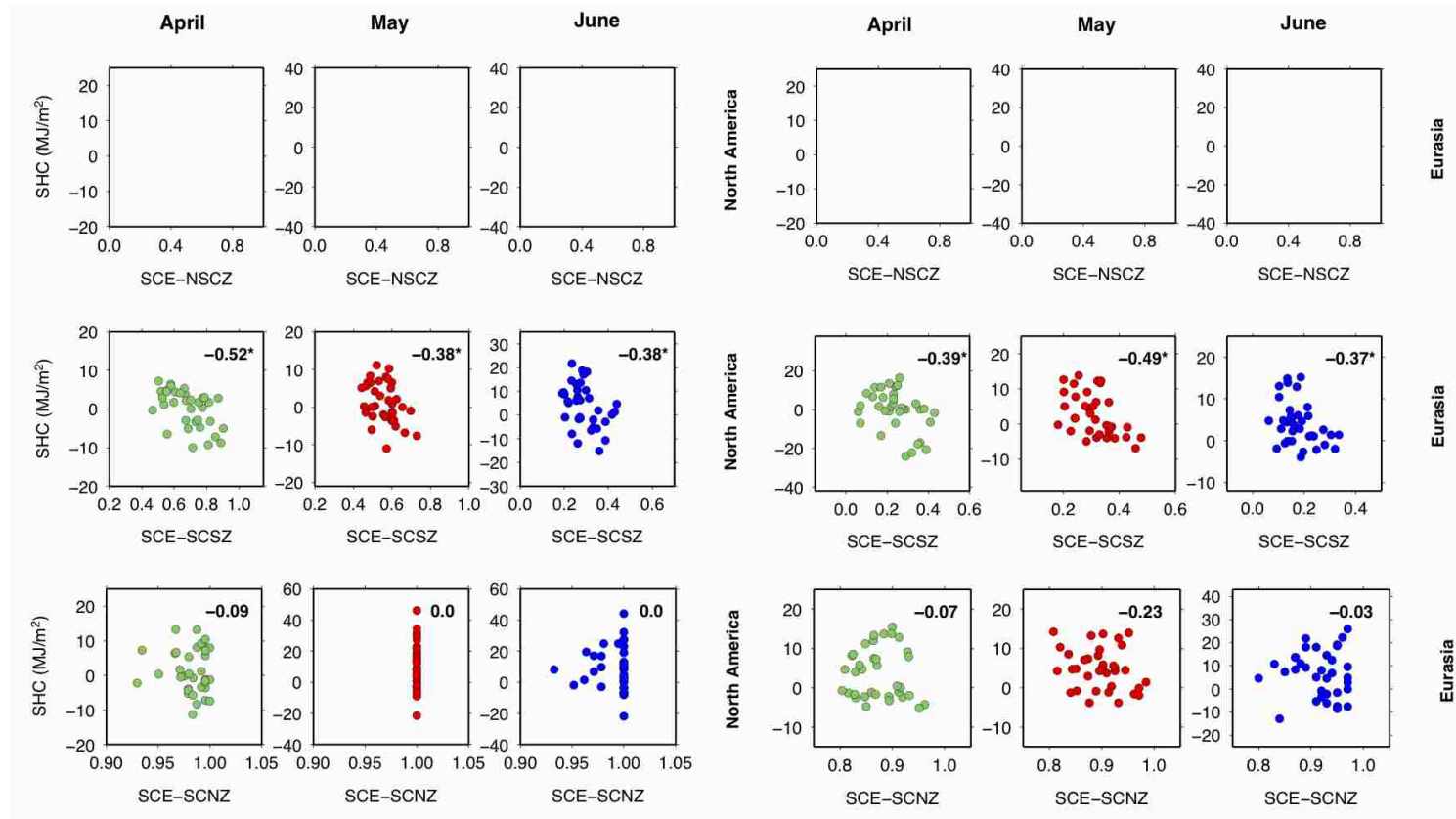


Figure 5.5. Correlations between NOAA-SCE and simulated SHC in NSCZ, SCSZ, and SCNZ over North America and Eurasia from April through June for the period 1972-2006. The correlation with asterisks is statistically significant at a level of $p < 0.025$ when its absolute value is greater than 0.34.

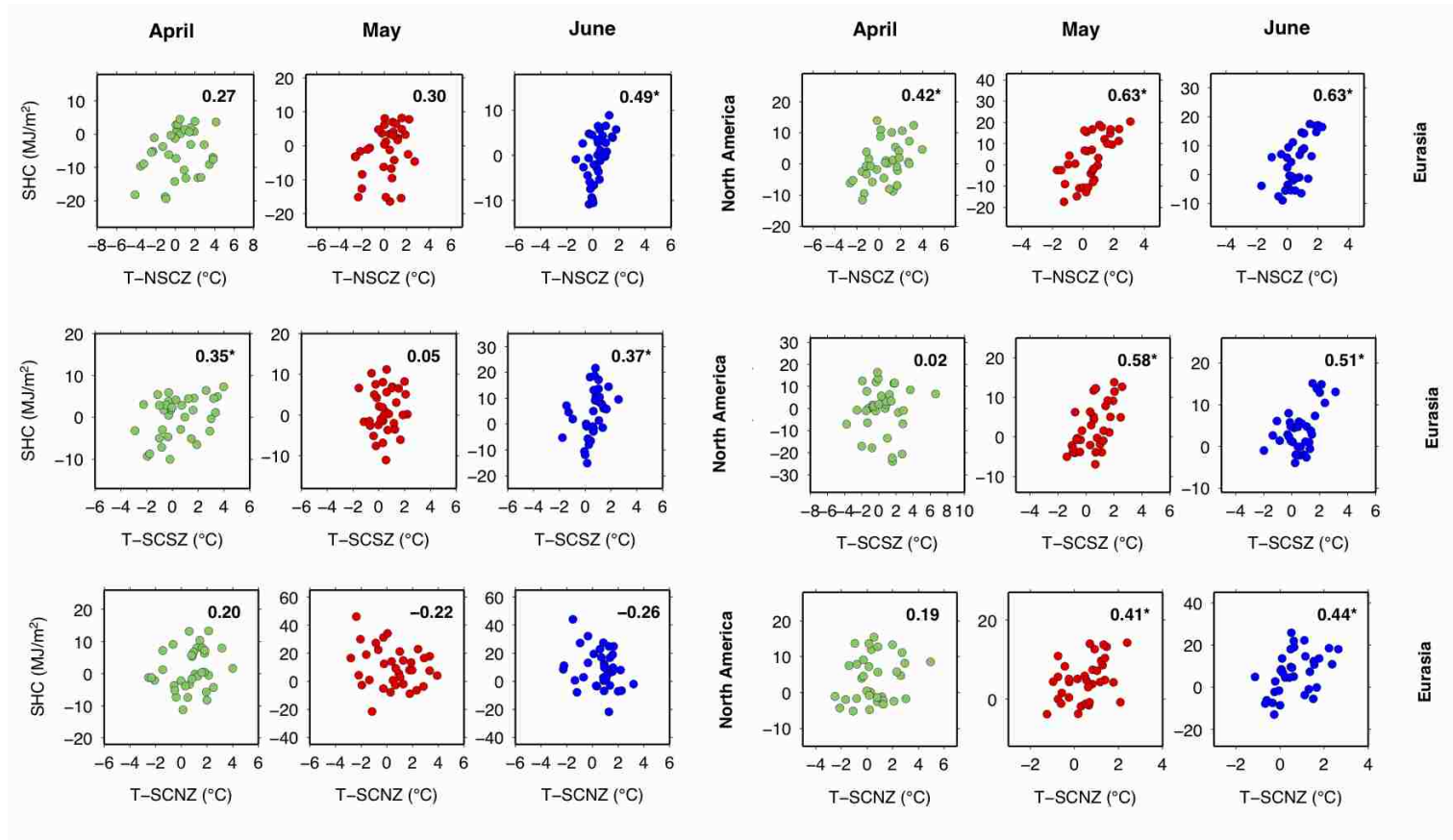


Figure 5.6. Correlations between observed SAT and simulated SHC in NSCZ, SCSZ and SCNZ over North America and Eurasia from April through June for the period 1972-2006. The correlation with asterisks is statistically significant at a level of $p < 0.025$ when its absolute value is greater than 0.34.

NSCZ. Moreover, SAT has greater influence on SHC over Eurasia than in North America as shown in Figure 5.6. All the correlations over Eurasia are statistically significant except for SCSZ and SCNZ in April, for which the increasing trends in SAT are not statistically significant.

The correlations described in Figures 5.5 and 5.6 were calculated on the time series of variables using the Pearson's product-moment method. Both the effects of secular trend and variability are included. We separated these two components and explored the relative roles of the linear trend and the variability (detrended) in the corresponding correlations. Table 5.4 summarizes correlation coefficients due to the linear trend and the variability between SHC derived from VIC and NOAA-SCE observations in SCSZ and SCNZ over North America and Eurasia for the period 1972-2006. The significance level (p -value) was calculated using a two-tailed Student t -test with 33 degrees of freedom. Basically, SHC and NOAA-SCE in NSCZ, SCSZ, and SCNZ are highly correlated due to the secular trend, except for May and June in SCNZ over North America, where the NOAA-SCE trends are zero. In contrast, the variability components are small without statistical significance. Obviously, the relationships between SHC and NOAA-SCE time series are mainly dominated by snow cover changes in each study zone over North America and Eurasia. We also applied the same analyses for the VIC-derived SHC and

Table 5.4. Correlation coefficients due to the linear trend and variability for SHC derived from VIC and NOAA-SCE observations in SCSZ and SCNZ over North America and Eurasia from April to June for the period 1972-2006. The significance level (p -value) was calculated using a two-tailed Student t-test with 33 degrees of freedom.

			April		May		June	
			$p <$	r	$p <$	r	$p <$	r
Correlation (Trend)	North America	SCSZ	0.025	-0.9	0.025	-0.7	0.025	-0.8
		SCNZ	0.025	-0.5	--	0.0	--	0.0
	Eurasia	SCSZ	0.025	-0.9	0.025	-1.0	0.025	-0.8
		SCNZ	0.025	0.9	0.025	-0.7	0.025	-0.7
Correlation (Variability)	North America	SCSZ	--	-0.2	--	-0.1	--	0.0
		SCNZ	--	0.0	--	0.0	--	0.0
	Eurasia	SCSZ	--	-0.0	--	-0.0	--	0.1
		SCNZ	--	-0.1	--	-0.1	--	0.1

Table 5.5. Correlation coefficients due to the linear trend and variability for SHC derived from VIC and CRU SAT in NSCZ, SCSZ, and SCNZ over North America and Eurasia from April to June for the period 1972-2006. The significance level (p-value) was calculated using a two-tailed Student t-test with 33 degrees of freedom.

			April		May		June	
			<i>p</i> <	<i>r</i>	<i>p</i> <	<i>r</i>	<i>p</i> <	<i>r</i>
Correlation (Trend)	North America	NSCZ	0.025	0.3	0.025	-0.7	0.025	0.7
		SCSZ	0.025	0.9	0.025	0.7	0.025	0.8
		SCNZ	0.025	0.5	--	0.0	--	0.0
	Eurasia	NSCZ	0.025	0.9	0.025	1.0	0.025	1.0
		SCSZ	0.025	0.9	0.025	1.0	0.025	0.8
		SCNZ	0.025	1.0	0.025	0.7	0.025	0.7
Correlation (Variability)	North America	NSCZ	--	0.2	0.025	0.4	--	0.37
		SCSZ	--	0.1	--	-0.2	--	-0.1
		SCNZ	--	-0.0	--	-0.2	--	-0.2
	Eurasia	NSCZ	--	0.2	--	0.1	--	0.2
		SCSZ	--	0.0	--	0.2	--	0.1
		SCNZ	--	0.1	--	0.1	--	0.1

CRU SAT, as reported in Table 5.5. The linear trends in SAT dominate the correlations between SHC derived from VIC and CRU SAT in NSCZ, SCSZ, and SCNZ over North America and Eurasia for the period 1972-2006. In contrast, the effect of SAT variability is weak and not statistically significant. Therefore, the relationships between SHC and SAT time series as shown in Figure 5.6 are mainly due to increasing SAT in each study zone over North America and Eurasia.

As described above, SHC changes are significantly affected by snow cover recession and increasing SAT from April through June over North America and Eurasia for the period 1972-2006. But the variability in NOAA-SCE and SAT has a insignificant effect on SHC.

Comparing the correlations in Figures 5.5 and 5.6 suggests that: (1) snow cover recession has a significant impact on SHC changes in SCSZ, which is similar for both continents; (2) SHC changes in SCSZ over North America during late spring and early summer are dominated by snow cover recession rather than increasing SAT; (3) over Eurasia, increasing SAT more strongly affects SHC than in North America; and (4) overall, increasing SAT has the greatest influence on SHC for North America and Eurasia, and reduced SCE plays a secondary role, which is only significant in SCSZ.

5.4. Conclusions

We defined three study zones (NSCZ, SCSZ, and SCNZ) within the North American and Eurasian portions of the pan-Arctic land area based on observed SCE trends. Using these definitions of zones, we focused on the effects of pan-Arctic snow cover and air temperature changes on SHC by exploring long-term trends in SHC, SCE, and SAT and their

corresponding correlations in NSCZ, SCSZ, and SCNZ for North America and Eurasia. We find that North American and Eurasian late spring and early summer (from April through June) SHC has increasing trends for the period 1972-2006. However, there are obvious differences between North America and Eurasia as to the magnitudes of SHC trend slopes and significance levels. For North America, SHC in SCSZ has mostly increased significantly, whereas in NSCZ and SCNZ, most thermal nodes show non-significant increasing trends. For Eurasia, almost all the thermal nodes in NSCZ, SCSZ, and SCNZ have statistically significant increasing trends, indicating that there are different effects of snow cover recession and increasing SAT on SHC changes between North America and Eurasia. By analyzing the corresponding correlations, we conclude that snow cover recession has a significant impact on SHC changes in SCSZ for North America and Eurasia from April through June. SHC changes in SCSZ over North America are dominated by snow cover recession rather than increasing SAT. Over Eurasia, increasing SAT more strongly affects SHC than in North America. Overall, increasing SAT during late spring and early summer has the greatest influence on SHC changes over the pan-Arctic, and reduced SCE plays a secondary role, which is only significant in SCSZ.

6. Conclusions

This dissertation has sought to investigate the possible causes of snow cover changes and their corresponding impact on frozen soils over the pan-Arctic region. In **Chapter 1**, I posed four research questions that motivated the research reported in **Chapters 2-5**. The first research question is “*To what extent are satellite data, reanalysis products and land surface model simulations consistent with in situ measurements of surface radiative fluxes over the pan-Arctic land region? What is the consistency of dominant temporal and spatial variability of these fluxes at the regional scale? Are there significant trends in these surface radiation fluxes?*” In **Chapter 2**, I showed that reanalysis products provide better estimates of the DSW diurnal cycle than do satellite products and a temperature index scheme based on station data. At the regional scale, all data sets have similar temporal patterns except for DLW in ISCCP and snow season albedo. In terms of dominant spatial variability, all data sets show large variability over the pan-Arctic. In addition, DSW and DLW show a similar latitudinal gradient. However, differences in albedo suggest a need for improvement of the reanalysis products. For a small number of stations with relatively long records, we analyzed long-term trends in DSW and found a turning point between 1985 and 1990. Before that, a dimming period exists, whereas brightening occurred thereafter.

The second research question I posed in **Chapter 1** is “*What are the relative roles of surface energy fluxes in snow cover changes over the pan-Arctic land region? Which are most responsible for the observed spring and summer SCE recession?*”. In **Chapter 3**, I showed

that ΔSNR is the primary energy source and ΔSH plays a secondary role in changes of SCE. Compared with ΔSNR and ΔSH , ΔLH has a minor influence on pan-Arctic snow cover changes.

The third research question I posed in **Chapter 1** is “*To what degree can a land surface model reconstruct spatial and temporal changes of SCE compared with corresponding satellite products? What are the relationships between snow cover and hydroclimate changes over each snow cover sensitivity zone for North America and Eurasia?*”. In **Chapter 4**, I showed that the Variable Infiltration Capacity (VIC) land surface hydrology model is able to reconstruct spatial and temporal changes of observed SCE over the pan-Arctic region. In the North American and Eurasian SCSZs, the relative roles of surface energy fluxes in snow cover changes are consistent with our previous findings. In addition, these changes in surface energy fluxes resulting in the pan-Arctic snow cover recession are mainly driven by statistically significant decreases in snow surface albedo and increased air temperatures, as well as statistically significant increased atmospheric water vapor pressure.

Finally, the fourth research question posed in **Chapter 1** is “*Are there significant trends in SHC over soil profiles? What are the effects of snow cover and air temperatures changes on SHC over the pan-Arctic land area?*”. In **Chapter 5**, I showed that North American and Eurasian late spring and early summer SHC has increasing trends for the period 1972-2006. However, there are obvious differences between North America and Eurasia as to the magnitudes of SHC trend slopes and significance levels. For North America, SHC in SCSZ has mostly increased significantly, whereas in NSCZ and SCNZ, most thermal nodes show non-significant increasing trends. For Eurasia, almost all the thermal nodes in NSCZ, SCSZ, and

SCNZ have statistically significant increasing trends, indicating that there are different effects of snow cover recession and increasing SAT on SHC changes between North America and Eurasia. By analyzing the corresponding correlations, I found that increasing SAT during late spring and early summer has the greatest influence on SHC changes over the pan-Arctic region, and reduced SCE plays a secondary role, which is only significant in SCSZ.

My dissertation provides insights into the reasons and potential impacts of historical snow cover changes over the pan-Arctic domain. Future work that could build from the studies reported here could proceed in several directions, of which I outline three here. First, an obvious extension to the work reported in Chapter 5 would focus on future changes in frozen soil heat content using climate model projections, and might investigate climate-induced changes on the interactions between snow cover extent and frozen soil heat content. Secondly, an issue of practical importance is the effect of snow cover recession on streamflow at the river basin level. A third direction would assess how permafrost and seasonally frozen ground are responding to climate change, and how these processes affect streamflow generation over large spatial scales.

Notwithstanding that the primary focus of my work is on technical issues associated with trends in high latitude moisture and energy fluxes, the work has broader implications that deserve mention. The importance of snow to high latitude energy fluxes, especially as a result of strong contrasts between the albedo of snow covered and snow free surfaces and hence the potential for positive climate impacts as the high latitudes warm, is well known. Furthermore, the low thermal conductivity of snow insulates the ground, and resultant contrasts in the snow surface temperature as contrasted with bare ground affect the transfer of heat to and from the

atmosphere (Barry et al. 2008). These factors can influence the climate not only of high latitude regions, but also, via teleconnections, of lower latitudes. More directly though, changes in snow cover patterns have major effects on water availability, industry, agriculture, and infrastructure and affect the livelihoods of the inhabitants of high latitude land regions. One of the most dramatic impacts of changing snow cover is on water resources. For example, over much of the pan arctic region, snow cover is the source of most streamflow, and hence water supplies. Melting of snow cover also is the source of water stored in the vast areas of lakes and wetlands across the region, which provide critical wildlife and fish habitat that provide sustenance for native people. Furthermore, certain industries depend heavily on snow cover and frozen soils. Oil and gas companies, for example, use ice roads in the Arctic to gain access to resource fields, and are negatively impacted by permafrost changes. Other industries would benefit from less snow, through reduced snow-removal costs. Another impact of snow cover changes is increased heat storage in frozen soils, which ultimately results in permafrost thawing. Thawing permafrost already has affected the stability of infrastructure over parts of the pan-Arctic domain, such as buildings, roads, railways, and pipelines. All of these potential impacts are related to the interaction of snow cover and soil freeze-thaw processes, and point to the importance of work like that reported herein in a broader context.

References

- ACIA, 2005: *Arctic Climate Impact Assessment*. Cambridge University Press, NY, 1042 pp.
- Adam, J. C., 2007: Understanding the causes of streamflow changes in the Eurasian Arctic. Ph.D. thesis, University of Washington, WA, 174pp.
- Adam, J. C., and D. P. Lettenmaier, 2003: Adjustment of global gridded precipitation for systematic bias. *J. Geophys. Res.*, **108**, 1-14.
- Adam, J. C., and D. P. Lettenmaier, 2008: Application of new precipitation and reconstructed streamflow products to streamflow trend attribution in northern Eurasia. *J. Climate*, **21**, 1807-1828.
- Adam, J. C., E. A. Clark, D. P. Lettenmaier, and E. F. Wood, 2006: Correction of global precipitation products for orographic effects. *J. Climate*, **19**, 15-38.
- Adam, J. C., I. Haddeland, F. Su, and D. P. Lettenmaier, 2007: Simulation of reservoir influences on annual and seasonal streamflow changes for the Lena, Yenisei, and Ob' rivers. *J. Geophys. Res.*, **112**, D24114.
- Allan, R. P., M. A. Ringer, J. A. Pamment, and A. Slingo, 2004: Simulation of the Earth's radiation budget by the European Centre for Medium-Range Weather Forecasts 40-year reanalysis (ERA40). *J. Geophys. Res.*, **109**, D18107, doi:10.1029/2004JD004816.
- Anderson, E. A., 1976: A point energy and mass balance model of a snow cover. NOAA Tech. Rep. ERL402-NHELM2, 91 pp.
- Andreadis, K. M., P. Storck, and D. P. Lettenmaier, 2009: Modeling snow accumulation and ablation processes in forested environments. *Water Resour. Res.*, **45**, W05429, doi:10.1029/2008WR007042.

- Armstrong, R. L., and M. J. Brodzik, 2007: Northern Hemisphere EASE-Grid weekly snow cover and sea ice extent version 3.1. National Snow and Ice Data Center, Boulder, CO, digital media. [Available online at <http://nsidc.org/data/nsidc-0046.html>.]
- Baker, D. G., D. L. Ruschy, R. H. Skaggs, and D. B. Wall, 1992: Air temperature and radiation depressions associated with a snow cover. *J. Appl. Meteorol.*, **31**, 247-254.
- Barry, R. G., R. Armstrong, T. Callaghan, J. Cherry, S. Gearheard, A. Nolin, D. Russell, and C. Zaeckler, 2007: *Chapter 4: Snow. In Global outlook for ice and snow*, ed. United Nations Environment Programme, 39-62, Hertfordshire, England.
- Bartlett, M. G., D. S. Chapman, and R. N. Harris, 2004: Snow and the ground temperature record of climate change. *J. Geophys. Res.*, **109**, F04008, doi:10.1029/2004JF000224.
- Bartlett, M. G., D. S. Chapman, and R. N. Harris, 2005: Snow effect on North American ground temperatures, 1950-2002. *J. Geophys. Res.*, **110**, F03008, doi:10.1029/2005JF000293.
- Bekryaev, R. V., I. V. Polyakov, and V. A. Alexeev, 2010: Role of polar amplification in long-term surface air temperature variations and modern Arctic warming. *J. Climate*, **23**, 3888-3906.
- Beltrami, H., E. Bourlon, L. Kellman, and J. F. Gonzales-Rouco, 2006: Spatial patterns of ground heat gain in the Northern Hemisphere. *Geophys. Res. Lett.*, **33**, L06717, doi:10.1029/2006GL025676.
- Beltrami, H., J. Smerdon, H. N. Pollack, and S. Huang, 2002: Continental heat gain in the global climate system. *Geophys. Res. Lett.*, **29**(8), 1167, doi:10.1029/2001GL014310.

- Betts, A. K., M. Köhler, and Y. Zhang, 2009: Comparison of river basin hydrometeorology in ERA-Interim and ERA-40 reanalyses with observations. *J. Geophys. Res.*, **114**, D02101, doi:10.1029/2008JD010761.
- Betts, A. K., M. Zhao, P. A. Dirmeyer, and A. C. M. Beljaars, 2006: Comparison of ERA40 and NCEP/DOE near-surface data sets with other ISLSCP-II data sets. *J. Geophys. Res.*, **111**, D22S04, doi:10.1029/2006JD007174.
- Boike, J., K. Roth, and O. Ippisch, 2003: Seasonal snow cover on frozen ground: Energy balance calculations of a permafrost site near Ny-Ålesund, Spitsbergen. *J. Geophys. Res.*, **108**, 8163.
- Bras, R. L., 1990: *Hydrology: An Introduction to Hydrologic Science*. Addison-Wesley Reading, Massachusetts, USA, 643pp.
- Brohan, P., J. Kennedy, I. Harris, S. Tett, and P. Jones, 2006: Uncertainty estimates in regional and global observed temperature changes: a new dataset from 1850. *J. Geophys. Res.*, **111**, D12106.
- Brown, R. D., 2000: Northern Hemisphere snow cover variability and change, 1915-97. *J. Climate*, **13**, 2339-2355.
- Brown, R., and D. A. Robinson, 2011: Northern Hemisphere spring snow cover variability and change over 1922–2010 including an assessment of uncertainty. *The Cryosphere*, **5**, 219-229.
- Brown, R., and P. W. Mote, 2009: The response of Northern Hemisphere snow cover to a changing climate. *J. Climate*, **22**, 2124-2145.
- Brown, R., C. Derksen, and L. Wang, 2007: Assessment of spring snow cover duration variability over northern Canada from satellite datasets. *Remote Sens. Environ.*, **111**,

367-381.

- Brown, R., C. Derksen, and L. Wang, 2010: A multi-data set analysis of variability and change in Arctic spring snow cover extent, 1967-2008. *J. Geophys. Res.*, **115**, D16111.
- Bowling, L. C., and D. P. Lettenmaier, 2010: Modeling the effects of lakes and wetlands on the water balance of arctic environments. *J. Hydrometeorol.*, **11(2)**, 276-295.
- Bowling, L. C., J. W. Pomeroy, and D. P. Lettenmaier, 2004: Parameterization of blowing-snow sublimation in a macroscale hydrology model. *J. Hydrometeorol.*, **5**, 745-762.
- Bowling, L. C., and Coauthors, 2003: Simulation of high-latitude hydrological processes in the Torne–Kalix basin: PILPS Phase 2(e): 1: Experimental description and summary intercomparisons. *Global Planet. Change*, **38**, 1–30.
- Brest, C. L., W. B. Rossow, and M. D. Roiter, 1997: Update of radiance calibrations for ISCCP. *J. Atmos. Oceanic Tech.*, **14**, 1091-1109,
- Bromwich, D. H., R. L. Fogt, K. I. Hodges, and J. E. Walsh, 2007: A tropospheric assessment of the ERA-40, NCEP, and JRA-25 global reanalyses in the polar regions. *J. Geophys. Res.*, **112**, D10111, doi:10.1029/2006JD007859.
- Brotzge, J. A., 2004: A two-year comparison of the surface water and energy budgets between two OASIS sites and NCEP-NCAR reanalysis data. *J. Hydrometeorol.*, **5(2)**, 311-326.
- Bulygina, O. N., V. N. Razuvaev, and N. N. Korshunova, 2009: Changes in snow cover over Northern Eurasia in the last few decades. *Environ. Res. Lett.*, **4**, 045026.
- Chapin, F. S., and Coauthors, 2005: Role of land-surface changes in Arctic summer warming. *Science*, **310**, 657-660.
- Cherkauer, K. A., and D. P. Lettenmaier, 1999: Hydrologic effects of frozen soils in the upper Mississippi River basin. *J. Geophys. Res.*, **104**, 19599-19610.

- Cherkauer, K. A., and D. P. Lettenmaier, 2003: Simulation of spatial variability in snow and frozen soil. *J. Geophys. Res.*, **108**, 8858.
- Choi, G., D. A. Robinson, and S. Kang, 2010: Changing Northern Hemisphere snow seasons. *J. Climate*, **23**, 5305-5310.
- Clark, M. P., M. C. Serreze, and D. A. Robinson, 1999: Atmospheric controls on Eurasian snow extent. *Int. J. Climatol.*, **19**, 27-40.
- Cline, D. W., 1997: Snow surface energy exchanges and snowmelt at a continental, midlatitude Alpine site. *Water Resour. Res.*, **33**, 689-701.
- Dai, A., 2006: Recent climatology, variability and trends in global surface humidity. *J. Climate*, **19**, 3589-3606.
- Derksen, C., and R. D. Brown, 2011: Terrestrial snow (Arctic) in state of the climate in 2010. *Bull. Am. Meteorol. Soc.*, **92**, S154-S155.
- Derksen, C., and R. D. Brown, 2012: Spring snow cover extent reductions in the 2008-2012 period exceeding climate model projections, *Geophys. Res. Lett.*, doi:10.1029/2012GL053387, in press.
- Derksen, C., R. D. Brown, and L. Wang, 2010: Terrestrial snow (Arctic) in state of the climate in 2009. *Bull. Am. Meteorol. Soc.*, **91**, S93-S94.
- Déry, S. J., and R. D. Brown, 2007: Recent Northern Hemisphere snow cover extent trends and implications for the snow-albedo feedback. *Geophys. Res. Lett.*, **34**, L22504, doi: 10.1029/2007GL031474.
- Déry, S. J., J. Sheffield, and E. F. Wood, 2005: Connectivity between Eurasian snow cover extent and Canadian snow water equivalent and river discharge. *J. Geophys. Res.*, **110**, D23106, doi: 10.1029/2005JD006173.

- Dye, D. G., 2002: Variability and trends in the annual snow-cover cycle in Northern Hemisphere land areas, 1972-2000. *Hydrol. Processes*, **16**, 3065–3077.
- Dyer, J. L., and T. L. Mote, 2002: Role of energy budget components on snow ablation from a mid-latitude prairie snowpack. *Polar Geogr.*, **26**, 87-115.
- Dyer, J. L., and T. L. Mote, 2007: Trends in snow ablation over North America. *Int. J. Climatol.*, **27**, 739-748.
- Flanner, M., C. Zender, P. Hess, N. Mahowald, T. Painter, V. Ramanathan, and P. Rasch, 2009: Springtime warming and reduced snow cover from carbonaceous particles. *Atmos. Chem. Phys.*, **9**, 2481-2497.
- Frauenfeld, O. W., T. Zhang, R. G. Barry, and D. Gilichinsky, 2004: Interdecadal changes in seasonal freeze and thaw depths in Russia. *J. Geophys. Res.*, **109**, D05101, doi:10.1029/2003JD004245
- Frei, A., and D. A. Robinson, 1999: Northern Hemisphere snow extent: Regional variability 1972-1994. *Int. J. Climatol.*, **19**, 1535-1560.
- Gates, D., 1980: *Biophysical Ecology*. Springer-Verlag, 611 pp.
- Gibson, J. K., P. Ka'llberg, S. Uppala, A. Hernandez, A. Nomura, and E. Serrano, 1999: *ERA-15 description, ECMWF Re-analysis. Proj. Rep.1, vers. 2*, Eur. Cent. for Medium-Range Weather Forecasts, Bracknell, U. K.
- Gilgen, H., M. Wild, and A. Ohmura, 1998: Means and trends of shortwave irradiance at the surface estimated from GEBA. *J. Climate*, **11**, 2042- 2061.
- Gold, L. W., 1963: Influence of snow cover on the average annual ground temperature at Ottawa, Canada. *IAHS Publ.*, **61**, 82-91.
- Goodrich, L. E., 1982: The influence of snow cover on the ground thermal regime. *Canadian*

Geotechnical J., **24**, 160-163.

Graversen, R. G., and M. Wang, 2009: Polar amplification in a coupled climate model with locked albedo. *Clim. Dyn.*, **33**(5), 629-643.

Gray, D. M. and D.H. Male 1981: *Handbook of Snow: Principles, Processes, Management and Use*. Pergamon Press, 776 pp.

Gray, D. M., and T. D. Prowse, 1993: *Snow and floating ice*. Vol. 7, McGraw-Hill: New York, 7.1-7.58.

Groisman, P. Y., T. R. Karl, R. W. Knight, and G. L. Stenchikov, 1994: Changes of snow cover, temperature, and radiative heat balance over the Northern Hemisphere. *J. Climate*, **7**, 1633-1656.

Hansen, J., and Coauthors, 2005: Earth's energy imbalance: Confirmation and implications. *Science*, **308**, 1431-1435.

Held, I., and B. Soden, 2000: Water vapor feedback and global warming. *Annu. Rev. Energy Environ.*, **25**, 441-475.

Hinzman, L. D., and D. L. Kane, 1992: Potential response of an Arctic watershed during a period of global warming. *J. Geophys. Res.*, **97**, 2811-2820.

Heimann, M., and M. Reichstein, 2008: Terrestrial ecosystem carbon dynamics and climate feedbacks. *Nature*, **451**, 289-292.

Hinzman, L., D. Kane, and R. Gieck, 1991: Regional snow ablation in the Alaskan Arctic. *Northern Hydrology: Selected Perspectives*, 122-139.

Hinzman, L. D., and Coauthors, 2005: Evidence and implications of recent climate change in northern Alaska and other arctic regions. *Climatic Change*, **72**, 251-298.

- Hirsch, R. M., J. R. Slack, and R. A. Smith, 1982: Techniques of trend analysis for monthly water-quality data. *Water Resour. Res.*, **18**, 107-121.
- Holland, M. M., C. M. Bitz, and B. Tremblay, 2006: Future abrupt reductions in the summer Arctic sea ice. *Geophys. Res. Lett.*, **33**, L23503, doi:10.1029/2006GL028024.
- Hollingsworth, A., and C. Pfrang, 2005: A preliminary survey of ERA-40 users developing applications of relevance to GEO (Group on Earth Observations). *ECMWF Newsletter*, **No. 104**, ECMWF, Reading, United Kingdom, 5-9.
- Isaac, V., and W. A. van Wijngaarden, 2012: Surface water vapor pressure and temperature trends in North America during 1948-2010. *J. Climate*, **25**, 3599-3609.
- Iwata, Y., M. Hayashi, and T. Hirota, 2008: Effects of snow cover on soil heat flux and freeze-thaw processes. *J. Agric. Meteorol.*, **64**, 301-308.
- Jol, A., F. Raes, and B. Menne, 2009: Impacts of Europe's changing climate-2008 indicator based assessment. *Earth Environ. Sci.*, **6**, 292042.
- Jones, P. D., and A. Moberg, 2003: Hemispheric and large-scale surface air temperature variations: An extensive revision and an update to 2001. *J. Climate*, **16**, 206-223.
- Kalnay, E., and Coauthors, 1996: The NCEP/NCAR 40-year reanalysis project. *Bull. Am. Meteorol. Soc.*, **77**, 437-471.
- Karl, T. R., P. Y. Groisman, R. W. Knight, and R. Heim, 1993: Recent variations of snow cover and snowfall in North America and their relation to precipitation and temperature variations. *J. Climate*, **6**, 1327-1344.
- Kimball, J., S. Running, and R. Nemani, 1997: An improved method for estimating surface humidity from daily minimum temperature. *Agr. Forest Meteorol.*, **85**, 87-98.
- Koivusalo, H., and T. Kokkonen, 2002: Snow processes in a forest clearing and in a coniferous

- forest. *J. Hydrol.*, **262**, 145-164.
- Kuusisto, E., 1986: The energy balance of a melting snow cover in different environment. in *Modeling Snowmelt-Induced Processes IAHS Publication, No.155*, Wallingford, Oxfordshire, UK: IAHS Press, 37-45.
- Lawrence, D. M., and A. G. Slater, 2010: The contribution of snow condition trends to future ground climate. *Clim. Dyn.*, **34**, 969-981, doi:10.1007/s00382-009-0537-4.
- Leathers, D. J., D. Graybeal, T. Mote, A. Grundstein, and D. Robinson, 2004: The role of airmass types and surface energy fluxes in snow cover ablation in the central Appalachians. *J. Appl. Meteorol.*, **43**, 1887-1899.
- Levitus, S., J. Antonov, and T. Boyer, 2005: Warming of the world ocean, 1955-2003. *Geophys. Res. Lett.*, **32**, L02604, doi:10.1029/2004GL021592.
- Levitus, S., J. Antonov, J. Wang, T. L. Delworth, K. Dixon, and A. Broccoli, 2001: Anthropogenic warming of the Earth's climate system. *Science*, **292**, 267-270.
- Li, Z., C. H. Whitlock, and T. P. Charlock, 1995: Assessment of the global monthly mean surface insolation estimated from satellite measurements using global energy balance archive data. *J. Climate*, **8**, 315-328.
- Liang, X., E. F. Wood, and D. P. Lettenmaier, 1996: Surface soil moisture parameterization of the VIC-2L model: Evaluation and modification. *Global Planet. Change*, **13**, 195-206.
- Liang, X., D. P. Lettenmaier, E. Wood, and S. Burgess, 1994: A simple hydrologically based model of land surface water and energy fluxes for general circulation models. *J. Geophys. Res.*, **99**, D17, 14415-14428.
- Lin, B., and Coauthors, 2008: Assessment of global annual atmospheric energy balance from satellite observations. *J. Geophys. Res.*, **113(D16)**.

- Liston, G. E., 1999: Interrelationships among snow distribution, snowmelt, and snow cover depletion: implications for atmospheric, hydrologic, and ecologic modeling. *J. Appl. Meteor.*, **36 (10)**, 1474-1487.
- Liston, G. E., C. A. Hiemstra, 2011: The changing cryosphere: pan-Arctic snow trends (1979–2009). *J. Climate*, **24**, 5691–5712.
- Liu, J., J. A. Curry, W. B. Rossow, J. R. Key, and X. Wang, 2005: Comparison of surface radiative flux data sets over the Arctic Ocean. *J. Geophys. Res.*, **110**, C02015, doi:10.1029/2004JC002381.
- Lugina, K. M., P. Ya Groisman, K. Ya Vinnikov, V. V. Koknaeva, and N. A. Speranskaya, 2005: Monthly surface air temperature time series area-averaged over the 30-degree latitudinal belts of the globe, 1881–2004. *Trends: A Compendium of Data on Global Change*, Carbon Dioxide Information Analysis Center, Oak Ridge National Laboratory, U.S. Department of Energy. [Available online at <http://cdiac.esd.ornl.gov/trends/temp/lugina/lugina.html>.].
- Mahlstein, I., and R. Knutti, 2011: Ocean heat transport as a cause for model uncertainty in projected arctic warming. *J. Climate*, **24(5)**, 1451-1460.
- Male, D., and R. Granger, 1981: Snow surface energy exchange. *Water Resour. Res.*, **17**, 609-627.
- Manabe, S., and R. J. Stouffer, 1994: Multiple-century response of a coupled ocean–atmosphere model to an increase of atmospheric carbon dioxide. *J. Climate*, **7**, 5-23.
- Manabe, S., M. J. Spelman, and R. J. Stouffer, 1992: Transient response of a coupled ocean–atmosphere model to gradual changes of atmospheric CO₂, Part II: Seasonal response. *J. Climate*, **5**, 105-126.

- Mann, H. B., 1945: Nonparametric tests against trend. *Econometrica: Journal of the Econometric Society*, 245-259.
- Marks, D., and J. Dozier, 1992: Climate and energy exchange at the snow surface in the alpine region of the Sierra Nevada 2. Snow cover energy balance. *Water Resour. Res.*, **28**, 3043-3054.
- Marsh, P., and J. Pomeroy, 1996: Meltwater fluxes at an Arctic forest-tundra site. *Hydrol. Processes*, **10**, 1383-1400.
- Maurer, E., A. Wood, J. Adam, D. Lettenmaier, and B. Nijssen, 2002: A long-term hydrologically based dataset of land surface fluxes and states for the conterminous United States. *J. Climate*, **15**, 3237-3251.
- McClelland, J. W., S. J. Déry, B. J. Peterson, R. M. Holmes, and E. F. Wood, 2006: A pan-arctic evaluation of changes in river discharge during the latter half of the 20th century. *Geophys. Res. Lett.*, **33**, L06715, doi: 10.1029/2006GL025753.
- McNally, A. P., 2002: A note on the occurrence of cloud in meteorologically sensitive areas and the implications for advanced infrared sounders. *Quart. J. Roy. Meteor. Soc.*, **128**, 2551-2556.
- Miller, J. R., and G. L. Russell, 2000: Projected impact of climatic change on the freshwater and salt budgets of the Arctic Ocean by a GCM. *Geophys. Res. Lett.*, **27**, 1183-1186.
- Moore, R. D., and I. F. Owens, 1983: Controls on advective snowmelt in a maritime alpine basin. *J. Climate App. Meteorol.*, **23**, 135-142.
- Niu, G. Y., and Z. L. Yang, 2007: An observation-based formulation of snow cover fraction and its evaluation over large North American river basins. *J. Geophys. Res.*, **112**, D21101.

- Ohmura, A., M. Wild, and H. Gilgen, 1989: *Global Energy Balance Archive, GEBA: World Climate Program, Water, Project A7*. Vol. 2, Verlag der Fachvereine.
- Oleson, K. W., and Coauthors, 2004: Technical description of the community land model (CLM). *NCAR Tech. Note TN-461+ STR*, **174**.
- Osterkamp, T. E., and V. E. Romanovsky, 1996: Characteristics of changing permafrost temperatures in the Alaskan Arctic, U.S.A. *Arct. Alp. Res.*, **28(3)**, 167-273.
- Osterkamp, T. E., and V. E. Romanovsky, 1999: Evidence for warming and thawing of discontinuous permafrost in Alaska. *Permafr. Periglac. Process.*, **10(1)**, 17-37.
- Overland, J. E., M. C. Spillane, D. B. Percival, M. Y. Wang, and H. O. Mofjeld, 2004: Seasonal and regional variation of pan-Arctic surface air temperature over the instrumental record. *J. Climate*, **17**, 3263-3282.
- Overpeck, J., K. Hughen, D. Hardy, R. Bradley, R. Case, M. Douglas, B. Finney, K. Gajewski, G. Jacoby, A. Jennings, S. Lamoureux, A. Lasca, G. MacDonald, J. Moore, M. Retelle, S. Smith, A. Wolfe, and G. Zielinski, 1997: Arctic environmental change of the last four centuries. *Science*, **278**, 1251-1256.
- Peterson, B. J., and Coauthors, 2002: Increasing river discharge to the Arctic Ocean. *Science*, **298**, 2171-2173.
- Pitman, A., and Coauthors, 1999: Key results and implications from phase 1 (c) of the project for intercomparison of land-surface parametrization schemes. *Clim. Dyn.*, **15**, 673-684.
- Pohl, S., and P. Marsh, 2006: Modelling the spatial-temporal variability of spring snowmelt in an arctic catchment. *Hydrol. Processes*, **20**, 1773-1792.
- Price, A., and T. Dunne, 1976: Energy balance computations of snowmelt in a subarctic area. *Water Resour. Res.*, **12**, 686-694.

- Prowse, T. D., and I. F. Owens, 1982: Energy balance over melting snow, Craigieburn Range, New Zealand. *J. Hydrol.*, **21**, 133-147.
- Raschke, E., S. Bakan, and S. Kinne, 2006: An assessment of radiation budget data provided by the ISCCP and GEWEX-SRB. *Geophys. Res. Lett.*, **33**, L07812, doi:10.1029/2005GL025503.
- Raschke, E., A. Ohmura, W. B. Rossow, B. E. Carlson, Y. C. Zhang, C. Stubenrauch, M. Kottke, and M. Wild, 2005: Cloud effects on the radiation budget based on ISCCP data, (1991–1995). *Internat. J. Climatol.*, **25**, 1103-1125.
- Rawlins, M. A., and Coauthors, 2010: Analysis of the arctic system for freshwater cycle intensification: Observations and expectations. *J. Climate*, **23**, 5715–5737.
- Robinson, D. A., 1986: Initiation of spring snowmelt over Arctic lands. in *Cold Regions Hydrology Symposium*, Fairbanks, AK: American Water Resources Association.
- Robinson, D. A., 2000: Weekly Northern Hemisphere snow maps: 1966-1999. Preprints, *12th Conf. on Applied Climatology*, Asheville, NC, Amer. Meteor. Soc., 12-15.
- Robinson, D. A., and A. Frei, 2000: Seasonal variability of Northern Hemisphere snow extent using visible satellite data. *The Prof. Geogr.*, **52**, 307-315.
- Robinson, D. A., K. F. Dewey, and R. R. Heim Jr, 1993: Global snow cover monitoring: An update. *Bull. Amer. Meteor. Soc.*, **74**, 1689-1696.
- Romanovsky, V., S. Smith, K. Yoshikawa, and J. Brown, 2002: Permafrost temperature records: indicators of climate change. *EOS, Transactions of AGU*, **83**, 589-594.
- Romanovsky, V. E., T. S. Sazonova, V. T. Balobaev, N. I. Shender, and D. O. Sergueev, 2007: Past and recent changes in air and permafrost temperatures in eastern Siberia. *Global Planet. Change*, **56**, 399-413.

- Rossow, W.B., and R.A. Schiffer, 1991: ISCCP cloud data products. *Bull. Amer. Meteor. Soc.*, **72**, 2-20.
- Rossow, W.B., and R. A. Schiffer, 1999: Advances in understanding clouds from ISCCP. *Bull. Am. Meteorol. Soc.*, **80**, 2261-2287.
- Santer, B., and Coauthors, 2007: Identification of human-induced changes in atmospheric moisture content. *Proc. Natl. Acad. Sci. USA*, **104**, 15 248-15 253.
- Screen, J. A., and I. Simmonds, 2010: The central role of diminishing sea ice in recent Arctic temperature amplification. *Nature*, **464**, 1334-1337.
- Sen, P. K., 1968: Estimates of the regression coefficient based on Kendall's tau. *J. Am. Stat. Assoc.*, 1379-1389.
- Serreze, M., and J. A. Francis, 2006: The Arctic Amplification Debate. *Clim. Change*, **76**, 241-264.
- Serreze, M. C., A. P. Barrett, J. C. Stroeve, D. N. Kindig, and M. M. Holland, 2009: The emergence of surface-based Arctic amplification. *The Cryosphere*, **3**, 11-19.
- Serreze, M., D. H. Bromwich, M. P. Clark, A. J. Etringer, T. Zhang, and R. Lammers, 2003: Large-scale hydro-climatology of the terrestrial Arctic drainage system. *J. Geophys. Res.*, **108**, 8160.
- Serreze, M., and Coauthors, 2000: Observational evidence of recent change in the northern high-latitude environment. *Clim. Change*, **46**, 159-207.
- Sheffield, J., et al., 2006: Development of a 50-year high-resolution global dataset of meteorological forcings for land surface modeling. *J. Climate*, **19(13)**, 3088-3111.
- Shepard, D. S., 1984: Computer mapping: The SYMAP interpolation algorithm. *Spatial Statistics Models*, Gaile, G. L., and C. J. Willmott, Eds., Kluwer, 133-145.

- Shi, X., A. W. Wood, and D. P. Lettenmaier, 2008: How essential is hydrologic model calibration to seasonal streamflow forecasting? *J. Hydrometeorol.*, **9**, 1350-1363.
- Shi, X., M. Wild, and D. P. Lettenmaier, 2010: Surface radiative fluxes over the pan-Arctic land region: Variability and trends. *J. Geophys. Res.*, **115**, D22104, doi:10.1029/2010JD014402.
- Shi, X., M. Sturm, G. E. Liston, R. E. Jordan, and D. P. Lettenmaier, 2009: SnowSTAR2002 transect reconstruction using a multilayered energy and mass balance snow model. *J. Hydrometeorol.*, **10**, 1151-1167.
- Shi, X., P. Y. Groisman, S. J. Déry, and D. P. Lettenmaier, 2011: The role of surface energy fluxes in pan-Arctic snow cover changes. *Environ. Res. Lett.*, **6**, 035204.
- Shi, X., S. J. Déry, P. Y. Groisman, and D. P. Lettenmaier, 2012: Relationships between recent pan-Arctic snow cover and hydroclimate trends. *J. Climate* (in press).
- Shiklomanov, A., R. Lammers, M. Rawlins, L. Smith, and T. Pavelsky, 2007: Temporal and spatial variations in maximum river discharge from a new Russian data set. *J. Geophys. Res.*, **112**, G04S53.
- Simmons, A., et al., 2006: ERA-Interim: New ECMWF reanalysis produces from 1989 onwards. in *ECMWF Newsletter*, edited, pp. 25-35, European Centre for Medium-Range Weather Forecasts, Reading, UK.
- Smith, N. V., S. S. Saatchi, and J. T. Randerson, 2004: Trends in high northern latitude soil freeze and thaw cycle from 1988 to 2002. *J. Geophys. Res.*, **109**, D12101, doi:10.1029/2003JD004472
- Solomon, S., D. Qin, M. Manning, M. Marquis, K. Averyt, M. M. B. Tignor, H. L. Miller Jr., and Z. Chen, 2007: *Climate Change 2007: The Physical Science Basis*. Cambridge

University Press, 1009 pp.

- Sorteberg, A, V. Katsov, J. Walsh, and T. Palova, 2007: The Arctic surface energy budget as simulated with the IPCC AR4 AOGCMs. *Clim Dyn.*, doi:10.1007/s00382-006-0222-9.
- Stackhouse, P. W., et al., 2004: 12-year surface radiation budget data set. *GEWEX News*, **14(4)**.
- Stieglitz, M., S. J. Déry, V. E. Romanovsky, and T. E. Osterkamp, 2003: The role of snow cover in the warming of arctic permafrost. *Geophys. Res. Lett.*, **30**, 1721, doi: 10.1029/2003GL017337.
- Stone, R. S., E. G. Dutton, J. M. Harris, D. Longenecker, 2002: Earlier spring snowmelt in northern Alaska as an indicator of climate change. *J. Geophys. Res.*, **107**, 4089, doi:10.1029/2000JD000286.
- Storck, P., D. P. Lettenmaier, and S. M. Bolton, 2002: Measurement of snow interception and canopy effects on snow accumulation and melt in a mountainous maritime climate, Oregon, United States. *Water Resour. Res.*, **38**, 1223.
- Stow, D. A., et al., 2004: Remote sensing of vegetation and land-cover change in arctic tundra ecosystems. *Remote Sens. Environ.*, **89**, 281-308.
- Sturm, M., C. Racine, and K. Tape, 2001: Climate change: Increasing shrub abundance in the Arctic. *Nature*, **411**, 546-547.
- Su, F., J. C. Adam, K. E. Trenberth, and D. P. Lettenmaier, 2006: Evaluation of surface water fluxes of the pan-Arctic land region with a land surface model and ERA-40 reanalysis. *J. Geophys. Res.*, **111**, D05110, doi:10.1029/2005JD006387.
- Su, F., J. C. Adam, L. C. Bowling, and D. P. Lettenmaier, 2005: Streamflow simulations of the terrestrial Arctic domain. *J. Geophys. Res.*, **110**, D08112, doi:10.1029/2004JD005518.
- Tan, A., J. C. Adam, and D. P. Lettenmaier, 2011: Change in spring snowmelt timing in

Eurasian Arctic rivers. *J. Geophys. Res.*, **116**, D03101.

Tennessee Valley Authority, 1972: Heat and mass transfer between a water surface and the atmosphere. Tennessee Valley Authority Laboratory Rep. 14, Water Resources Rep. 0-6803, 166 pp.

Thornton, P. E., and S. W. Running, 1999: An improved algorithm for estimating incident daily solar radiation from measurements of temperature, humidity, and precipitation. *Agr. Forest Meteorol.*, **93**, 211-228.

Trenberth, K. E., et al., 2007: Observations: Surface and atmospheric climate change. in *Climate Change 2007: The Physical Science Basis, contribution of working group I to the fourth assessment report of the intergovernmental panel on climate change*, edited by S. Solomon et al., 235-336, Cambridge Univ. Press, New York.

Troy, T. J., 2010: The hydrology of northern Eurasia: uncertainty and change in the terrestrial water and energy budgets. Ph.D. thesis, Princeton University, Princeton, NJ, 164pp.

Troy, T. J., and E. F. Wood, 2009: Comparison and evaluation of gridded radiation products across northern Eurasia. *Environ. Res. Lett.*, **4**, 045008.

Troy, T. J., J. Sheffield, and E. F. Wood, 2011: Estimation of the terrestrial water budget over northern Eurasia through the use of multiple data sources. *J. Climate*, **24**, 3272-3293.

Troy, T. J., J. Sheffield, and E. F. Wood, 2012: Accelerating soil heat accumulation across northern Eurasia. *J. Climate* (submitted).

Uppala, S. M., and Coauthors, 2005: The ERA-40 re-analysis. *Q. J. R. Meteorol. Soc.*, **131(612)**, 2961-3012.

- Uppala, S., and Coauthors, 2008: Towards a climate data assimilation system: Status update of ERA_Interim. in *ECMWF Newsletter*, edited, pp. 12-18, European Centre for Medium-Range Weather Forecasts, Reading, UK.
- U.S. Army Corps of Engineers, 1956: *Snow Hydrology, Summary Report of the Snow Investigations*. U.S. Government Printing Office, 433 pp.
- Vincent, L. A., W. A. van Wijngaarden, and R. Hopkinson, 2007: Surface temperature and humidity trends in Canada for 1953-2005. *J. Climate*, **20**, 5100-5113.
- Viterbo, P., and A. K. Betts, 1999: Impact on ECMWF forecasts of changes to the albedo of the boreal forests in the presence of snow. *J. Geophys. Res.*, **104**, 27803-27810.
- Voeikov, A.I. 1889: Snow cover, its effects on soil, climate, and weather and methods of investigations (in Russian), *Notes of Russian Geographical Society on General Geography*. **18**(2).
- Wagener, T., D. P. Boyle, M. J. Lees, H. S. Wheater, H. V. Gupta, and S. Sorooshian, 2001: A framework for development and application of hydrological models. *Hydrol. Earth Syst. Sci.*, **5**, 13-26.
- Walsh, J. E., W. L. Chapman, and D. H. Portis, 2009: Arctic cloud fraction and radiative fluxes in atmospheric reanalyses. *J. Climate*, **22**, 2316-2334.
- Wang, L., M. Sharp, R. Brown, C. Derksen, and B. Rivard, 2005: Evaluation of spring snow covered area depletion in the Canadian Arctic from NOAA snow charts. *Remote Sens. Environ.*, **95**, 453-463.
- Wang, X., J. R. Key, and Y. Liu, 2010: A thermodynamic model for estimating sea and lake ice thickness with optical satellite data. *J. Geophys. Res.*, **115**, C12035, doi:10.1029/2009JC005857.

- Westermann, S., J. Lüers, M. Langer, K. Piel, and J. Boike, 2009: The annual surface energy budget of a high-arctic permafrost site on Svalbard, Norway. *The Cryosphere*, **3**, 245-263.
- White, D., and Coauthors, 2007: The arctic freshwater system: Changes and impacts. *J. Geophys. Res.*, **112**, G04S54, doi:10.1029/2006JG000353.
- Wiesnet, D. R., C. F. Ropelewsk, G. J. Kuklaand, and D. A. Robinson, 1987: A discussion of the accuracy of NOAA satellite-derived global seasonal snow cover measurements. in *Large Scale Effects of Seasonal Snow Cover IAHS Publication*, **No.166**, ed. Goodison, B. E., R. G. Barry, and J. Dozier, Wallingford, Oxfordshire, UK: IAHS Press.
- Wild, M., 2009: Global dimming and brightening: A review. *J. Geophys. Res.*, **114**, D00D16, doi:10.1029/2008JD011470.
- Wild, M., A. Ohmura, H. Gilgen, and J. J. Morcrette, 1998: The distribution of solar energy at the earth's surface as calculated in the ECMWF re-analysis. *Geophys. Res. Lett.*, **25**, 4373-4376.
- Willmott, C. J., and K. Matsuura, 2009: Terrestrial air temperature and precipitation: Monthly and annual time series (1930-2004). [Available online at http://climate.geog.udel.edu/~climate/html_pages/archive.html.]
- Woo, M. K., D. Yang, and K. L. Young, 1999: Representativeness of arctic weather station data for the computation of snowmelt in a small area. *Hydrol. Processes*, **13**, 1859-1870.
- Yang, D., D. Robinson, Y. Zhao, T. Estilow, and B. Ye, 2003: Streamflow response to seasonal snow cover extent changes in large Siberian watersheds. *J. Geophys. Res.*, **108**, 4578.

- Yang, K., R. T. Pinker, Y. Ma, T. Koike, M. M. Wonsick, S. J. Cox, Y. Zhang, and P. Stackhouse, 2008: Evaluation of satellite estimates of downward shortwave radiation over the Tibetan Plateau. *J. Geophys. Res.*, **113**, D17204, doi:10.1029/2007JD009736.
- Zhang, J., and J. E. Walsh, 2007: Relative impacts of vegetation coverage and leaf area index on climate change in a greener north. *Geophys. Res. Lett.*, **34**, L15703, doi:10.1029/2007GL030852.
- Zhang, T., 2005: Influence of the seasonal snow cover on the ground thermal regime: An overview. *Rev. Geophys.*, **43**, RG4002, doi:10.1029/2004RG000157.
- Zhang, T., and K. Stamnes, 1998: Impact of climatic factors on the active layer and permafrost at Barrow, Alaska. *Permafr. Periglac. Process.*, **9**, 229-246.
- Zhang, T., T. E. Osterkamp, and K. Stamnes, 1997: Effects of climate on the active layer and permafrost on the North Slope of Alaska, U.S.A. *Permafr. Periglac. Process.*, **8**, 45-67.
- Zhang, T., R. G. Barry, D. Gilichinsky, S. S. Bykhovets, V. A. Sorokovikov, and J. P. Ye, 2001: An amplified signal of climatic change in soil temperatures during the last century at Irkutsk, Russia. *Clim. Change*, **49**, 41-76.
- Zhang, Y. C., W. B. Rossow, and P. W. Stackhouse, 2006: Comparison of different global information sources used in surface radiative flux calculation: radiative properties of the near-surface atmosphere. *J. Geophys. Res.*, **111**, D13106.
- Zhang, Y. C., W. B. Rossow, and P. W. Stackhouse, 2007: Comparison of different global information sources used in surface radiative flux calculation: radiative properties of the surface. *J. Geophys. Res.*, **112**, D01102.
- Zhang, Y. C., and Coauthors, 2004: Calculation of radiative fluxes from the surface to top of atmosphere based on ISCCP and other global data sets: Refinements of the radiative

transfer model and the input data. *J. Geophys. Res.*, **109**, D19105,
doi:10.1029/2003JD004457

Zhao, H. X., and R. Fernandes, 2009: Daily snow cover estimation from Advanced Very High Resolution Radiometer Polar Pathfinder data over Northern Hemisphere land surfaces during 1982-2004. *J. Geophys. Res.*, **114**, D05113, doi:10.1029/2008JD011272.

Zhu, C., and D. P. Lettenmaier, 2007: Long-term climate and derived surface hydrology and energy flux data for Mexico: 1925-2004. *J. Climate*, **20**, 1944-1954.

Curriculum Vitae

1. ACADEMIC BACKGROUND:

University of Washington, Ph.D., 2012

- Department of Civil and Environmental Engineering
- Dissertation Title: “Understanding the causes and impacts of recent pan-Arctic snow cover changes”
- Advisor: Dr. Dennis P. Lettenmaier

McMaster University, M.A.S., 2005

- Department of Civil Engineering
- Thesis Title: “Impact of climate change on future design standards of drainage infrastructure”
- Advisor: Dr. Paulin Coulibaly

Tianjin University, M.E. (part-time), 2000

- School of Civil Engineering
- Thesis Title: “An application of a theory of modern bargaining to dispute management”
- Advisor: Dr. Xiheng Sun

Tianjin University, B.E., 1997

- Department of Hydraulic Engineering
- Thesis Title: “A dimensional analysis in the sand density calculation”
- Advisor: Dr. Jinliang Yang

2. PUBLICATIONS:

Peer-reviewed publications (published/in press):

- 1) **Shi, X.**, S. J. Déry, P. Y. Groisman, and D. P. Lettenmaier, 2012: Relationships between recent pan-Arctic snow cover and hydroclimate trends. *J. Climate (in press)*.

- 2) **Shi, X.**, P. Y. Groisman, S. J. Déry, and D. P. Lettenmaier, 2011: The role of surface energy fluxes in pan-Arctic snow cover changes. *Environ. Res. Lett.*, **6**, 035204.
- 3) **Shi, X.**, M. Wild, and D. P. Lettenmaier, 2010: Surface radiative fluxes over the pan-Arctic land region: Variability and trends. *J. Geophys. Res.-Atmospheres*, **115**, D22104.
- 4) Gao, H., Q. Tang, **X. Shi**, C. Zhu, T. J. Bohn, F. Su, J. Sheffield, M. Pan, D. P. Lettenmaier, and E. F. Wood, 2010: Water budget record from variable infiltration capacity (VIC) model, *In Algorithm Theoretical Basis Document for Terrestrial Water Cycle Data Records (in press)*.
- 5) **Shi, X.**, M. Sturm, G.E. Liston, R.E. Jordan, and D.P. Lettenmaier, 2009: SnowSTAR2002 transect reconstruction using a multilayered energy and mass balance snow model, *J. of Hydrometeorology*, **10(5)**, 1151-1167.
- 6) **Shi, X.**, A.W. Wood, and D.P. Lettenmaier, 2008: How essential is hydrologic model calibration to seasonal streamflow forecasting? , *J. of Hydrometeorology*, **9(6)**, 1350-1363.
- 7) **Shi, X.**, 2002: An application of a theory of modern bargaining to the project dispute management. *Port Engineering Technology*, **1**, 30-32.
- 8) **Shi, X.**, 1999: The simplified analysis of risk assessment for a large terminal project. *J. of China Harbor Engineering*, **5**, 62-63.
- 9) **Shi, X.**, 1999: A dimensional analysis of the calculation of sand density in the backfill behind the gravity wharf. *Tianjin Port*, **6**, 23-25.

Non-peer reviewed publications:

- 10) Dibike, Y. B, **X. Shi**, and P. Coulibaly, 2006: Assessing climate change impact on design standards of hydraulic structures, *Proceedings of the 7th International Conference on Hydroinformatics*, Nice, France.

11) Coulibaly, P., and **X. Shi**, 2005: The impact of climate change on future design standards of drainage infrastructure in Ontario, *Ministry of Transportation of Ontario, Canada, technical reports*, available at:
http://www.cspi.ca/english/technical_publications.html.

3. PRESENTATIONS:

- 1) **Shi, X.**, and D. P. Lettenmaier, 2012: The impact of pan-Arctic snow cover on frozen soil heat content, *AGU Fall meeting*, San Francisco, CA.
- 2) **Shi, X.**, 2012: The role of surface energy fluxes in pan-Arctic snow cover changes, *UBC/UW Hydrology and Water Resource Symposium*, Seattle, WA.
- 3) **Shi, X.**, S. J. Déry, P. Y. Groisman, and D.P. Lettenmaier, 2012: The role of surface energy fluxes in pan-Arctic snow cover changes, *International Polar Year (IPY) Montreal Conference*, Montreal, QC.
- 4) **Shi, X.**, and D.P. Lettenmaier, 2011: The role of surface energy fluxes in pan-Arctic snow cover changes, *MIT/Woods Hole Graduate Climate Conference*, Cape Cod, MA.
- 5) **Shi, X.**, M. Wild, and D.P. Lettenmaier, 2011: Surface radiative fluxes over the pan-Arctic land region: variability and trends, *EGU General Assembly*, Vienna, Austria.
- 6) Wood E. F., T. Troy, M. Pan, M. Rawlins, and **X. Shi**, 2011: Documenting the uncertainty of the terrestrial water cycle across NESSPI and its effect on trend and attribution studies, *EGU General Assembly*, Vienna, Austria.
- 7) **Shi, X.**, M. Wild, and D. P. Lettenmaier, 2010: Surface radiative fluxes over the pan-Arctic land region: variability and trends, *Steve Burges Retirement Symposium*, Seattle, WA.
- 8) **Shi, X.**, P. Y. Groisman, S. J. Déry, and D. P. Lettenmaier, 2010: The role of surface energy fluxes in pan-Arctic snow cover changes, *AGU Fall meeting*, San Francisco, CA.

- 9) **Shi, X.**, and D.P. Lettenmaier, 2010: The role of surface energy fluxes, temperature and precipitation in spring and summer snow cover retreat over the pan-Arctic, *The UW Program on Climate Change Summer Institute*, Friday Harbor Labs, San Juan Island, WA.
- 10) **Shi, X.**, M. Wild, and D. P. Lettenmaier, 2009: Surface radiation over the pan-Arctic land region: temporal variability and trends, *AGU Fall Meeting*, San Francisco, CA.
- 11) **Shi, X.**, M. Wild, and D. P. Lettenmaier, 2009: Surface radiative fluxes over the pan-Arctic land region: variability and trends, *UBC/UW Hydrology and Water Resource Symposium*, Vancouver, BC.
- 12) **Shi, X.**, M. Sturm, G. E. Liston, R. E. Jordan, and D. P. Lettenmaier, 2009: SnowSTAR2002 transect reconstruction in Alaska, *UW Water Center Annual Review of Research*, Seattle, WA.
- 13) **Shi, X.**, M. Wild, and D.P. Lettenmaier, 2009: Surface radiative fluxes over the pan-Arctic land region: variability and trends, *NASA Energy and Water Cycle Study Annual PI Meeting*, Columbia, MD.
- 14) **Shi, X.**, and D.P. Lettenmaier, 2009: The spatial and temporal variability of surface radiative fluxes over the pan-Arctic, *The Third Annual Graduate Climate Conference*, Pack Forest Conference Center, Seattle, WA.
- 15) **Shi, X.**, M. Sturm, G. E. Liston, R. E. Jordan, and D. P. Lettenmaier, 2008: SnowSTAR2002 transect reconstruction using a multilayered energy and mass balance snow model, *AGU Fall Meeting*, San Francisco, CA.
- 16) **Shi, X.**, D. P. Lettenmaier, 2008: The role of satellite data on the understanding of land surface water and energy fluxes in the pan-Arctic, *NASA Energy and Water Cycle Study Annual PI Meeting*, Baltimore, MD.
- 17) **Shi, X.**, and D. P. Lettenmaier, 2008: SnowSTAR2002 transect reconstruction using a multilayered energy and mass balance snow model, *UBC/UW Hydrology and Water Resource Symposium*, Seattle, WA.

- 18) Lettenmaier, D. P., E. F. Wood, P. Y. Groisman, **X. Shi**, and T. J. Troy, 2008: The role of satellite data on the understanding of land surface water and energy fluxes in the pan-Arctic, *NASA Energy and Water Cycle Study Annual PI Meeting*, Baltimore, MD.
- 19) **Shi, X.**, A.W. Wood, and Dennis P. Lettenmaier, 2008: The effect of hydrologic model calibration on seasonal streamflow forecast performance, *88th AMS Annual Meeting*, New Orleans, LA.
- 20) **Shi, X.**, A.W. Wood, and Dennis P. Lettenmaier, 2007: The effect of hydrologic model calibration on seasonal streamflow forecasts, *AGU Fall Meeting*, San Francisco, CA.
- 21) **Shi, X.**, and D. P. Lettenmaier, 2007: Hydroclimatology of North America 2: The accelerated water cycle and extreme events, *Hydro Seminar*, University of Washington, Seattle, WA.
- 22) **Shi, X.**, and D. P. Lettenmaier, 2007: Hydroclimatology of North America 1: The nature of hydrologic variables, *Hydro Seminar*, University of Washington, Seattle, WA.
- 23) **Shi, X.**, 2005: Climate change impact on future design standards of drainage infrastructure, *UBC/UW Hydrology and Water Resource Symposium*, Vancouver, BC.
- 24) **Shi, X.**, Y. B. Dibike and P. Coulibaly, 2004: Downscaling GCM output with genetic programming model, *AGU/CGU 2004 Joint assembly*, Montreal, QC.